8-1-1984

A signal-to-noise ratio analysis of an autoradiographic image enhancement process

Donald R. Williams

A SIGNAL-TO-NOISE RATIO ANALYSIS OF AN AUTORADIOGRAPHIC IMAGE ENHANCEMENT PROCESS

by

Donald R. Williams

A.A.S. ROCHESTER INSTITUTE OF TECHNOLOGY

(1978)

A thesis submitted in partial fulfillment
of the requirements for the degree of
Master of Science in the School of
Photographic Arts and Sciences in the
College of Graphic Arts and Photography
of the Rochester Institute of Technology

August, 1984

Signature of the Author..... Donald R. Williams
Photographic Science and
Instrumentation Division

Accepted by..... Ronald Francis
Coordinator, M.S. Degree Program

College of Graphic Arts and Photography
Rochester Institute of Technology
Rochester, New York

CERTIFICATE OF APPROVAL

M.S. DEGREE THESIS

The M.S. Degree Thesis of Donald R. Williams
has been examined and approved
by the thesis committee as satisfactory
for the thesis requirement for the
Master of Science degree

Edward M. Grahger
Dr. Edward M. Grahger, Thesis Advisor

John Carson
Mr. John Carson

James Jakubowski
Mr. James Jakubowski

8/18/84
Date

A
SIGNAL-TO-NOISE RATIO ANALYSIS
OF AN AUTORADIOGRAPHIC IMAGE ENHANCEMENT
PROCESS

by

Donald R. Williams

Submitted to the
Photographic Science and Instrumentation Division
in partial fulfillment of the requirements
for the Master of Science degree
at the Rochester Institute of Technology

ABSTRACT

A signal-to-noise ratio(SNR) analysis of a S-35 thiourea autoradiographic image enhancement process incorporating subproportional bleaches is performed, with emphasis on diagnostic medical imagery. Quantifying SNR through a spatial frequency definition of DQE and NEQ, these metrics were compared between donor and receiver-composite stages. While improvements in radiometric speed and gamma were noted in the receiver-composite, these gains were more than offset in a SNR sense by correspondingly lower MTF and higher Wiener spectrum values. As a result the donor's $DQE_{max.}$ of .30 exceeded that of the receiver-composite's $DQE_{max.}$ by 50%. Similarly, the donor's $NEQ_{max.}$ exceeded that of the receiver composite's by 350%. The donor's DQE and NEQ continued to exceed that of the receiver-composite even on an equi-exposure basis.

ACKNOWLEDGEMENTS

The author wishes to thank the following for both technical and facility support in the completion of this thesis:

Dr. E.M.Granger, Mr. John Carson, & Mr. James Jakubowski for both technical support, and in their capacity as thesis committee members.

Mr. Phillip Bunch and his colleagues at the Kodak Research Laboratories, Rochester,N.Y..

Xerox Corp., Webster, N.Y., for microdensitometer and computer facility access.

Dr. Plewes and Dr. Owunwanne of Strong Memorial Hospital, University of Rochester, Rochester, N.Y.

and

Mr. Roland Porth for use of the MTF computer programs.

TABLE OF CONTENTS

LIST OF FIGURES

1. INTRODUCTION

1.1 Autoradiography

As photography evolved from an art to a science, a natural consequence was the evaluation and extension of the photographic image as an information medium. This spawned a plethora of techniques to enhance the photographic image information beyond what was considered to be normal. Even to this day new techniques continue to be proposed. However, only a handful of these methods survived the gauntlet of practicality and success.

One of these processes which, at first, did not appear especially appealing from an image enhancement perspective was a radiation emission method[1,2]. Over the years this method has come to be known as autoradiography. Basically, the procedure involves toning the original silver image(the donor) with a radioactive material. When the toned image was placed in contact with another unexposed silver halide material (the receiver), the decay properties of the radioactive material led to a subsequent latent image in the receiver. Since the amount of toner and with it radiation emission(i.e., exposure) is proportional to the amount of silver at a given location, wherever there was a high density in the donor there was a proportional amount of latent image or, after development, density. Likewise, low donor densities led to low receiver densities. Therefore, upon development, the receiver was a duplicate positive image of the donor.

While this method was originally intended as a duplication scheme, it eventually found a use as an image enhancement method[3]. The idea behind the enhancement is to radioactively tag the donor's image silver that does not contribute significantly to the optical density yet does contain image information. Most of this information is in the toe region of the characteristic curve and is associated with individual image grains rather than a large number of grains. By radioactively tagging this silver one hopes that the information in this region will manifest

itself in the receiver, and in turn increase the photographic speed.The feasability of recent efforts using this scheme has suffered however due to inherent radiation hazards, equipment considerations and unacceptable image quality.[4,5]

Be that as it may, one process that has shown considerable promise and seems to circumvent some of the above mentioned problems is an autoradiographic image intensification method developed by Askins[6]. Similar to the radiation emission method, the original silver image of the donor is reacted with radioactive nuclides. For Askins's process these are beta-particle emitting nuclides and because of their low energy tend to optimize the enhanced image's resolution.[7] These nuclides take the form of thiourea S-35 in an activating or toner bath.

Once the donor has been bathed in this activating bath it is dried, and one then has a radioactive image whose radioactive flux at any location is proportional to the amount of silver at that point. This radiotoned film is then placed in contact for a given duration of time with another silver halide emulsion, the receiver, and subsequently developed as one would a normal image from silver halide materials.

The chemical mechanism behind the procedure can best be described through work done by James and Vanselow[8]. It is believed that the silver ion reacts with the thiourea through the thione yielding $RCNH_2{=}S{-}{-}Ag^+$. In the presence of OH^- ion , the following reaction occurs:

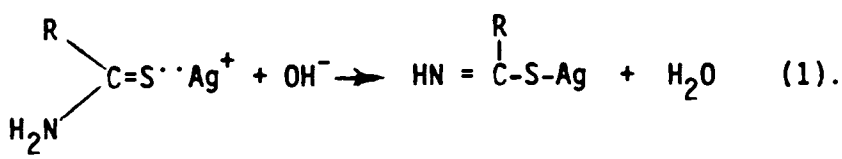

$$\begin{matrix} R \\ \diagdown \\ \quad C{=}S\cdot\cdot Ag^+ \\ \diagup \\ H_2N \end{matrix} + OH^- \longrightarrow \begin{matrix} \quad\quad R \\ \quad\quad | \\ HN = C\text{-}S\text{-}Ag \end{matrix} + H_2O \qquad (1).$$

However, at higher pH the silver thiourea compound reacts via the equation:

$$HN = C\text{-}\underset{\displaystyle R}{\overset{\displaystyle |}{S}}\text{-}Ag^{+} + Ag^{+} + OH^{-} \rightarrow Ag_2S + RC = N + H_2O \qquad (2).$$

With respect to Askin's process, any silver existing in the donor material is aerially oxidized to Ag^{+}. This oxidized silver is then reacted with the radioactive S-35 to form silver sulphide as outlined in equation 2. In essence, the silver image in the donor has been radioactivated. The difference between this and classical two stage imaging systems though is the fact that the silver in the first stage no longer acts to stop radiation but rather to create it.

Previous and existing work with this process in the field of medical radiography has led to reports of increases in speed, visual detection, and resolution in the receiver image when compared to the donor image.[9,10,11] However, one of the major problems in the receiver images has been the high fog levels. This is a direct result of the non-selective nature of the chemical reactions in distinguishing between image and non-image silver. In an effort to diminish these fog levels Vachon[10] and Wheaton[12] studied the effects of subproportional reducers at various stages of the processing and achieved encouraging results from a signal-to-noise ratio viewpoint.

The attributes of the receiver image that were encouraging were not only the speed increases, but also the increased characteristic curve gammas and lower fog levels. These latter two are of keen interest from a signal detection viewpoint. To see how they figure into signal detection a signal-to-noise ratio (SNR) analysis is appropriate. The necessary background for this analysis follows.

1.2 Signal Detection and Signal-to-Noise Ratio

A film's sensitivity or speed has typically been of

primary concern in the evaluation and development of photographic materials. To be sure, optimizing a film's speed is a desirable parameter in many applications. Unfortunately, it alone tells the user nothing about the signal detection capabilities of the film. More than anything, it only informs the user of how well the film will act as a density meter. The point to be made is that speed by itself is of little concern when trying to detect faint stars in distant galaxies, or to distinguish tumors or cancerous cells in the human body. One may be using the fastest film available on the market, but it will be of limited utility if upon processing one is unable to discern signals on it because of the inherent noise in the film.

With this in mind, one may question the relative merits of different systems of speed measurements when in many practical cases one is interested in not only speed but also signal detection. Thus, a marriage of the two parameters would seem in order rather than treating them seperately. The latter may have still been the case had it not been for Rose[13] and his introduction of the concept of efficiency. Important subsequent work on this concept was performed by Jones[14], Fellgett[15], Shaw[16], and various other workers[17,18,19]. To understand how the concept of efficiency evolved and its relation to speed and signal detection, it would be helpful to first understand the parameters that affect a detector's ability to distinguish any given signal.

A signal in the photographic sense manifests itself as a change in density against some uniform background density. The strength of this signal will of course determine how well it is detected. However, in most detection problems the strength of the signal is minimal, and as implied above, the real limiting factor becomes the amount of noise that corrupts the signal. Noise in this case, can be quantified by the root-mean-square(rms) fluctuations. From a thermodynamic point of view, the least amount of noise that one can expect from an ideal radiation detector would be that due to the photon noise of the incident radiation. Assuming that this

radiation is governed by Poisson statistics, the photon noise associated with an ideal detector working at some mean exposure level, q, is $\sqrt{q}$ .The signal-to-noise ratio (SNR) for the perfect detector then becomes:

$$SNR_{in} = \frac{q}{\sqrt{q}} = \sqrt{q} \qquad (3)$$

The subscript "in" implies input. It is imperative to recognize at this point that the signal and noise are referred to in the exposure domain. The need for this becomes evident shortly.

From purely heuristic arguments, one measure of how well a system will perform would be to compare the noise associated with the ideal detector as defined above with that of a detector at hand. In a sense one is not faulting the system under evaluation for noise that was introduced by the incident photons. This measure of the signal detecting efficiency has been termed the Comparative Noise Ratio.[20] Other equivalent terms found in the literature for this measure are Detective Quantum Efficiency(DQE), Equivalent Quantum Efficiency(EQE), and Detective Efficiency. For the sake of convention, DQE will be adopted throughout this paper. The working equation for quantifying DQE experimentally can be developed by knowing the way in which the output and input noise characteristics are related relative to the same criteria.

For photographic films, output fluctuations are made relative to density, whereas measurements of the input noise are made relative to exposure. As mentioned above, to compare these noise levels on an equal basis, it is necessary to make use of the characteristic (D-Log q) curve.

It is well known that

$$\gamma = \frac{dD}{d(\log q)} = \frac{dD}{dq} \cdot \frac{q}{\log_{10} e} \qquad (4)$$

where γ = Differential gamma along the D-log q curve
D = Optical density
q = Average quantum exposure per unit area

If the mean square fluctuations in density, σ_D^2, obey Selwyn's Law, then:

$$G = \sigma_D^2 \cdot A \qquad (5)$$

where σ_D is the rms density fluctuations as measured with an aperture of area A, and G is a constant referred to as Selwyn's constant. These density fluctuations are related to an equivalent number of quantum fluctuations within an area A, $\Delta\bar{q}^2$, by equation 4. Mathematically, this relation is

$$\Delta\bar{q}^2_{out} = \sigma_D^2 \left(\frac{dq}{dD} \right)^2 = \frac{G}{A} \left(\frac{A \cdot q}{\gamma \cdot \log_{10} e} \right)^2 \qquad (6)$$

$$\Delta\bar{q}^2_{out} = G \cdot A \left(\frac{q}{\gamma \cdot \log_{10} e} \right)^2$$

In other words, $\Delta\bar{q}^2_{out}$ is a measure of the output fluctuations as measured with an aperture area A, expressed in terms of an equivalent number of input quanta. The assumption being made in equation 6 that allows us to do this is that the measured output fluctuations σ_D are small enough to be approximated by the differential dD. This, therefore, restricts its use to quantum limited signals.

Recall from equation 3 that the mean square input fluctuations, $\Delta\bar{q}^2_{in}$, are related to the mean number of input quanta q_{in} within an area A, by

$$\Delta\bar{q}^2_{in} = q_{in} = q \cdot A \qquad (7)$$

Therefore, by comparing the input fluctuations as defined in equation 7 with the output fluctuations in equation 6, the ratio between the two, - thus the term, comparative noise ratio - or DQE becomes:

$$DQE = \frac{\gamma^2 \, (\log_{10} e)^2}{G \cdot q} \quad . \qquad (8)$$

Through equation 8 it becomes constructive to recognize alternate interpretations of DQE. By noticing that 1/q is a speed measure and that G is a granularity measure, one common interpretation of DQE has become a speed-to-granularity ratio. It seems logical that for a given speed film, signal detection would be inversely related to the granularity. Generally, this is the case.

A more intuitive feel for DQE can be gained by recalling from equation 3,

$$SNR_{in} = \frac{q}{\sqrt{q}} = \sqrt{q}$$

or

$$(SNR_{in})^2 = q \qquad (9)$$

By defining the output SNR in equivalent exposure terms as

$$(SNR_{out})^2 = \left[\frac{\text{Signal}}{\text{Equiv. Noise}}\right]^2 = \left[\frac{q}{G\cdot\left(\frac{dq}{dD}\right)}\right]^2$$

One finds that

$$\frac{(SNR_{out})^2}{(SNR_{in})^2} = \frac{\gamma^2 (\log_{10}e)^2}{G\cdot q} \qquad (10)$$

The result of course is identical to the expression for DQE in equation 8. Therefore, one finds that

$$DQE = \frac{(SNR_{out})^2}{(SNR_{in})^2} \qquad (11)$$

Insight into the principle of DQE is best reflected through equation 11. The SNR_{out} will always deteriorate relative to the SNR_{in}, since occurances to the contrary would violate laws of statistical entropy. The exception, of course, exists for an ideal detector where the above SNR's are equal.

Also, since an efficiency of any kind can usually be described as some ratio, Rose's concept of efficiency finally becomes more evident from equation 11. To develop this idea thoroughly, we know that

$$DQE = \frac{(SNR_{out})^2}{(SNR_{in})^2} = \frac{(SNR_{out})^2}{q}$$

In order to maintain the integrity of the above equation we may define

$$q' = (SNR_{out})^2 = \frac{\gamma^2 \cdot (\log_{10} e)^2}{G} \qquad (12)$$

or

$$DQE = \frac{q'}{q}$$

By examining equation 12 one may think of the system as working at some SNR associated with an exposure level q', whereas if inefficiencies in the system did not exist at all(i.e. DQE = 100%) the system would be working at some greater SNR associated with an exposure level q. It is as if in attempting to count q quanta, the system was only successful in counting q' quanta[21].

The exposure value q' as defined in equation 12 has come to be known as the Noise Equivalent Quanta(NEQ) per unit image area. The utility of NEQ arises from SNR optimization considerations. While DQE is a measure of SNR per unit energy, NEQ measures the SNR per unit image area. Therefore, one finds that for applications where exposure criteria is critical(i.e., the recording stage) one would want to base exposure on maximum DQE. On the other hand, if there was no limit to the amount of available energy(i.e., the printing stage) the exposure would be based on maximum NEQ values. It is important to differentiate between these SNR measures and to determine which is to be used for the application at hand.

In an effort to keep a numerical and less abstract perspective on matters, it may be helpful at this point to realize some typical DQE and NEQ values of silver halide materials arrived at through experimentation. Most of these DQE values lie within a range of 1%-4% at their maximum value. Compared to other detectors like photomultiplier tubes with DQEs approaching 100%, silver

halide materials then, are sadly outperformed. There have been various schemes to increase these low values however, that work quite well. Most of them are implemented at the emulsion design step and have been studied via the existing models[22]. The main factors that lend towards these low values are the threshhold/saturation nature of the individual receptors(i.e., grains), random spatial array and size distribution of the receptors, variable grain sensitivities, and fog. Typical NEQ values of silver halide materials lie between .1 and .2 quanta/um^2.

In early experimental work many of the reported DQE values were actually in error. This was due to the overriding assumption in the previous analysis that the noise parameter as measured on the film, σ_D, is done so with apertures that are large in comparison to the size of the grains. From a frequency analysis viewpoint then, one is only measuring the fluctuations at low spatial frequencies since the aperture is prefiltering the higher ones. For the general case, this aperture dependent DQE then is not desirable. However, this situation was rectified through work performed by Shaw[23]. By describing the input and output fluctuations via the Wiener Spectrum, a more complete frequency analysis of DQE was described. A synopsis of Shaw's work is derived below via the equations already defined.

It follows from equation 6 that the output fluctuations are

$$\sigma^2_{out} = \sigma^2 \cdot A\left(\frac{q}{\gamma \cdot \log_{10} e}\right)^2 \qquad (13)$$

In keeping with the more complete frequency analysis, the output noise parameter, ^{2}, is replaced with the two dimensional Wiener spectrum of the density fluctuations, arriving at

$$\sigma^2_{out}(u,v,q) = W(u,v,q) \cdot A \cdot \left(\frac{q}{\gamma \cdot M(u,v) \cdot (\log_{10} e)}\right)^2 \qquad (14)$$

where u, v = Rectangular spatial frequency coordinates

$W(u,v,q)$ = The two-dimensional Wiener spectrum of the density fluctuations corresponding to an exposure level q.

$M(u,v)$ = The two-dimensional Modulation Transfer Function.

It is necessary to introduce $M(u,v)$ into the denominator of equation 14 due to the possibility of the output noise becoming less than the input noise at higher frequencies. Assuming that the input has a flat Wiener spectrum, the input noise then becomes

$$\sigma^2_{in}(u,v) = q \cdot A$$

Combining this with equation 14, and assuming an isotropic imaging system, the spatial frequency definition of DQE becomes

$$DQE(w,q) = \frac{(\log_{10}e)^2 \cdot (\gamma(q))^2 \cdot (MTF(w))^2}{q \cdot W(w,q)} \qquad (15)$$

where w = rotationally symmetric spatial frequency

Through this manner of definition, one finds that DQE is no longer dependent on the aperture size and that both a micro- and macroscopic formulation of DQE exist. A complete SNR analysis of a film system can now be achieved by knowing its D-absolute log q curve, MTF, and Wiener spectrum.

By using the above analysis, several authors[24-26] have demonstrated the application of DQE to particular disciplines. One of these areas which plan to be investigated in this work, medical radiography, has especially benefitted due to the exploding field of medical diagnostic imaging. Knowing the DQE and NEQ is genuinely useful in this area since one is interested in not only detecting weak signals for maximum exploitation(i.e., NEQ), but also doing

it with a minimum of X-Ray exposure to the patient(i.e., DQE). Indeed, this is exactly what DQE and NEQ indicate about a detector! By knowing the exposure for maximum DQE, one can most efficiently detect any given signal. Once this signal is detected, it can then be amplified in the signal to noise sense in the second stage process by knowing the film's NEQ characteristics. Both DQE and NEQ become important. DQE to detect the signal with as little exposure as possible, and NEQ to help in the interpretation of that signal by making its detection highly probable. The two must go hand-in-hand in this application.

1.3 Statement of the Problem

Through research efforts on the thiourea S-35 autoradiographic process, much has been learned of the macroscopic image characteristics of the process as it applies to medical radiography. Included in these efforts were evaluations of resolution and signal detection using tri-bar targets and phantoms.[9,10] It was reported that both resolution and signal detection increased. Resolution was determined through inspection of the tri-bar targets and signal detection through evaluation by medical personnel of the phantom images. Due to the nature of the evaluation techniques very little insight was lent as to why these increases occurred. One only knows that according to the authors' observations these changes did occur. As suggested previously, one way of gaining insight into these changes is through a signal detection or SNR analysis. Specifically the measurement of DQE and NEQ for the process in question.

Recall that the autoradiographic process employing subproportional bleaches appeared especially appealing from a SNR viewpoint. In addition to increased speed(1/q) and gamma(γ) of the receiver image when compared to that of the donor, the high fog problem in the receiver image was also alleviated. Inspection of equation 7 would then suggest that DQE and NEQ might increase from

donor to receiver images. The decreased fog would also help in extending the latitude DQE and NEQ.

Two key measures that would verify this are lacking however: namely the MTF and Wiener spectrum. Qualitatively, one might expect that when generating the second(receiver) image from the first(donor) image, the MTF would decrease and the Wiener spectrum values increase. This of course is likely to offset any possible DQE or NEQ gains offered by increases in gamma and speed. Indeed, the nature of entropy would almost dictate it. If this is so though, and one accepts SNR as a basic visual detection criteria, how then does one reconcile the reported increases in visual detection pointed out earlier?

With these thoughts in mind, The experimental objectives of this research are twofold. They are:

1) Measure the DQE and NEQ of a subproportional bleaching autoradiographic process with specific emphasis on medical diagnostic imagery.
2) Evaluate the results and draw conclusions on the donor and receiver image processes as "de facto" image systems based on the DQE and NEQ measurements.

In achieving these objectives, several questions hope to be answered. They are:

1) Is the $DQE_{max.}$ or $NEQ_{max.}$ greater in the donor or donor-receiver combination?
2) How do the DQE and NEQ between donor and donor-receiver images compare on an equi-exposure basis?

and

3) When treated as a two stage expose-to-print process is the exposure at maximum DQE in the donor step the same as the exposure for maximum NEQ in the donor-receiver step?

This last question will determine if the two steps truly complement each other from a SNR viewpoint and is of certain interest for this intensification process's optimization.

Finally, because of the largely positive results with the autoradiographic process for image intensification, the hypothesis for this research is

Hypothesis: When treated as "de-facto" imaging systems the receiver imaging process outperforms the donor process in a SNR sense at some point along the exposure domain.

The way in which these objectives, questions and hypothesis plan to be addressed are outlined in the experimental section that follows. It is in this section that the definitions of the donor and receiver processes are given along with the method of implementation for data capture and processing.

2. EXPERIMENTAL

As pointed out earlier, the measurement of DQE and NEQ is one of the prime experimental objectives of this work. This being the case, this experimental section bears heavily on the validity and interpretation of the results. For, it is here that the measurement foundations are laid. Once this is done, the approach is defined and the actual work of sample generation and measurement takes place.

The cornerstone to all of this is of course defining the actual image system to be analyzed, followed by a statement of what parameters of the system need to be measured. All of this is accomplished in the first section, 2.1, on Image System Definition. Other sections relating to generating the necessary samples and subsequent methods of data capture and analysis follow. Occasionally, certain input/output relationships are referred to throughout this section, however, their exhibition is held for the results section and the reader is asked to be patient. With this as a background, let us begin.

2.1 Image System Definition

From the introduction, it should be clear that two entities of the autoradiographic process, namely the donor and receiver steps, need defining before any measurement work can be performed. Furthermore, they must be defined within the context of an operational medical imaging environment. Therefore, a short scanario of this environment might prove helpful.

Classical medical imaging is always done by means of an X-ray flux passing through some medium. The structure of this medium (i.e. bone, muscle, etc.) differentially attenuates the flux and therefore gives rise to a potential image. Next, some way of detecting and recording this image becomes necessary. This is accomplished by means of a film cassette placed beyond, but in close proximity to, the object being imaged. Figure 1 illustrates

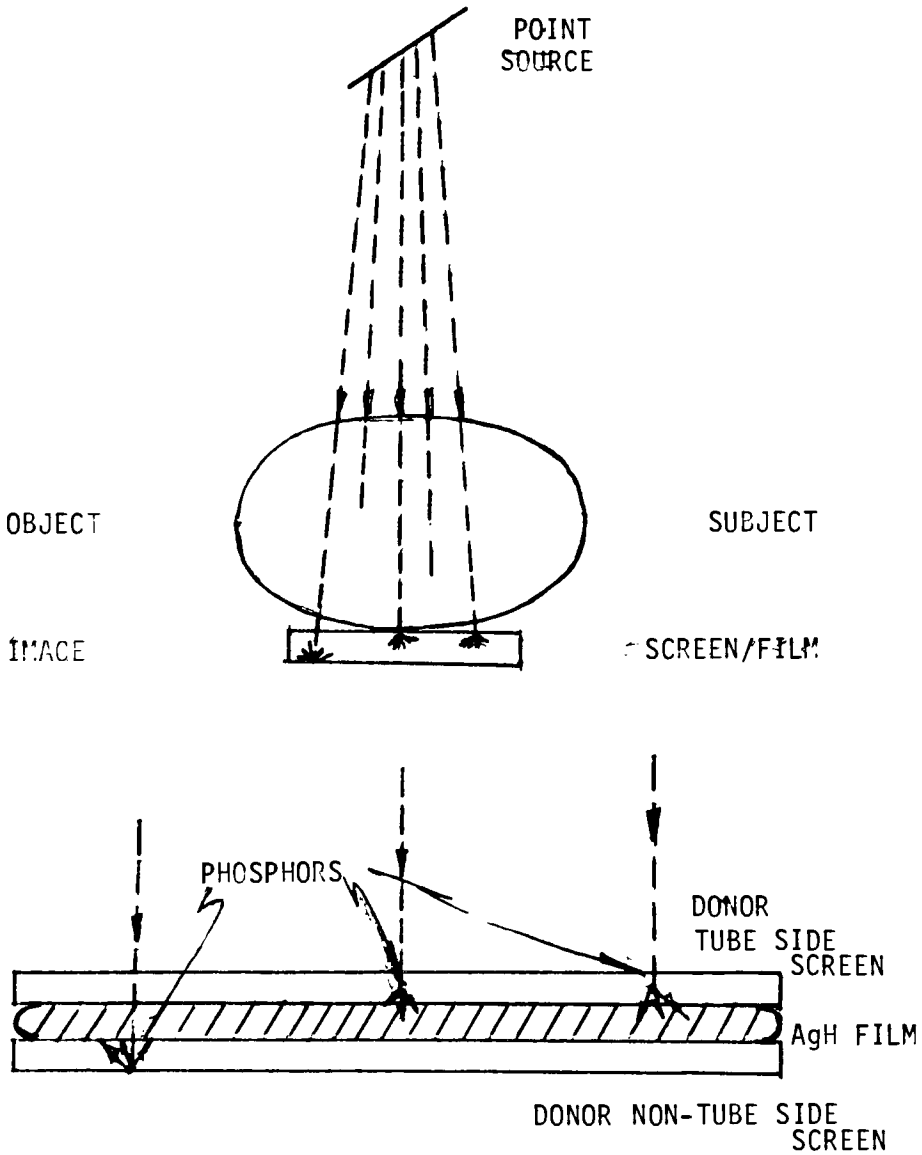

FIGURE 1. Typical Medical X-Ray Exposure Scenario (top), and Cross-section of Screen/Film combination cassette(bottom).

this scenario along with an enlarged cross section of the film cassette as it applies to the donor image generation.

In figure 1 we find that this cassette actually consists of a silver halide photographic material sandwiched between two phosphor screens. It is the screens which make possible most medical imaging as we know it today. They do this by literally translating the energy of the incident X-ray flux, via the phosphors, into an energy band to which the photographic material is sensitive. Because of these phosphors, X-ray exposures many many times less that of direct X-ray imaging is possible. From a patient viewpoint then, it goes without saying that this is a desirable result.

Since no X-ray focusing is done between the object(subject) and image(screen/film) planes, the image that one obtains upon development is in essence a negative shadow of the medium and its internal structure. Areas that absorb X-rays, like bone, image with less density than flesh and muscle tissue which tend to let the X-ray flux pass. For instance, in identifying a broken bone, the image of the break will be dark against the relatively light surround of the bone. This is because the void created by the break allows the X-rays to pass, thus creating a higher density in the image. To a first order, this is the basic nature of the image used for medical diagnosis.

It is logical then to characterize the primary image of a medical environment by evaluating the image generated by an X-ray screen/film system. Similarly, if any image enhancements are to be performed, it is on this screen film image that they would likely be done. With reference to the autoradiographic process then, it is natural in a medical imaging environment to define the donor as the screen/film image. Therefore, by definition, we have:

Donor- That image as generated by an X-ray exposure onto a single screen/film system, and normal chemical development.

From this point on then, the term "donor" will be consistent with the above definition. When necessary to distinguish only a portion of the donor system, that portion will be specifically stated; for example, donor film, or donor processing.

Recall that the receiver is necessarally born from the donor. That is, the steps leading to the receiver image are not only those of the toning(or activating) and contact exposure steps but also of the entire donor sequence. In order to avoid confusion, the receiver as referred to earlier will from this point on be termed the "receiver-composite". It is defined as:

Receiver-composite- That image as generated by the contact exposure of the activated donor to the receiver photographic material. This includes the normal chemical development of the receiver material.

For clarification, figure 2 gives a block diagram of both the donor and receiver-composite systems. Having defined these, the necessary measurements to arrive at the DQE and NEQ of these steps should be reviewed.

From equation 15 we have

$$DQE(w,q) = \frac{(\log_{10}e)^2 \cdot (\gamma(q))^2 \cdot (MTF(w))^2}{q \cdot W(w,q)}$$

where
- q = Absolute log exposure in photons per unit area
- w = Rotationally symmetric spatial frequency
- γ = Differential gamma(first derivative) of the D-log q curve
- MTF = Modulation Transfer Function
- W = Wiener spectrum

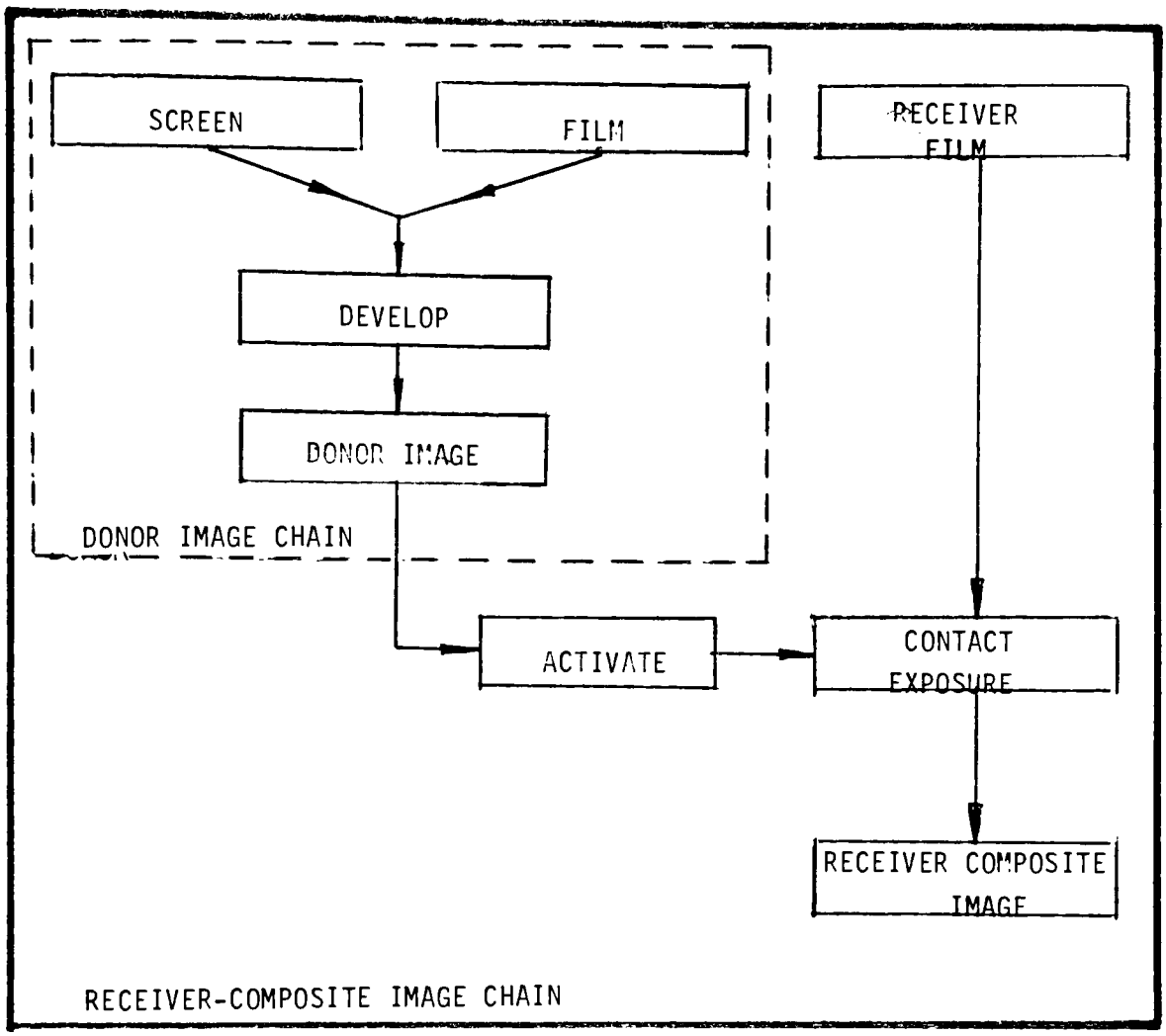

FIGURE 2. Block Diagram defining Donor(dash) and Receiver Composite(bold solid) stages.

In order to calculate the DQE and NEQ then, three primary measurements for both the donor and receiver-composite are necessary. Along with the type of samples required, these measurements are

1. Density vs. absolute log exposure(D-log q) or characteristic curves from stepped density patches to give $\gamma(q)$ and q.
2. Modulation Transfer Function from edge images to give MTF(w).
3. Wiener Spectrum from uniformly exposed and processed density patches to give W(w,q).

Once the samples are obtained, their corresponding functions can be measured and calculated according to equation 15 to arrive at the DQE and NEQ metrics.

To insure an understanding of the image chain, figure 3 gives a block diagram of the steps involved in generating the donor and receiver-composite samples. It also indicates points along the image chain where the necessary parameters are measured or merged. Keep in mind that all three sample types(i.e. step tablets, edges, and densiy patches) are being generated in this process. While the details concerning the step tablet densities are discussed in this section, those for the edge(MTF(w)) and density patches(W(w,q)) are addressed in section 2.3. An entire listing of the major equipment used in the data capture phase of this experiment is given in Appendix A.

2.2 Sample Generation

In performing the work described herein, every effort was made to reflect the conditions of a typical medical imaging environment. In this way, the work involved with extending the experimental results to the applied world should be minimized.

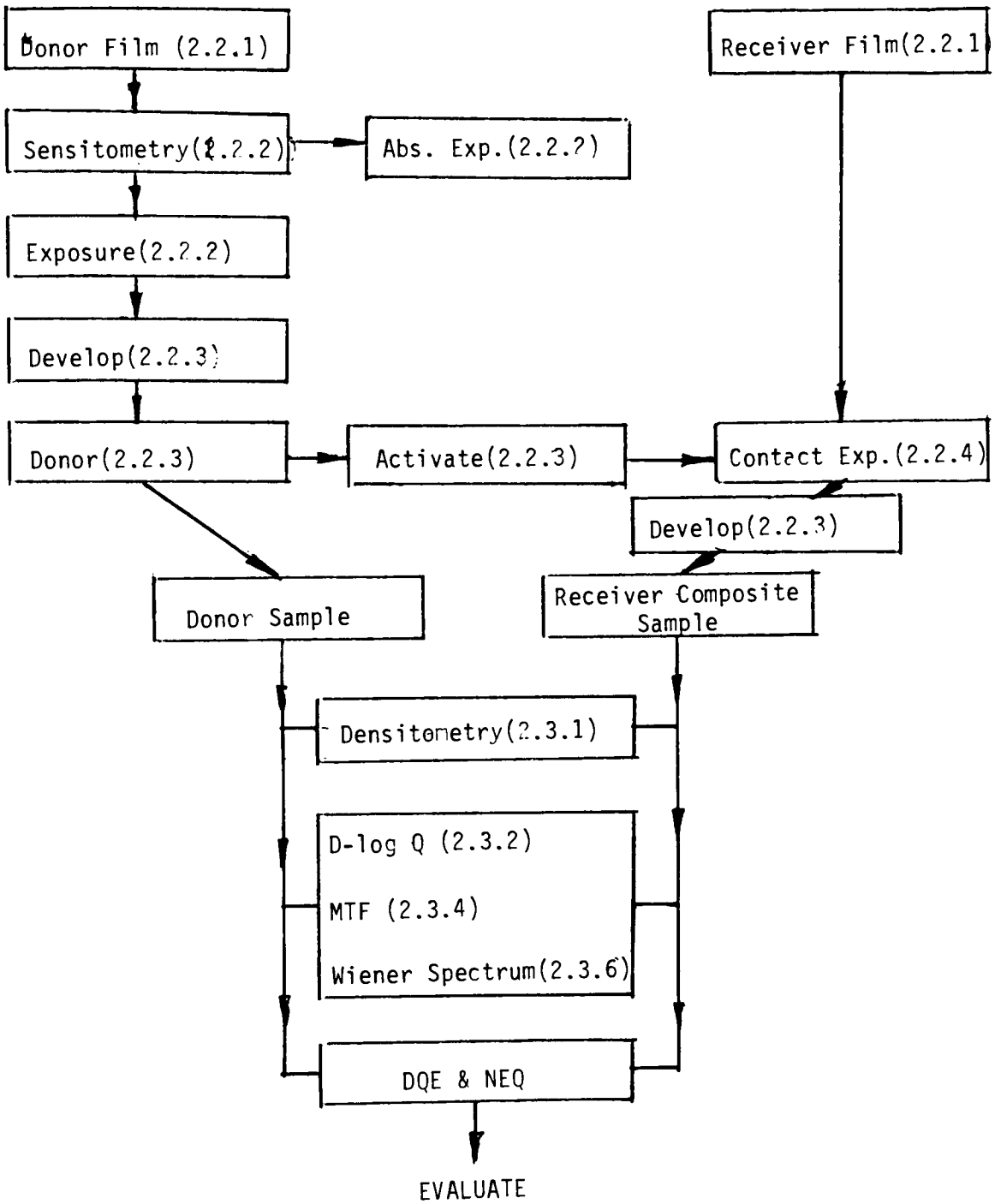

FIGURE 3. Block Diagram for the experimental procedure

2.2.1 Donor and Receiver Photographic Materials

The donor film was Kodak XG Medical Radiographic film. This is a double sided green sensitive silver halide film with an emulsion thickness on either side of the film base of approximately 40 micrometers. The XG film was used in conjunction with a Kodak X-Omat Regular screen. This is a barium strontium sulfate screen and when used with the XG film is considered a "medium" speed screen/film system.

The receiver film was Kodak NMC Nuclear Medicine film. This was a single coated silver halide film and was chosen primarily because of the promising results with it in work by Vachon[10] and Wheaton[12].

2.2.2 Donor Screen/Film Exposure and Sensitometry

As indicated in figure 3 this portion of the experiment is critical in determining the absolute exposure, q, necessary for the DQE and NEQ metrics. The exposing X-ray radiation was at a nominal 70 Kvp(Kilovolts peak), 30 Mas(Milliamp seconds), with .5 mm of copper and 1 mm of aluminum filtration. The spectral power distribution for these conditions is shown in Appendix A, and was calibrated at 1.12 meters from the X-ray source. This corresponded to 1.204 milliroentgens with a 1% error from twelve replicate measurements made with an ion chamber dosimeter. Exposure corrections for a temperature of $68^{o}F$ and barometric pressure of one atmosphere were made from this and then converted to units of photons/cm^2 via the standard photon fluence equation[27]. An example of this calculation is given in Appendix B.

Once the absolute exposure at the above distance was determined, corresponding exposures at other distances were calculated using the inverse square law. The densities corresponding to these exposures gave the usual stepped density modulation used in obtaining the donor and receiver-composite

characteristic curves. It was felt that this inverse square law sensitometry was most accurate since it avoided any scattering effects associated with stepped lead targets.

The edge images were created by contacting a copper edge on top of the screen/film sandwich and exposing at a number of distances from the source. This same trial-and-error technique was also used for exposure of the uniform Wiener spectrum samples. Upon development, those samples meeting the proper requirements(to be described) were then selected for measurement.

2.2.3 Chemical Processing

Two forms of chemical processing existed in this work. The one consisted of the usual latent image to filamentary silver development. This portion was carried out for both the donor and receiver films in a Kodak X-Omatic film processor under the manufacturer's suggested conditions.

The other chemical processing involved the activating solution of the subproportional bleach and S-35 nuclide. The choice of this particular solution was made because of the success that both Wheaton[12] and Vachon[10] had with this process. This particular processing combined the bleaching and activating of the donor in one toner step and eliminated many of the time consuming wash stages. From Wheaton's work, there appeared to be no adverse effects with these shortcuts. The composition of the activating solution along with the step by step toning procedures are given in Appendix A.

At this point, it becomes worthwhile to mention that before the donor samples were activated, they were physically cut in half lengthwise. One portion was retained for the donor characterization while the other was used for further processing in characterizing the receiver-composite. In this way, the error caused by duplicate processing was minimized.

2.2.4 Receiver Film Exposure

Once the activated donor was dried, it was placed emulsion-to-emulsion with the receiver film. This combination was then placed in a screen cassette and contact printed for 1.5 hours followed by the development process. This yielded the final receiver-composite.

Certain considerations were made in this step to allow for the double-sided nature of the donor film. Because the low energy beta particles of the S-35 nuclides are unable to penetrate the film base, only one of the donor emulsions was actually contributing to the receiver film exposure. The particular emulsion side chosen for contact to the receiver film was that side closest to the X-ray source(tube side) at the initial exposure. This choice was made because of its greater effective radiometric speed relative to the distant emulsion side(non-tube side). Since the tube side is closer to the X-ray source this result might be expected and is in fact confirmed in the results. Other reasons for knowing the tube and non-tube characteristics are made clear in the following Data Capture and Processing section.

2.3 Data Capture and Processing

From the previous section we have seen how the physical film samples to be measured were actually generated. Recall that these samples were stepped density tablets for the D-log q curve, edge images for the MTF, and uniform density patches for the Wiener spectrum. It now comes time to examine the densitometric measurement of these samples.

Keep in mind that while all of the measurements are eventually refered back to exposure space through the D-log q curve(see Introduction), the basis for the original measurements

lie in the initial densitometry metrics. With this in mind we will begin with the densitometry technique.

2.3.1 Densitometry- Macro & Micro

Macro-densities of the stepped tablets were read with a Macbeth TD-504 densitometer in a visual diffuse mode equipped with a 3 mm diameter circular aperture. The edge images and uniform density noise patches on the other hand were measured on a scanning microdensitometer. This was a modified Zeiss microscope/photometer with a photomultiplier detector and a computer interface for rapid digitization(see Appendix A). For all microdensitometry, transmission values were the initial capture form. In order to lessen the effects of inherent electrical noise in the microdensitometer, the recorded transmission values were an average of three replicate readings at each sampled point. These values were recorded over 0-225 counts corresponding to a 0-1 transmission range.

Whenever equivalent macro-diffuse density values were required, the micro transmission values, t_o, were converted to micro-density(i.e., $-\log(t_o)$) which in turn were converted to macro diffuse density via a linear calibration curve. A different calibration curve was used for the donor and receiver-composite characterization and was arrived at through a simple linear regression of the macro(ordinate) vs. micro(abscissa) densities of no less than fourteen(14) different density patches over the range of expected density values.

Since the configuration of the microdensitometer for the MTF and Wiener spectrum measurements were identical in many ways, the common parameters of the microdensitometer setup for the two are listed in Appendix A. The selection of these parameters was based on an average source wavelength of 550 nm, diffraction limited optics, 1.5 index of refraction for the emulsion, and a 40.0 micrometer depth-of-focus criteria. Microdensitometer

linearity and effective incoherence conditions as described by Swing[28] were also observed for an image scanning, overfill mode at a sampling interval of 12.5 micrometers. The calculations for the depth-of-focus, microdensitometer linearity, and effective incoherence conditions are listed in Appendix B.

2.3.2 Characteristic Curve Data Acquisition

Data for all characteristic curves were read and reported as macro-diffuse densities above base. From microdensitometry considerations that will become clear soon, seperate density readings for the donor's tube and non-tube side were necessary. This was done by stripping the emulsion from the appropriate side of the film and measuring the remaining density on the substrate.

2.3.3 Characteristic Curve Data Processing

Remember from equation 15 that the DQE and NEQ analysis required a differential gamma along each point of the D-log q curve. To facilitate in determining this, all characteristic curves were fit to a continuous function. The parametric equation for this function was

$$D(x) = \frac{D_{max} - D_{min}}{1 + e^{-\gamma(x-x_o)}} + D_{min} \qquad (16)$$

where

D = Density

D_{max} = Maximum Density

D_{min} = Fog Density

γ = A parameter proportional to the maximum first derivative of the D-log q curve

x_o = Shift parameter in log exposure

x = Independent variable in log exposure

Once the fit was satisfactory, the first derivative with respect to log q (i.e.,dD/dx in equation 16) was calculated in order to arrive at the differential gamma along any point of the characteristic curve. Qualitatively, this function worked quite well for the purposes at hand. RMS errors for the fits are listed in Appendix B along with examples of the raw and smoothed data.

2.3.4 MTF Data Acquisition

The edge images used for the MTF measurement existed over the non-zero slope portion of the characteristic curves and subsequently digitized in transmission. Because of effective exposure linearity considerations[29] every effort was made to keep the density differences over the edge images to less than 0.30. The edges were imaged over three different mean density levels for the donor and two different mean density levels for the receiver-composite. Though these densities were all in the toe portion of their respective characteristic curves it was assumed that the MTFs obtained from them were representative for all mean density levels. The validity of this assumption was not verified. For each edge image, fifteen replicate edge scans(i.e. same sample, different region) were read. Each scan consisted of 200 points and was measured with an effective slit dimension of 25 x 700 micrometers. All other microdensitometer conditions for the MTF data capture are summarized in Appendix A.

As mentioned previously, the double sided nature of the donor film deserved special consideration for both the MTF and Wiener spectrum measurements. This was so because of the relatively large depth-of-focus needed to collect data from both the tube and non-tube sides of the donor emulsion simultaneously. This total thickness was 280 micrometers. Using an average wavelength of 550 nm and an emulsion refractive index of 1.5, one finds that a .036 numerical aperture(N.A.)efflux objective would have been necessary for concurrent-sided microdensitometry measurements (see

calculation in Appendix B). This efflux objective being unavailable, an alternative solution was sought. This solution is outlined below.

By stripping the emulsion from the appropriate side of the donor, the edge images corresponding to the tube and non-tube side of the donor were measured seperately. These seperate measurements allowed a relaxation of the depth-of-focus criteria to that of a single emulsion thickness(i.e, 40.0 micrometers). This criteria was therefore more easily satisfied(N.A.$\leq$.096) and was accomplished with an available .08 N.A. for the efflux optics. In actuality then, there were six(6) edge image samples measured for the donor, two for each of the three mean density levels.The way in which the seperate edge image scans were combined to arrive at the total donor MTF is covered in the following section. Since the receiver film was only a single sided film considerations of this sort were unnecessary.

2.3.5 MTF Data Processing

Having collected the edge scan transmission values, each individual scan was converted to macro-diffuse density and in turn effective exposure through the D-log q curve. All MTF processing was therefore done under the assumption that these systems were linear in effective exposure. While not within the scope of this research to confirm this, there was every reason to believe that at the very least the donor system under consideration was not prone to the classical non-linear adjacency effects often associated with silver halide photographic materials. This is supported by the use of non-viscous development and the unlikelihood of any appreciable laminar layer on the film when using the X-Omatic processor. Likewise, since all exposures were done at 30 Mas, there was no reason to believe that the sensitometry was affected by reciprocity affects, another non-linearity often associated with silver halide photographic systems.

Because the fifteen replicate edge scans within a data set did not all begin at the same spatial coordinates, some effort was needed to place the fifteen scans in phase with each other. This was necessary to avoid any positive bias errors in the averaging of individual MTF estimates. This "in-phase" operation was carried out visually as described below.

After plotting the points for the individual edge scans, the scans within each set were literally shifted along the distance axis and note made of the amount of shift for a satisfactory visual coincidence. The data files for each scan were then shifted in software according to the previously noted shift values. The result was a single 3000 point(i.e 200 points/scan times 15 scans/set) edge scan for each mean density level. The actual MTF calculation began upon completing this operation.

The method used for estimating the MTF was an edge gradient Fourier transform scheme developed by Porth[30]. Using this method, each 3000 point edge data set was fit with a constrained(zero-slope endpoint) least square cubic spline. Knot positions for the spline were visually selected so as to minimize the rms error yet retain the expectations of an edge profile. Usually five, and no more than six knots were needed to fit a particular edge data set satisfactorily. The Fortran callable subroutine that calculated the spline, SPL2Z, and its intermediate values, SPLVAL, are listed in Appendix D along with other supporting subroutines. Following the spline calculation the MTF was estimated by calculating the Fourier transform of the spline's first derivative. This was done via the subroutine SPLFTZ. An example of an edge fit with the splines is given in Appendix B. According to Porth[30] a typical 40:1 signal to noise ratio associated with our edge data would give approximately a 1%-2% error in the MTF at .50 modulation.

Although differences between the MTFs for the tube and non-tube sides of the donor were expected[31] no qualitative differences in the MTF estimates between sides were noted(see

Appendix C). Therefore, after removing the microdensitometer's optical and aperture transfer function degradations, the six donor MTF estimates were averaged and taken as the MTF of the donor. The same was done for the two receiver-composite estimates. In these cases the MTF averaging was rationalized because of the small number of estimates combined.

2.3.6 Wiener Spectrum Data Acquisition

Digital transmission data for the Wiener spectrum was collected over ten different mean density levels ranging from .04 to 1.0 (above base) for a single side of the donor. The same number of density levels was also measured for the receiver-composite film and ranged from .14 to 2.68(above base). The specific density levels chosen were such that they corresponded to as near equal density increments as possible. The effective slit dimension for scanning was 25 x 700 micrometers, and 52 data blocks of two-hundred points each were collected at each density level. This corresponds to a $(2/52)^{.5}$ percent error in the Wiener spectrum at all intermediate frequencies and $(1/52)^{.5}$ error at the zero and Nyquist frequencies[32]. Other microdensitometer parameters are as outlined in Appendix A.

2.3.7 Wiener Spectrum Data Processing

The Wiener spectrum for each mean density level was estimated by direct digital computation of the equivalent macro-diffuse data from the uniform density patches. This involved the block average technique which averages the Fourier transform modulus squared of a number of spectrum estimates at each frequency. In this work, fifty-two(52) estimates per frequency (f=.40 mm^{-1}) were averaged. Further details of the block average technique can be found in work by Dainty and Shaw[33].

Upon calculating the Wiener spectrum from the transmission values, the equivalent macro-diffuse density Wiener spectrum was in turn determined[33]. The error associated with this transformation never exceeded .4%[34]. A final correction on the spectrum was then made for the effects of the aperture and optical MTFs of the microdensitometer. The Fortran computer program, CLAUDE, that performed the initial Wiener spectrum estimation and subsequent corrections can be found in Appendix D.

Since the Wiener spectrum estimates were only for discrete density levels(ten per film type) and frequencies, some interpolation scheme to completely describe the donor and receiver-composite Wiener spectra over a continuum of densities and frequncies was necessary. This was accomplished by choosing an appropriate underlying function for the Wiener spectrum estimates W(w). A descriptive parametric equation was then derived from this function from least square considerations and applied as the interpolation operator over all frequencies. This function used for both donor and receiver-composite Wiener spectra was

$$W(w) = h\left(1 - \left(\frac{w}{w_{max}}\right)^2\right)^q + b \qquad (17)$$

A normalized (i.e.,h=1, b=0, and w_{max}=1) family of curves for this function is illustrated in Appendix B. The parameter w_{max} was chosen as 25 mm^{-1} since Wiener spectrum values beyond this frequency appeared to remain unchanged .The parameters h and b are essentially scaling factors and values for them were chosen by visually inspecting the log-log plots of the low(w=.4 mm^{-1}) and high(w= 25 mm^{-1}) frequency Wiener spectrum values respectively at each mean density level. In order to interpolate across density then a simple piecewise function was used to describe h and b. This then characterized the rise and fall of the Wiener spectra as a function of density. In this way, the Wiener spectra and in turn

DQE and NEQ can be characterized over a density and frequency continuum. An example of a functional fit to equation 17 can be found in Appendix B.

Keep in mind that special care had to be taken for the double-sided donor film. This was handled by measuring and characterizing the Wiener spectrum for the single sided densities of the donor as described above. Once this was done, the equivalent double-sided Wiener spectrum was arrived at by simply adding the Wiener spectrum values from the tube and non-tube side densities. Choosing which two single sided densities to use was accomplished through previous knowledge of the tube and non-tube characteristic curves.

The adding of the Wiener spectrum(variance) in this way is well founded[35] and assumes that the two image density patches are independent realizations. It also assumes that the final detection system's depth-of-field criteria covers the double-sided film thickness. For normal viewing distances this is certainly the case for the human visual system[36] and becomes important since it is likely that NEQ could proportionally track with visual detection performance.

3. RESULTS

With all of the measurements needed for the DQE and NEQ characterization of the donor and receiver-composite in hand, the exposition and outcome of these measurements are presented in this section. The individual results of the characteristic curves, gamma, MTF, and Wiener spectrum are presented first. These results are then unified into NEQ and DQE parameters. Finally, none of the above would be complete without the proper error analysis. This is presented at the chapters end.

Whenever possible, an attempt has been made to compare or verify the forthcoming results with that of previous work in the field. This is done primarily as a check to confirm that the metrics from this work reflect expected values and that no gross errors in the measurements were made.

Since the nature of this research cuts across the medical, physical, and engineering disciplines, the units, presentation, and nomenclature sometimes proved a problem in the preparation of this section. The decision was made to present the information in a manner consistent with the image science community. When appropriate however, supplementary graphs with a variety of formats are supplied in Appendix C. They are described and cited in the text whenever relevant. In an effort to promote uninterrupted reading of the text, all figures are presented at the end of the section.

3.1 Characteristic Curves - Gamma(γ) and Absolute Exposure(q)

The resulting family of absolute characteristic curves for the different stages of the autoradiographic process are shown in figure 4. That is, the seperate tube and non-tube sides of the donor, the tube plus non-tube sides of the donor, and the receiver-composite. The necessary parameters derived from these curves are gamma(dD/d(log q)) and exposure(q). Since DQE and NEQ have their basis in photon statistics, the exposure units chosen in figure 4 are in terms of

photons/cm^2. Supplemental graphs in Appendix C(figures C1 & C2) are plotted in exposure units of roentgens, and ergs/cm^2.

One possible point of confusion for the reader in these graphs may be the interpretation of exposure for the receiver-composite curves. One should not interpret this exposure as the contact exposure from the beta particle flux. Rather, it should be thought of as an effective exposure resulting from the enhancement of the donor. In other words, the densities for the receiver-composite were plotted at the same log exposure as those densities which created them in the donor. With this behind us, let us proceed.

Below, table 1 gives a summary of the important points to be drawn from figure 4.

TABLE 1
Donor and Receiver-composite
Characteristic Curve Comparisons

Parameter	Donor	Rec.-Comp.	Comment
1) Fog density	.048	.035	lower in receiver-composite
2) Speed	.89	3.16	Approximate 2 stop increase in rec.-comp.
3) $D_{max.}$	4.23	2.91	Higher in Donor
4) Gamma	4.2	5.8	Peak gamma higher in receiver-composite
5) Log Exp.shift	-------.08-----		Between opposite tube sides

With regard to the first four items, both Vachon's[10] and Wheaton's[12] work with this process confirm the general nature of the differences. Supporting graphs for item #2 are given in figure 5 and illustrate gamma as a function of log exposure. Complementing graphs for gamma vs. density are given in Appendix C(figure C4). Also, as

suggested from discussions with Plewes[37] the .08 log exposure shift of item #5 accurately reflects the often used rule-of-thumb that for a given amount of incident energy the non-tube side receives 80% as much exposure as the tube side. For this experiment it was 83% as much. The reader is warned however, the exposure shift between tube and non-tube side as exhibited in figure 4 should not be interpreted as an absolutely greater screen/film speed for the tube side , but rather as a means of segmenting the curves according to effective incident exposure.

It was found that the shape of the donor characteristic curve of figure 4 was in very good agreement with the results of work performed at the U.S. Department of Health and Human Services (HHS)[38] for the same screen/film combination and development process(see Appendix C, figure C18, for comparison). Likewise, the exposure needed to attain a density of 1.0 was comparable to values published by Taylor[39] under similar operating conditions(75 Kvp, but with a moving bucky grid). His results were within 1 stop of those in this experiment.

3.2 Modulation Transfer Function - MTF(w)

Figure 6 shows the measured modulation transfer function for the donor and receiver-composite. Additional curves plotted on log-log axes are given in Appendix C(figure C3) and may prove beneficial in conjunction with the Wiener spectrum analysis. Both MTFs had the general form of a negative exponential(i.e., $e^{-|x|}$) with the donor MTF cutoff at 8.0 mm^{-1} and the receiver-composite cutoff at 4.0 mm^{-1}.

Using Bracewell's[40] definition of equivalent bandwidth as a mono-numeric for MTF comparisons, one finds that the donor's equivalent bandwidth is $\approx$1.8 mm^{-1} compared to $\approx$1.2 $mm^{-1}$for the receiver-composite(shown in figure 6). This would indicate that for the mid frequencies the MTF for the donor is 50% greater than for the receiver-composite. Checking this figure with the mid-frequencies (.05-1.5 mm^{-1}) generally confirms this. The guide used to check the

results of the donor MTF was from previosly mentioned work at the U.S. Dept. of HHS[38]. For the same screen/film combination,their MTF results compare favorably with the results of this work. A graphical comparison between the two is given in Appendix C(figure C2D).

3.3 Wiener spectrum - W(w,q)

The final component needed before computing DQE and NEQ is the Wiener spectrum. Representative curves for the donor and receiver-composite Wiener spectra at a density of 1.D above base are given in figure 7. Included are the 95% confidence intervals.

From figure 7 some observations can be made. They are,

1. The spectrum shapes are "well behaved". That is, both donor and receiver-composite Wiener spectra exhibit the characteristically large low frequency values , gradually giving way to and riding on a lesser, but constant, "white noise" component[41]. This shape is common for screen/film radiographic imaging systems.
2. The Wiener spectrum "whitens" for the donor and receiver-composite spectra at $\approx$25. mm^{-1}.
3. The spectrum shapes are different from one another in that the inflection point of the donor's spectrum(in log-log coordinates) occurs at fairly low frequencies while that for the receiver-composite appears at the higher frequencies.
4. For low spatial frequencies and equal densities, the Wiener spectrum of the receiver-composite is approximately an order of magnitude greater than for the donor.

In addition to this, the absolute values of the Wiener spectrum forthe donor conforms well to the measurements of reference 38. These are illustrated in Appendix C(figure C19).

Although figure 7 and the above results are instructive, one must keep in mind that in order to characterize the DQE & NEQ according to equation 15, it must be done with respect to two

independent variables, spatial frequency(w) and exposure(q). Since the Wiener spectrum is a function of these variables, it should be analyzed from this perspective.

An attempt in depicting the three dimensional(x,y,& z) Wiener spectra is illustrated via contour plots in figures 8 and 9. The x axis is spatial frequency; y axis log exposure; and z axis(coming out of the page) Wiener spectrum. Shown are contours of equal log Wiener spectrum values in absolute units of D^2um^2, and most are labeled to avoid any confusion. Each successive contour signifies an equal log Wiener spectrum difference from its nearest neighbor, and corresponds to an approximate 26% change from it. Appendix C gives additional plots with density and spatial frequency as the independent variables. These are presented to convey the "well behaved" nature of the spectra with respect to both spatial frequency and exposure.

By taking a log exposure cross-section of figures 8 and 9, at particular frequencies a clear picture of the Wiener spectra values behavior at these frequencies as a function of exposure is evident. Choosing $.40mm^{-1}$ as the Wiener spectrum frequency of peak value, and $2.0\ mm^{-1}$ as a compromise frequency for the half peak Wiener spectrum value of donor and receiver-composite, figure 10 illustrates that the shape of the Wiener spectrum vs. log exposure relationship for the donor and receiver-composite is largely insensitive to spatial frequency. Therefore, in order to simplify the analysis, most of the discussion from here on will imply a low frequency(i.e.,$.40\ mm^{-1}$) definition of the Wiener spectrum and in turn,DQE and NEQ. Any necessary extensions to the higher frequencies can be had through figures 7,8, or 9, or the contour plots in Appendix C.

Using the above approach in figure 11, one can observe the trend of the low frequency Wiener spectrum as a function of log exposure. Included in figure 11 are accompanying plots of the donor and receiver-composite characteristic curves to help with interpretation in density space. From this, one finds that the Wiener spectrume is fairly linear with log exposure level. That is, at least in the case of those exposures leading to densities of less than 1.2

for both donor and receiver-composite. Beyond this density,a sharp Wiener spectrum falloff of the receiver-composite occurs along with a more gradual flattening of the donor Wiener spectrum at ≈2.0 density.

3.4 DQE and NEQ

Finally, the DQE and NEQ of the donor and receiver-composite are calculated by unifying all of the previous results according to equation 15. The results for the donor are illustrated in figure 12 for a frequency of .40 mm^{-1}. The characteristic curve in relative density is also given for comparison purposes. Additional contour plots for the entire bandwidth are given in Appendix C(figures C9-C16) and support the previous contention of shape insensitivity with spatial frequency.

Both the DQE and NEQ of figure 12 compare well with the few SNR values that exist for X-ray screen/film systems. Work by Wagner and Muntz[43] predict maximum DQEs on the order of 30% while Wagner alone[44] lists NEQ values at typical operating points of ≈.05 um^{-2}. For the donor screen/film system tested the values just cited both occur at a density above base of 0.63.

DQE and NEQ results for the receiver-composite are given in figure 13 with the appropriate contour plots in Appendix C. The shape of the DQE and NEQ curves for both the donor and receiver-composite along with the location of their maxima along the characteristic curve are consistent with most silver halide film systems. DQEs will typically reach a maximum in the toe of the characteristic curve, while maximum NEQ occurs at maximum gamma. Physically, this is due to the thresholding and saturation nature of the silver halide "receptors". A summary of the important points from figures 12 and 13 are listed in table 2.

TABLE 2

Maximum DQE & NEQ @ .4 mm^{-1}

	Donor (Fig. 12)	Receiver-comp. (Fig. 13)
DQE_{max}	0.30	0.21
Log Exp. (photons/cm^2)	7.26	6.78
Density (above base)	0.63	0.75
NEQ_{max} (um^{-2})	0.08	D.018
Log Exp. (photons/cm^2)	7.55	7.03
Density (above base)	1.80	1.90

With these results presented, an estimate of the error involved with their calculation is now in order. Therefore, as a fitting ending to this section, that which follows will detail the proper error analysis of DQE and NEQ from their component measurements.

3.5 DQE and NEQ Error Analysis

Throughout the experimental section, figures for percent error(σ_x/x) in each of the measurements were estimated whenever possible. These estimates are listed in Table 3 below, along with some reasonable guesses for the gamma error. Before proceeding however, some background is necessary.

One can determine the total percent error in DQE due to the components in table 3 through equation 18 below. It is

$$\left[\frac{\sigma_{DQE}}{DQE}\right]^2 = \left[2\frac{\sigma_\gamma}{\gamma}\right]^2 + \left[2\frac{\sigma_{MTF}}{MTF}\right]^2 + \left[\frac{\sigma_q}{q}\right]^2 + \left[\frac{\sigma_{W.S}}{W.S}\right]^2 \qquad (18)$$

In each case, σ_x/x signifies the percent error associated with the subscripted metric. Equation 18 assumes that no bias or proportional(calibration) errors exist, and only considers random zero-mean errors from uncorrelated parameters. Bevington[45] gives a very readable treatment of this analysis along with several examples.

By actually substituting the component percent errors of table 3 into equation 18, the right most column of the table was generated .It should give the reader an idea of the way that the component errors are propagated.

TABLE 3

Percent Error Values in Calculating DQE and NEQ

$\bar{\omega}_{mm^{-1}}$	$\frac{\sigma_\gamma}{\gamma}$	$\frac{\sigma_Q}{Q}$	$\frac{\sigma_{WS}}{WS}$	$\frac{\sigma_{MTF}}{MTF}$	$\frac{\sigma_{DQE}}{DQE}$
0.	10.	1.	20.	0.	28.
.4	10.	1.	13.	2.	24.
0.	5.	1.	20.	0.	22.
.4	5.	1.	13.	2.	17.
0.	2.	1.	20.	0.	20.
.4	2.	1.	13.	2.	14.

One finds that while most of the individual errors are within reason, the fact that they are either multiplied or even worse, squared, leads to some unacceptable errors in DQE. In fact, by performing an actual calculation one will find that the largest contributors to the DQE error are the individual gamma and MTF(the only difference between DQE and NEQ is the exposure term in the denominator. Therefore, since the exposure error is relatively small in this case the same

conclusions for the error in DQE can also be made for NEQ). Indeed, this is why many researchers are reluctant to measure it[46].

With this in mind then, certain doubts may be cast upon the precision of this experiment. This author makes no claim to the contrary. Let it be known though that as a result of the assumptions in the above analysis, those figures cited, are to be interpreted as a root-mean-square error and not as one of miscalibration or bias. It is clearly a difference between the definitions of "accuracy" and "precision". Therefore,"on the average" the results of this experiment are certainly accurate, and as with any measurement the user must be aware of how far to extend the results to his particular application. Further discussion of these results follows.

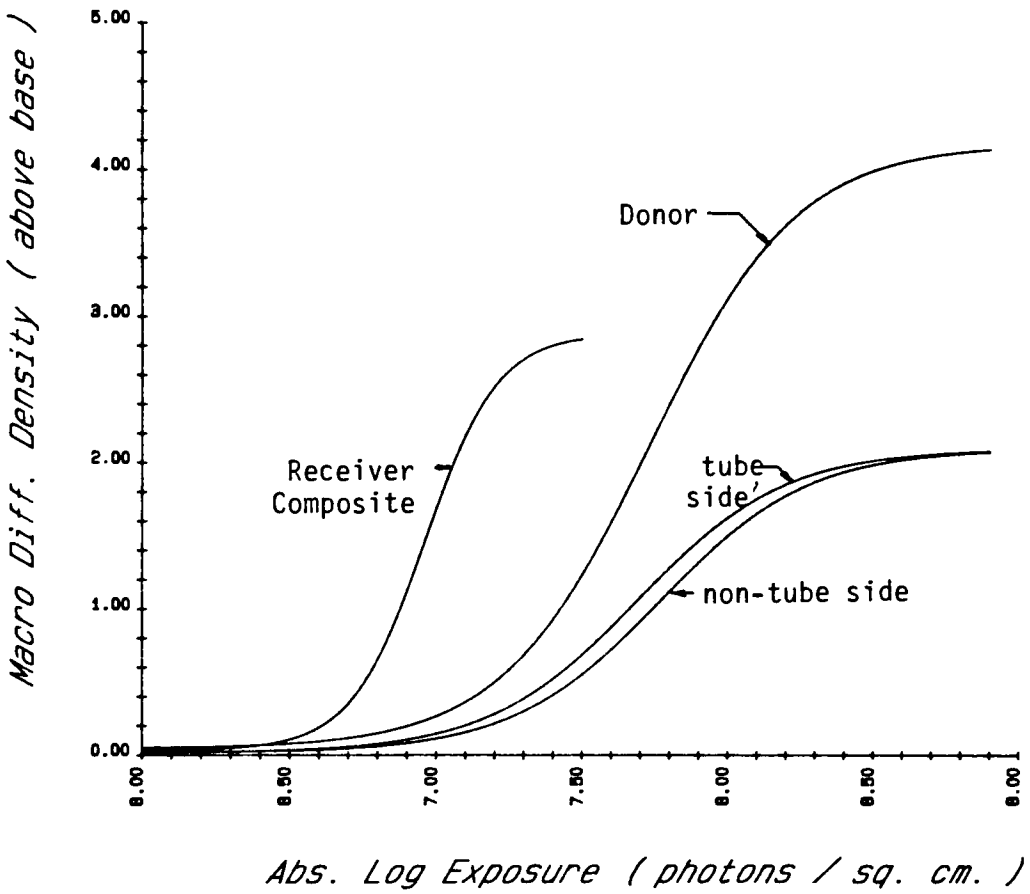

Figure 4: Characteristic curves for different stages of the Autoradiographic system tested

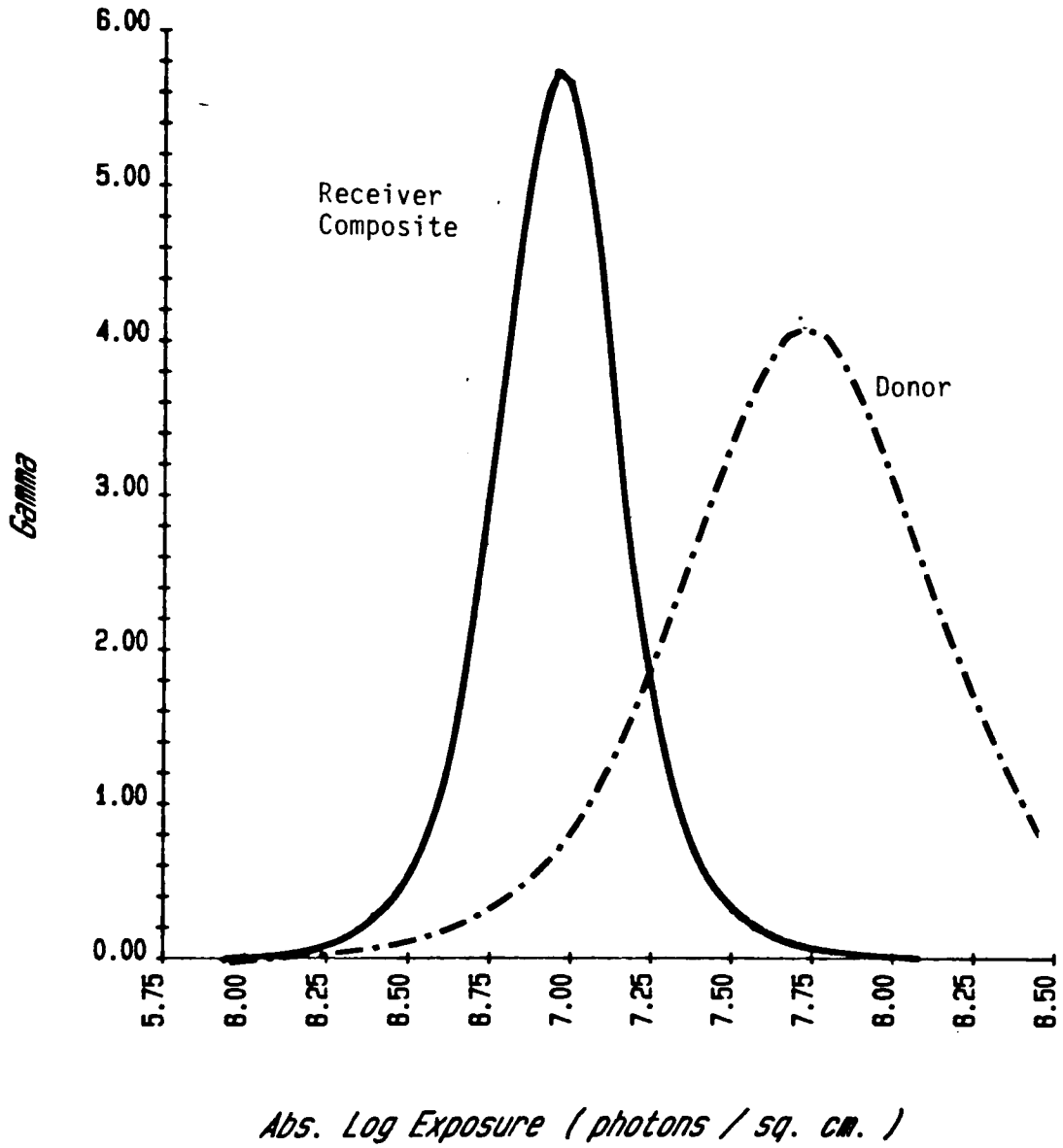

Figure 5: Differential gamma vs. log exposure for Donor and Receiver Composite

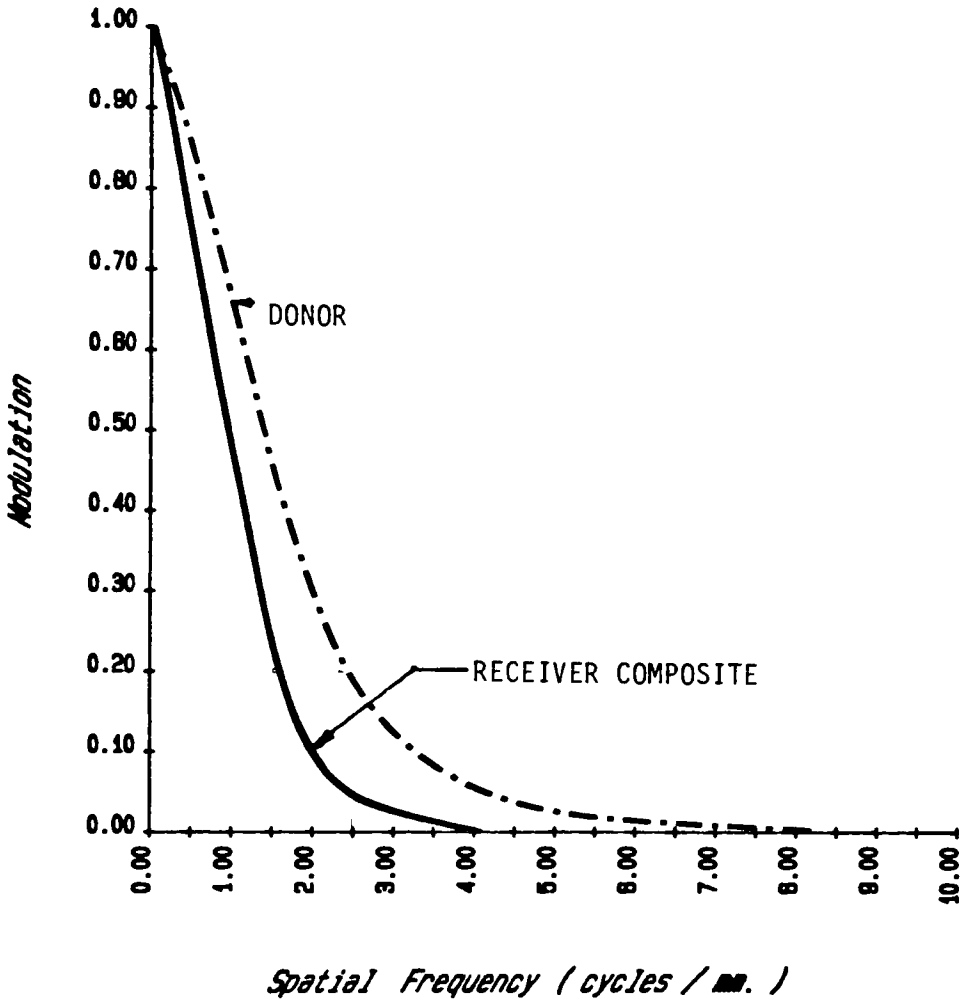

Figure 6: Modulation Transfer Functions for Donor(dash) and Receiver Composite(solid) stages

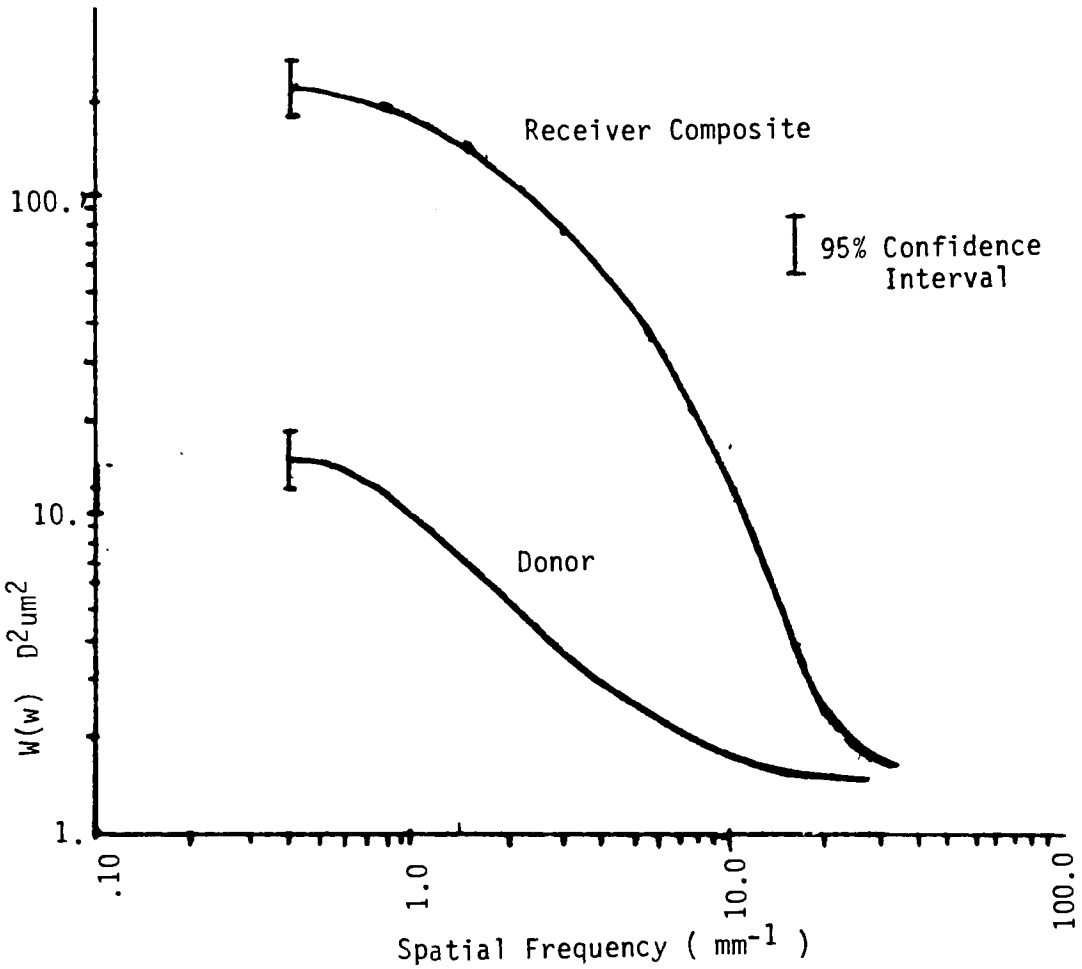

Figure 7: Wiener spectrum(W(w)) for Donor and Receiver Composite at 1.0 Density above base

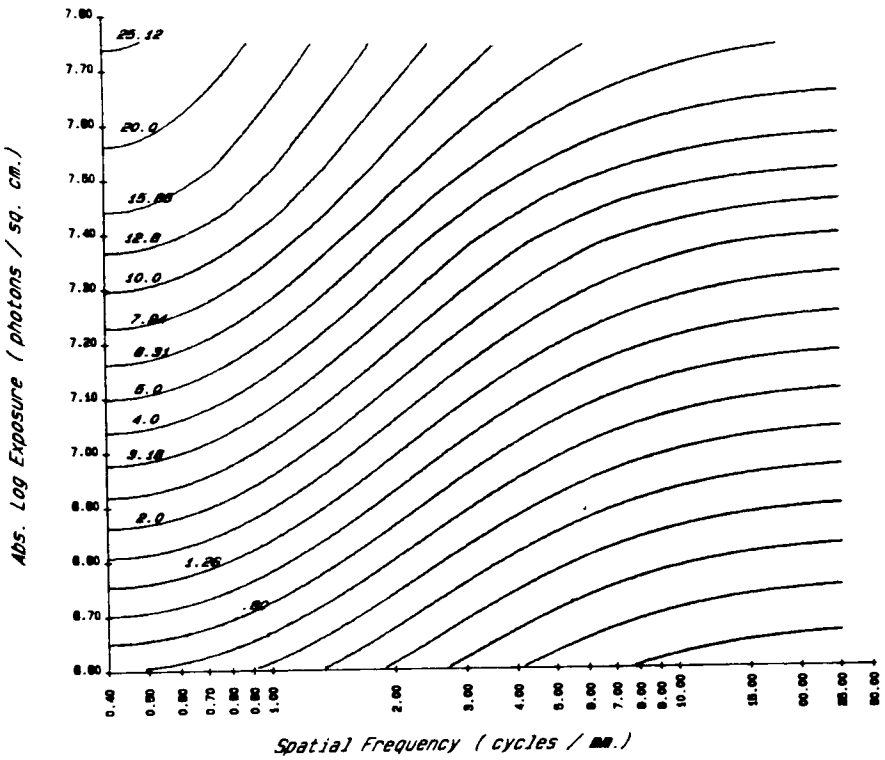

Figure 8: Wiener spectrum contour plots for Donor. Equal log noise power intervals

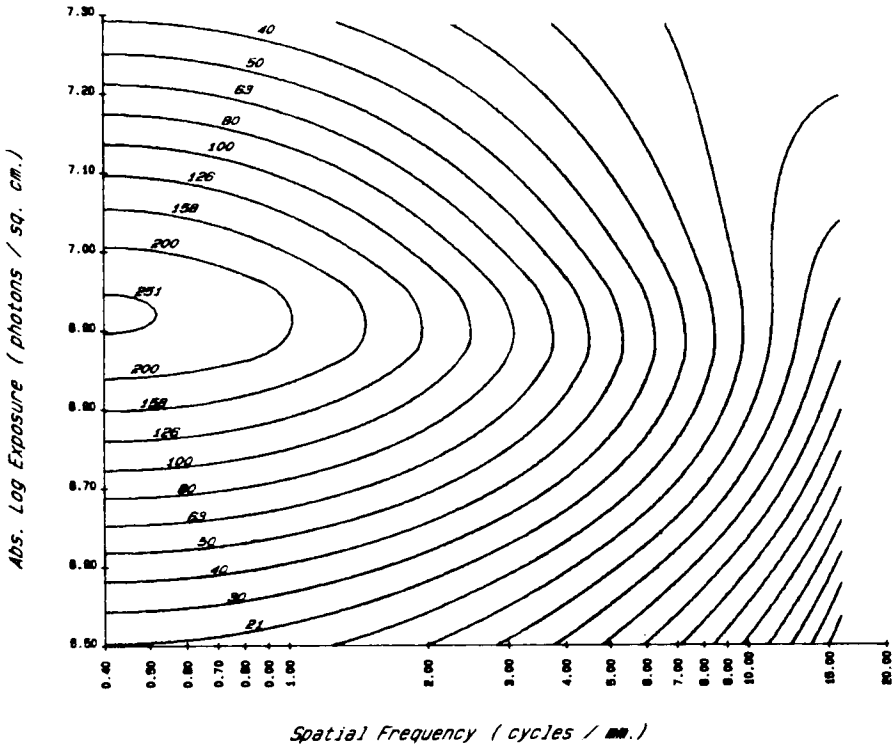

Figure 9: Wiener spectrum contour plots for Receiver Composite. Equal log noise power intervals

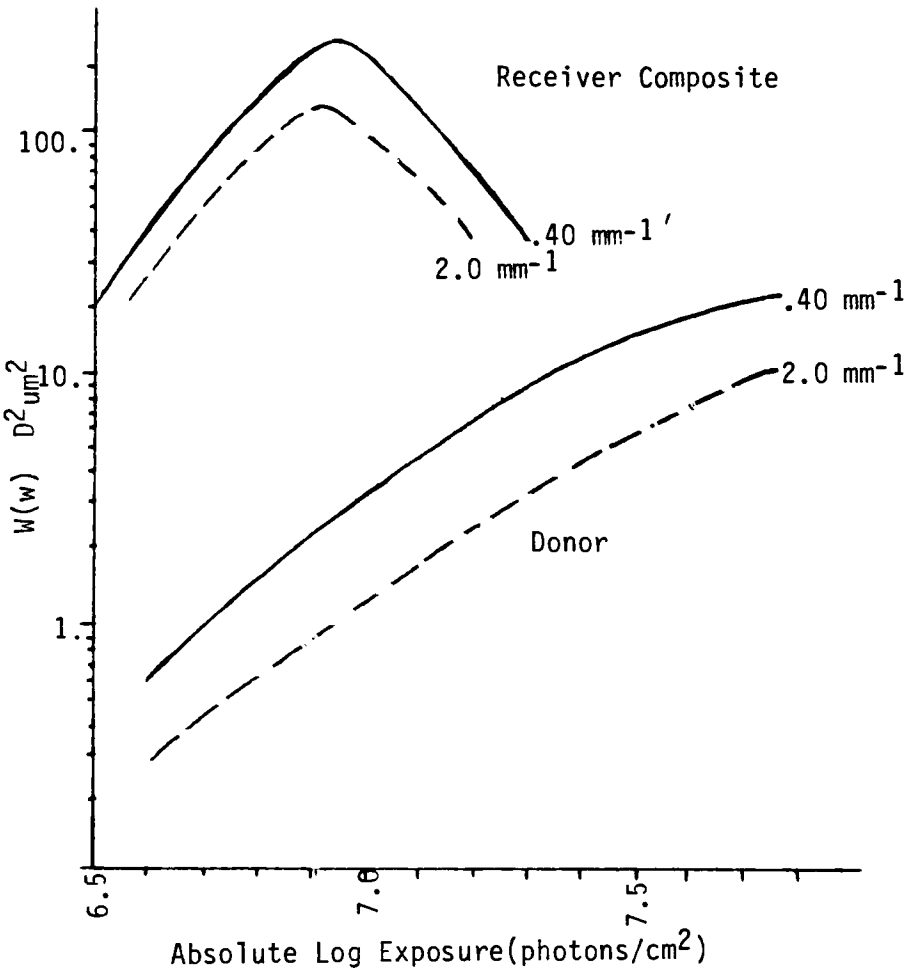

Figure 10: Wiener spectra values @ .40 mm^{-1} (solid) & 2.0 mm^{-1} (dash) for Donor & Receiver-composite

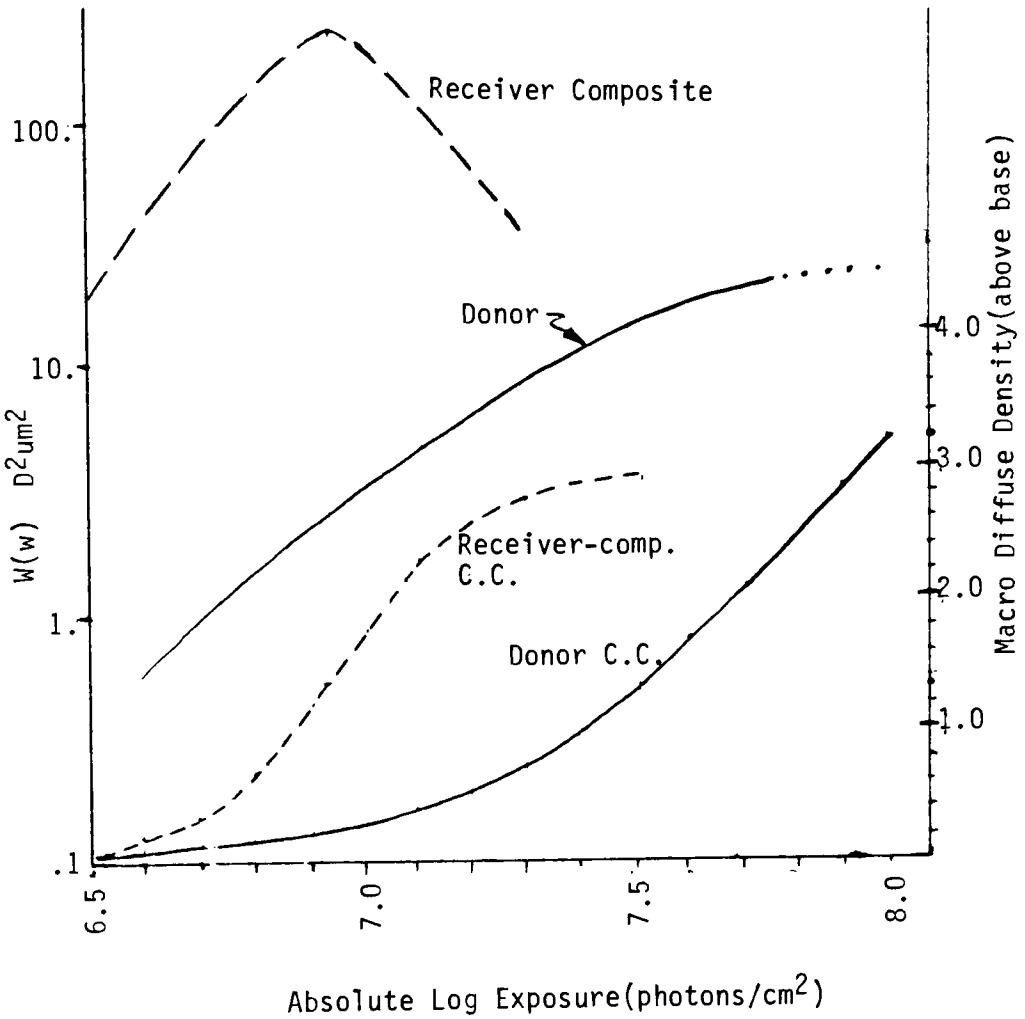

Figure 11. W(.40) for Donor(solid) and Receiver Composite(dash) compared to respective characteristic curves Wiener spectrum on left ordinate & density on right ordinate

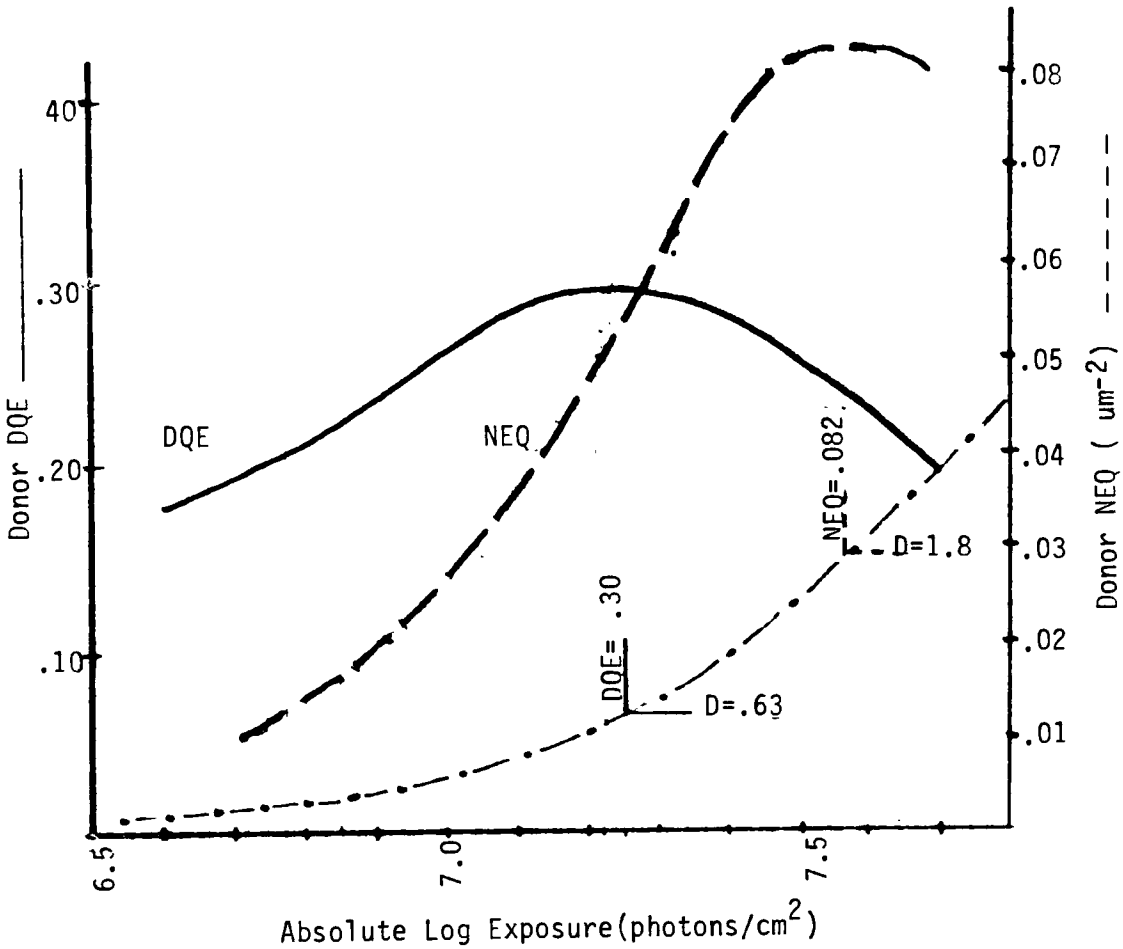

Figure 12: Donor DQE(solid) and NEQ(single dash) curves @ .40 mm^{-1}. Relative Density characteristic curve for comparison.

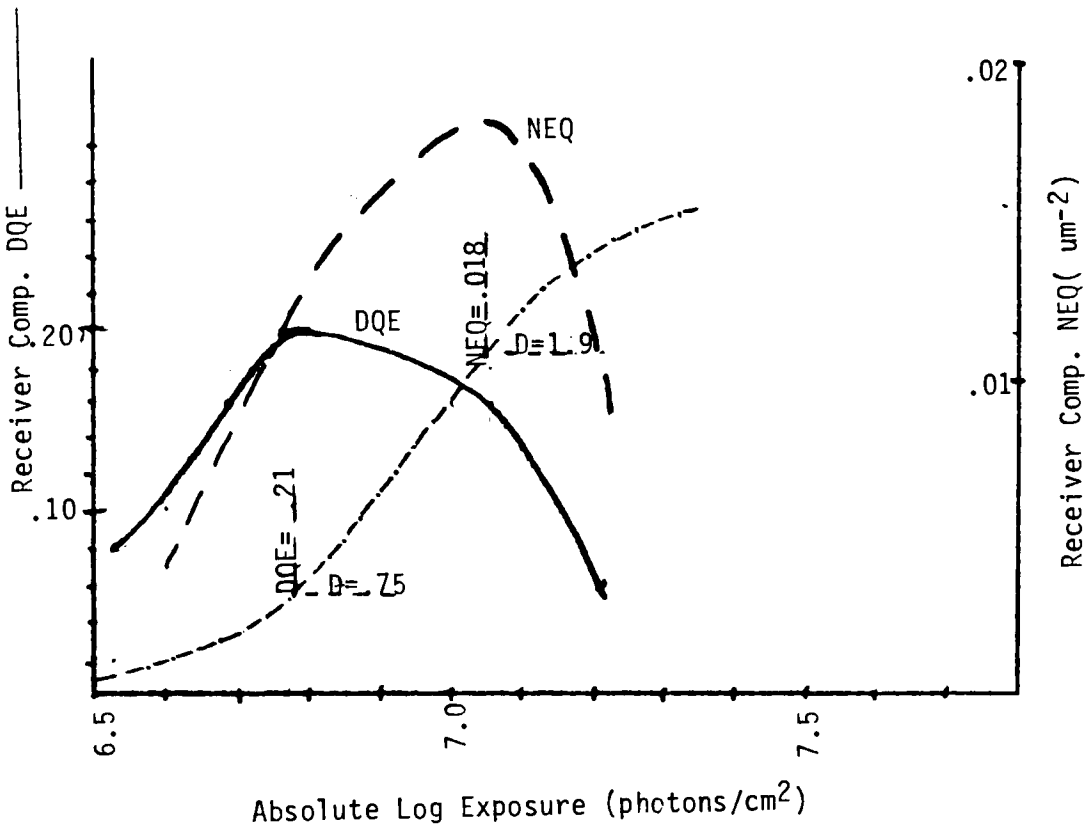

Figure 13: Receiver Composite DQE(solid) & NEQ(single dash) curves @ .40 mm^{-1}. Relative Density characteristic curve for comparison

4. DISCUSSION

With the results of the measurements having just been presented, questions relating to the "how?" and "why?" of these results need to be answered. It is the purpose of this discussion section to answer these questions or, at the very least, speculate on them. If appropriate, recommendations for further research will also be made.

Although DQE and NEQ are the primary metrics of interest in this study, it would be wise to investigate the fundamental quantities that influence them. In this way, any efforts to improve system performance can be directed toward those components offering the greatest gains. These components are speed(1/q), gamma(γ), MTF, and Wiener spectrum. Recall that they are mathematically related to DQE through equation 15 which is restated below.

$$DQE(w,q) = \frac{(\log_{10}e)^2 \cdot (\gamma(q))^2 \cdot (MTF(w))^2}{q \cdot W(w,q)} \qquad (15)$$

Simply put, equation 15 tells us that the speed, and the squares of MTF and gamma lead to proportional changes in DQE, while the Wiener spectrum yields reciprocal changes. Of course, with the exception of the speed criteria the same holds for NEQ.

The chronology in this section is similar to the others. By beginning with an analysis of the characteristic curve, the influences of speed and gamma on DQE are studied. This is followed by a discussion of the influences of the final two components, MTF and Wiener spectrum. All four components are then unified under the DQE and NEQ section along with some appropriate applications.

4.1 Characteristic Curves

The gains in speed and gamma in going from donor to receiver-composite were expected, and as cited in the Introduction, are consistent with past results[9-12]. This is because the S-35 nuclides are able to amplify the individual silver grains in the

extreme toe of the donor curve that are usually undetected by typical optical densitometric techniques. This amplification has led to a resultant speed in the receiver-composite that is consistent with "fast" X-ray screen/film systems[38,46]. Earlier, it was stated that the donor screen/film system was considered "medium" speed. By analogy then, we have effectively gone from a "medium" to a "fast" screen/film system.

Relative to previous S-35 processes, the speed and gamma increases are due to a considerable reduction in the receiver-composite fog level. A receiver-composite with lower fog decreases the Wiener spectrum values in the toe of the characteristic curve, and in so doing enhances the DQE and NEQ. This was shown by Shaw[47] in a model that revealed that fog acts not only as a seperate noise source, as one might expect, but also in a multiplicative way on the input photon noise. This multiplicative effect is a result of the fog grains reducing the film gamma in the toe of the characteristic curve. From equation 15 then, it is plain to see that DQE along with NEQ are affected multiplicatively by the square of the gamma. Hence, any significant change in this parameter is likely to have a profound effect on the DQE and NEQ.

Based on these facts alone, it might appear that the DQE and NEQ of the receiver-composite are prone to exceed those of the donor. This is suggested by the large gamma differences between the two stages. These differences are made clear in figure 14 and show that there is a maximum 10x difference between the receiver-composite and donor gammas for any particular exposure. Though this opportunity for large signal enhancement might appear appealling at first, there are tradeoffs that go with it.

One of these tradeoffs is shortened exposure latitude. Indeed, from figure 4, this is exactly what has happened for the receiver-composite, and it is made worse by the fact that the NMC film used for the receiver-composite has a lower D_{max} than the donor's XG film. Therefore, while one might expect a shift in the DQE and NEQ "exposure latitude"(not strictly defined for DQE and NEQ) to lower

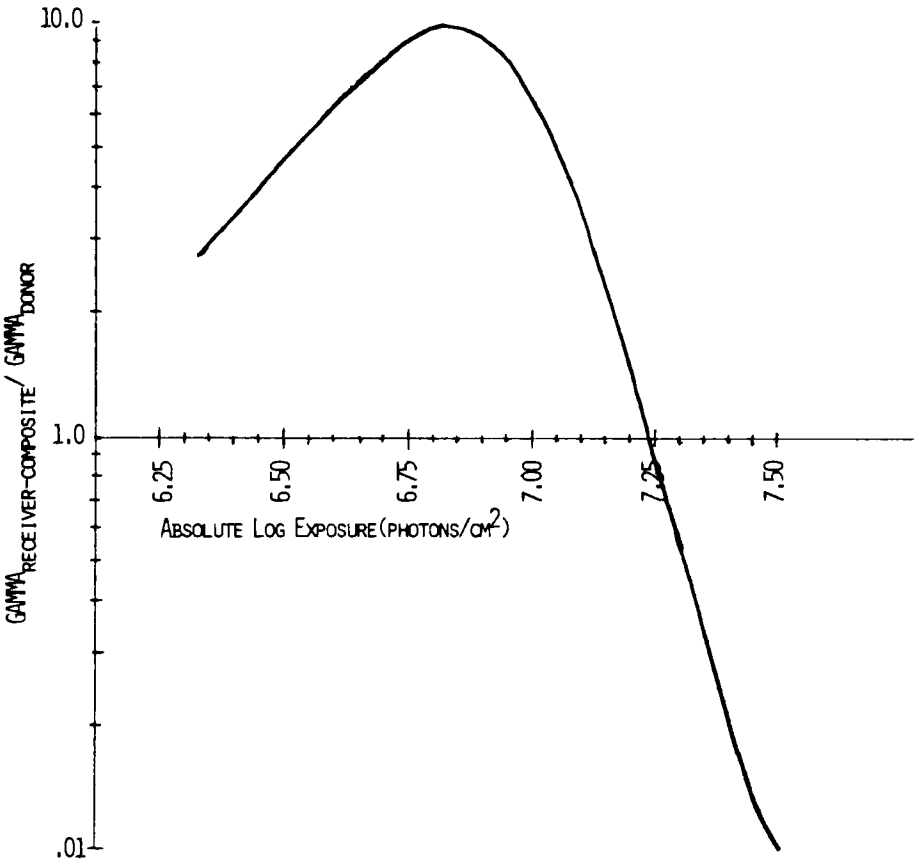

Figure 14: Ratio of Receiver-Composite gamma:
Donor gamma vs. log exposure

exposures due to the speed increase, an extension of this latitude to these exposures does not occur. This is due to the low $D_{max.}$ of the receiver-composite film which by necessity leads to a premature falloff of its gamma in the exposure region where the donor's gamma is still maintained.(Figures 12 and 13 should help in visualizing this.) The other tradeoff of the receiver-composite's increased gamma is corresponding noise enhancement. This, of course, is covered through the Wiener spectrum characterization of the receiver-composite. Before analyzing it though, we will consider the MTF and its influence on DQE and NEQ.

4.2 Modulation Transfer Function (MTF)

Considering the many opportunities for scatter and refraction afforded in an X-ray screen/film system, the MTFs of figure 6 are not surprising. They are consistent with not only the physical aspects of the imaging system (grain size, # of interfaces, thickness), but also with parameters from previous experiments[38] on medium speed screen/film systems. Specifically, these parameters are equivalent bandwidth, shape, and cutoff frequency.

Just as the donor's MTF parallels a "medium" speed screen/film system, the MTF of the receiver-composite is similar to a typical "fast" screen/film system[38]. Figure 15 illustrates these comparisons for both donor and receiver-composite analogies. For the receiver-composite, it shows that while the low frequency modulation of the receiver-composite is similar to a "fast" screen/film system, the cutoff frequency for most of these systems extend beyond that of the receiver-composite. If, however, one is willing to overlook this lack of equivalence, it can generally be stated that, for the same tradeoffs in speed and MTF, going from donor to receiver-composite is comparable to going from a "medium" to a "fast" screen/film system.

Since much of the DQE and NEQ analysis is done at $.40mm^{-1}$, the difference in MTF from donor to receiver-composite at this frequency should be noted. For the donor, MTF(.40) = .95, and for the

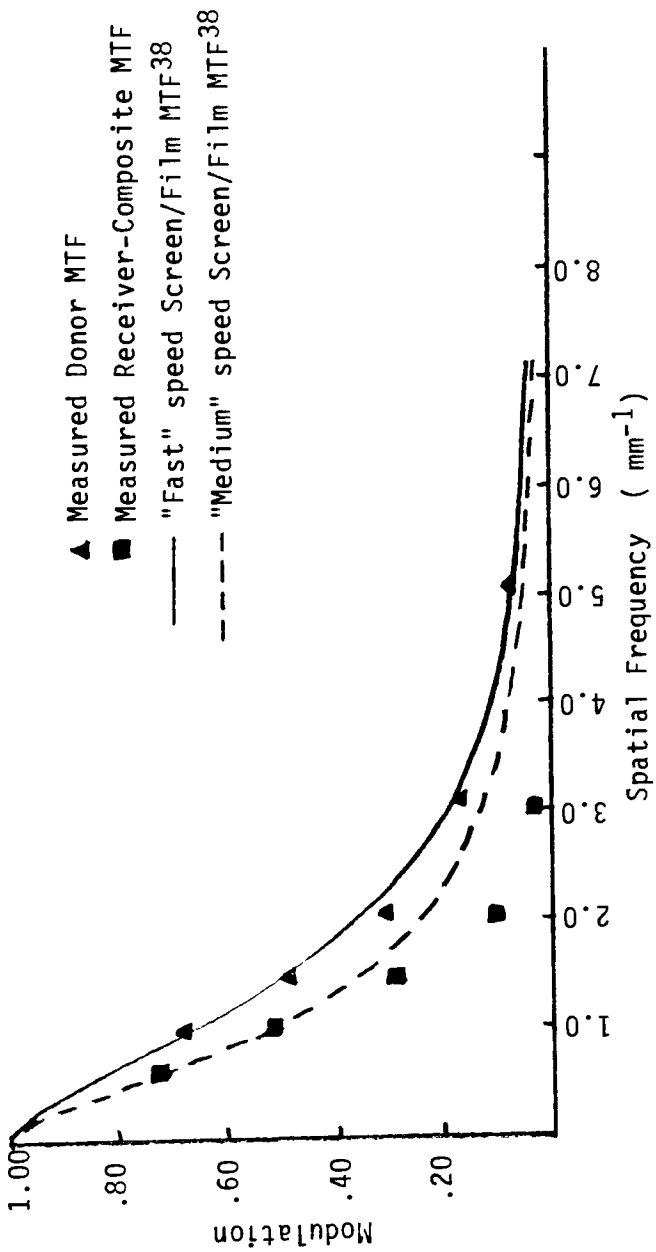

Figure 15: Comparison of Donor and Receiver-Composite MTFs
with typical fast and maedium speed screen/film systems

receiver-composite, MTF(.4) = .90. These figures will also affect the DQE and NEQ by the square of their respective values. One should be reluctant however to translate these into any meaningful measure of radiographic image quality. This is so because of the combined effects from several sources[48], the most prominent of which is photographic noise. An analysis of this noise for the processes at hand follow.

4.3 Wiener Spectrum

A distinguishing feature of medical radiographs is the somewhat splotchy nature of the image structure. This characteristic noise or mottle has appropriately come to be known as 'quantum mottle' since it arises mainly from the statistical nature of the X-ray quanta. When analyzed via the Wiener spectrum, one finds that this mottle manifests itself as a dominant low frequency component that gradually gives way to, and rides upon additive noise contributions from screen structure and inherent film grain. For most screen/film systems the mottle component completely falls off at $\approx$ 25 mm.$^{-1}$. From this frequency to about 50 mm.$^{-1}$ the sole contribution to the Wiener spectrum is from the screen and film grain sources. Beyond this, the Wiener spectrum is typically nil. These characteristics of X-ray screen/film systems' Wiener spectra have been modeled by Rossman[41] and further studied through exposure radiation experiments by Halmshaw[49]. A diagram of Rossman's model along with its functional form is given in figure 16.

Since the Wiener spectra of both the donor and receiver-composite assume the general shape of Rossman's model, it would be interesting to analyze them from that point of view. For instance, as far as the shape of the donor and receiver-composite Wiener spectra are concerned, both appear to conform quiet well to that of Rossman's model: low frequency quantum mottle gradually giving way to higher frequency screen structure and grain noise. Since the mottle is a direct consequence of the X-ray/screen interaction though, one may question why this same effect appears in the

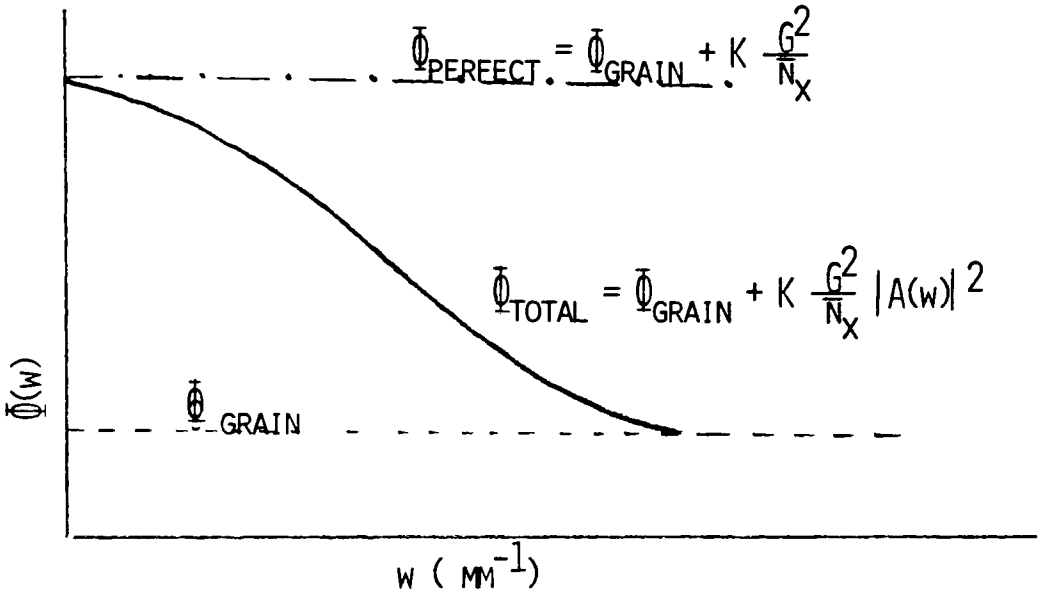

ROSSMAN'S MODEL FOR X-RAY SCREEN/FILM SYSTEM
WIENER SPECTRA

$\bar{\Phi}$ = WIENER SPECTRUM OR NOISE POWER
G = SYSTEM GAIN
$\bar{N}_X$ = AVG. ABSORBED QUANTA/AREA
A(w) = SYSTEM TRANSFER FUNCTION

Figure 16: Schematic of Rossman's Wiener spectrum model for radiographic film/screen systems

receiver-composite spectrum when in fact no screen is used to expose the receiver-composite film itself.

It is speculated that the low frequency mottle of the receiver-composite is simply a manifestation of that in the donor. That is, some sort of grain "print through" effect is probably occurring in the contact exposure between the donor and receiver-composite films. Whether or not this print through of the autoradiographic process is governed by the same theories[50] put forward for classical two-stage printing processes is certainly an area for further studies.

By further extending Rossman's model to our results however, a quantitative discrepancy occurs. That is, the experimental results of this research do not support the low frequency falloff of the Wiener spectra with the square of the MTF as predicted by Rossman's model. For both donor and receiver-composite, the Wiener spectra clearly fall off slower than this (see figure 17), thus indicating sources of noise that are not influenced by the MTF[43]. This anamolous behavior is more pronounced for the receiver-composite and qualitatively might be expected from the complex nature of the process up to that point.

Having analyzed the Wiener spectrum as a function of frequency via Rossman's model, it now becomes appropriate to discuss this same Wiener spectrum values as a function of density. Doing so, yet another departure of the Wiener spectra from a past model occurs. This model is Selwyn's Law[42]. While Selwyn's Law predicts a linear relation between Wiener spectrum values and mean density level, this study shows otherwise, and is illustrated in figure 18 for the donor and receiver-composite at .40 mm^{-1}. For those familiar with the pragmatic end of photographic science, this should come as no surprise. Because assumptions in Selwyn's Law governing grain statistics are violated at higher densities, almost all silver halide photographic materials exhibit this behavior. The donor and receiver-composite densities are no exception. An analysis in this regard shows that for the donor the departure from any semblance of linearity occurs at a density of $\simeq$60, and appears to approach an

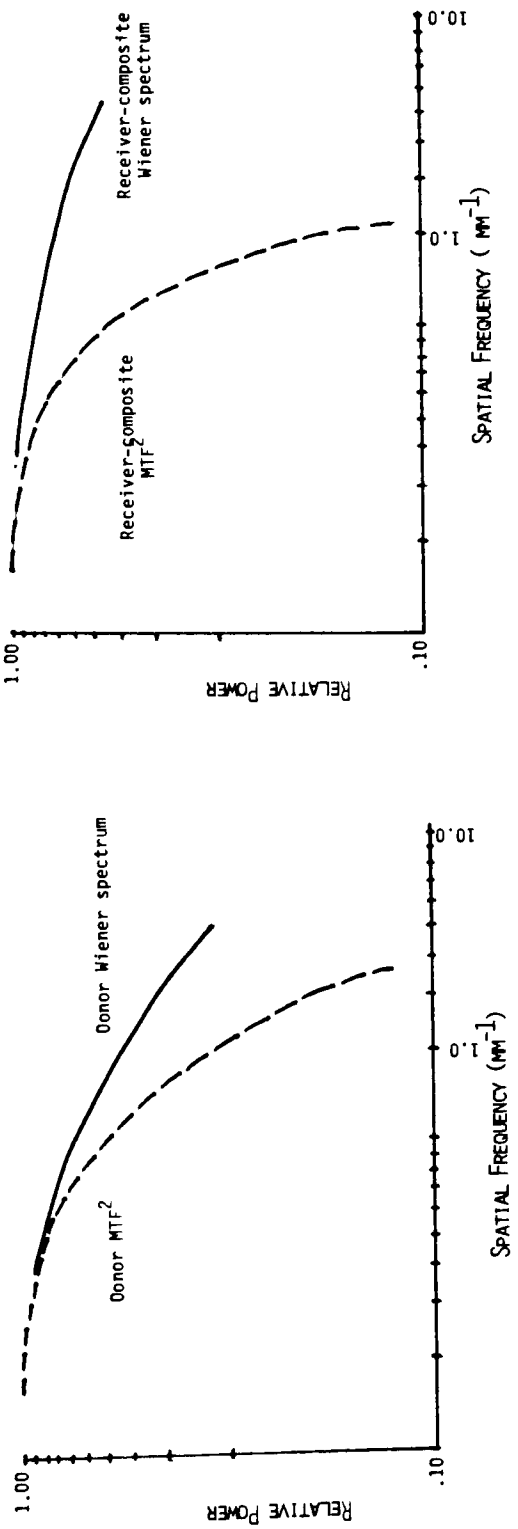

Figure 17: Comparison of Donor(left) and Receiver-composite(right) Wiener spectra against their respective MTF^2.

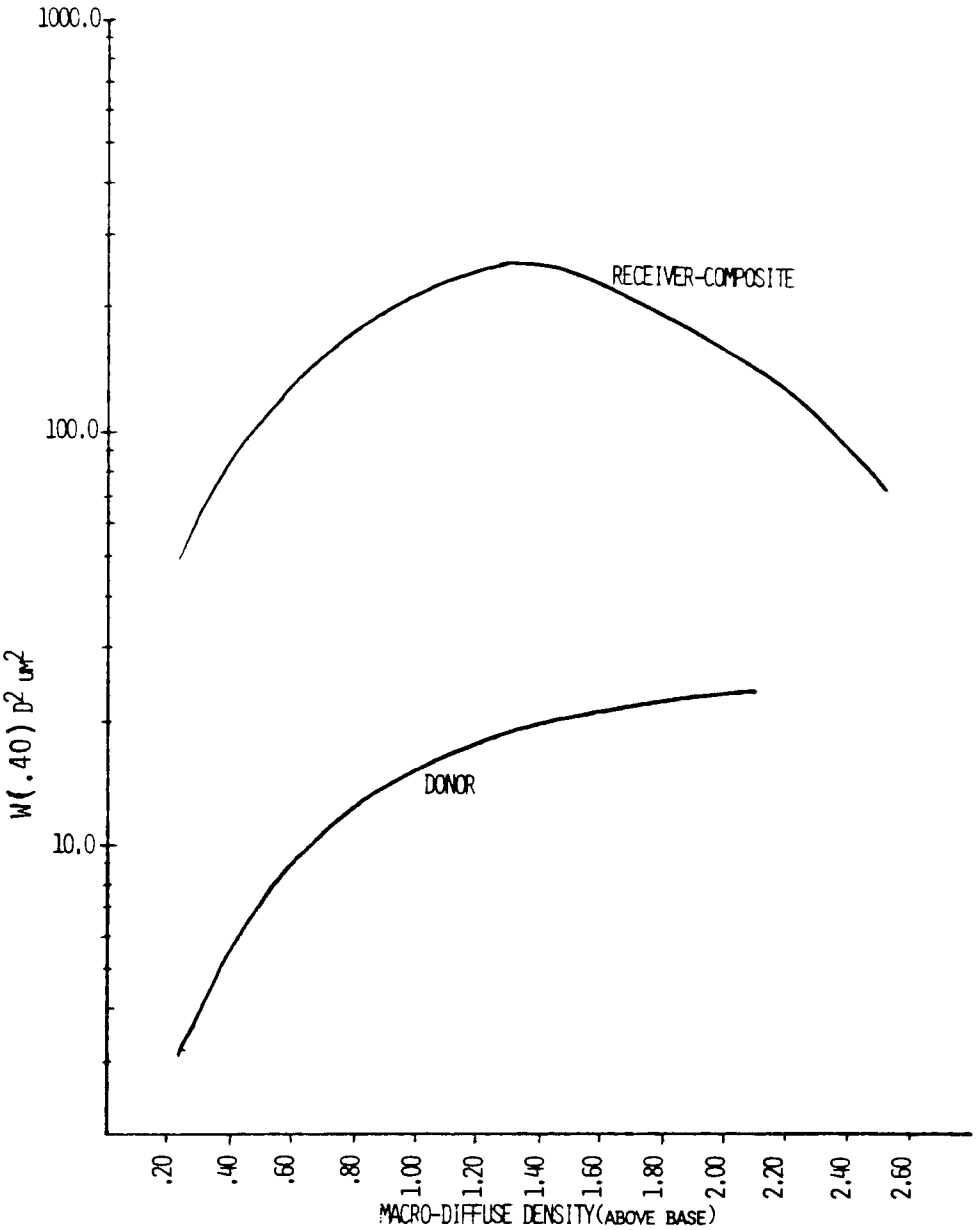

Figure 18 : Low frequency(.40 mm^{-1}) Wiener spectrum value for Donor and Receiver-Composite vs. Macro-diffuse density

asymptote at 25 D^2um^2. For the receiver-composite, the Wiener spectrum is characterized by a nearly symmetrical rise and fall about a density of 1.30. Based on new models of image structure[36], this falloff of the Wiener spectrum at higher densities is likely attributable to grain clumping.

Up to this point, we have analyzed the donor and receiver-composite Wiener spectra in and of themselves. If however, there is a greater interest in SNR gains from donor to receiver-composite a comparison of the spectra is in order. This comparison should indicate whether gains in signal power (gamma or MTF) are offset by equal or greater gains in the Wiener spectrum. This, of course, would suggest a net loss in SNR transferring from donor to receiver-composite and thus lower the DQE and NEQ in the receiver-composite.

The increase of the receiver-composite gamma might be chiefly responsible for such an effect. This is supported in both Rossman's model and classical noise transfer theory[50] which requires the Wiener spectrum of a printed density be proportional to the gamma squared of the printing process's characteristic curve. Therefore in attempting to predict whether the receiver-composite's Wiener spectrum might outweigh any signal increase, the square of the receiver-composite's gamma would be a useful predictor.Since it is presumed that the donor gamma at a given exposure leads to a receiver-composite gamma at the same exposure, it is only proper that comparisons of the Wiener spectrum be done on an equi-exposure basis. This being the case, one finds that the receiver-composite's maximum gamma of 6 (figure 5) would only account for a portion of the large measured increase in equi-exposure Wiener spectrum.

Interpreting this in terms of DQE and NEQ it is found that although a 36(i.e.,6^2) fold signal increase results in the numerator of equation 15, this is more than offset by the average 2 order of magnitude noise increase from donor to receiver-composite (figure 11). The fact that the Wiener spectrum does increase by greater than γ^2 of the receiver-composite may tell us that classical noise transfer

theory is not applicable to the autoradiographic process. This was alluded to earlier when it was pointed out that unlike typical two-stage expose-to-print processes, the silver in the first stage(donor) no longer acts to attentuate radiation but rather to create it. Herein may lie the reasoning to the large noise increases in the receiver-composite, and is certainly an area for further research in understanding noise transfer for the autoradiographic process.

From this information then, increases in DQE and NEQ for the receiver-composite step would not be anticipated. We find that this is indeed the case despite the folding in of MTF & exposure influences. A detailed discussion including the implications, interpretation, and significance of this follows.

4.4 DQE and NEQ

In the introduction, it was pointed at that three questions along with the hypothesis were to be answered and addressed. These questions were

1. Is the DQE_{max} or NEQ_{max} greater in the donor or receiver-composite?
2. How do the DQE and NEQ between donor and receiver-composite compare on an equi-exposure basis?
3. When treated as a two stage expose-to-print process, is the exposure at DQE_{max} in the donor step the same as that for NEQ_{max} in the receiver-composite step?

The reader is reminded to keep these questions in mind in this particular section since, all of them ultimately deal with DQE and NEQ. It is the author's intention to answer these questions in the forthcoming discussion.

For the receiver-composite, the $DQE_{max.}$ of .21 exhibited a substantial decrease from the donor's DQE_{max} of .30. Based on these

peak values then, one could conclude that when treated as seperate imaging systems, the receiver-composite offers no advantage over the donor in efficiently detecting incident quanta. Indeed, at their maximum DQE values, the receiver-composite was only 66% as efficient as the donor. A much greater decrease was evidenced with respect to the NEQ values. The difference in the maximum NEQ of nearly 350, % clearly indicates the superiority of the donor in a SNR sense. The answer to the first of the above questions then is, the donor exhibits greater maximum DQE and NEQ than the receiver-composite.

The overall lower DQEs and NEQs exhibited by the receiver-composite were no doubt due to the greatly boosted Wiener spectrum values in the intensification step . From this, it would appear that, the worse fear concerning the intensification step's enhanced gamma increasing not only the signal but also the noise was realized. That is, along with signal amplification came disproportionate noise amplification. This was especially evident for the NEQ parameter since the increased speed of the receiver-composite did not figure in its calculation. This additional speed contribution of the receiver-composite did help to bring the $DQE_{max.}$ for this step to within a reasonable limit of that of the donor, and is encouraging when one analyzes the donor and receiver-composite on an equi-exposure basis.

Recall that the appropriate analysis for certain cases may not be one of comparing maximum DQE and NEQ as much as comparing these parameters for a given exposure. In this way a normalizing of the quanta noise is achieved and comparisons can be commensurate over all exposures. The extent and nature of the DQE and NEQ transfer should likewise be realized from this. These comparisons are illustrated in figure 19. Here the ratio of receiver-composite:donor DQE levels are plotted against log exposure. Should this ratio exceed unity(1) for any given exposure, the intensification process would be worthwhile to exploit at these exposures. Though it is plain to see from figure 18 that this is not the case, the fact that a ratio of unity was closely approached at an exposure of $10^{6.75}$ photons/cm^2does offer promise.

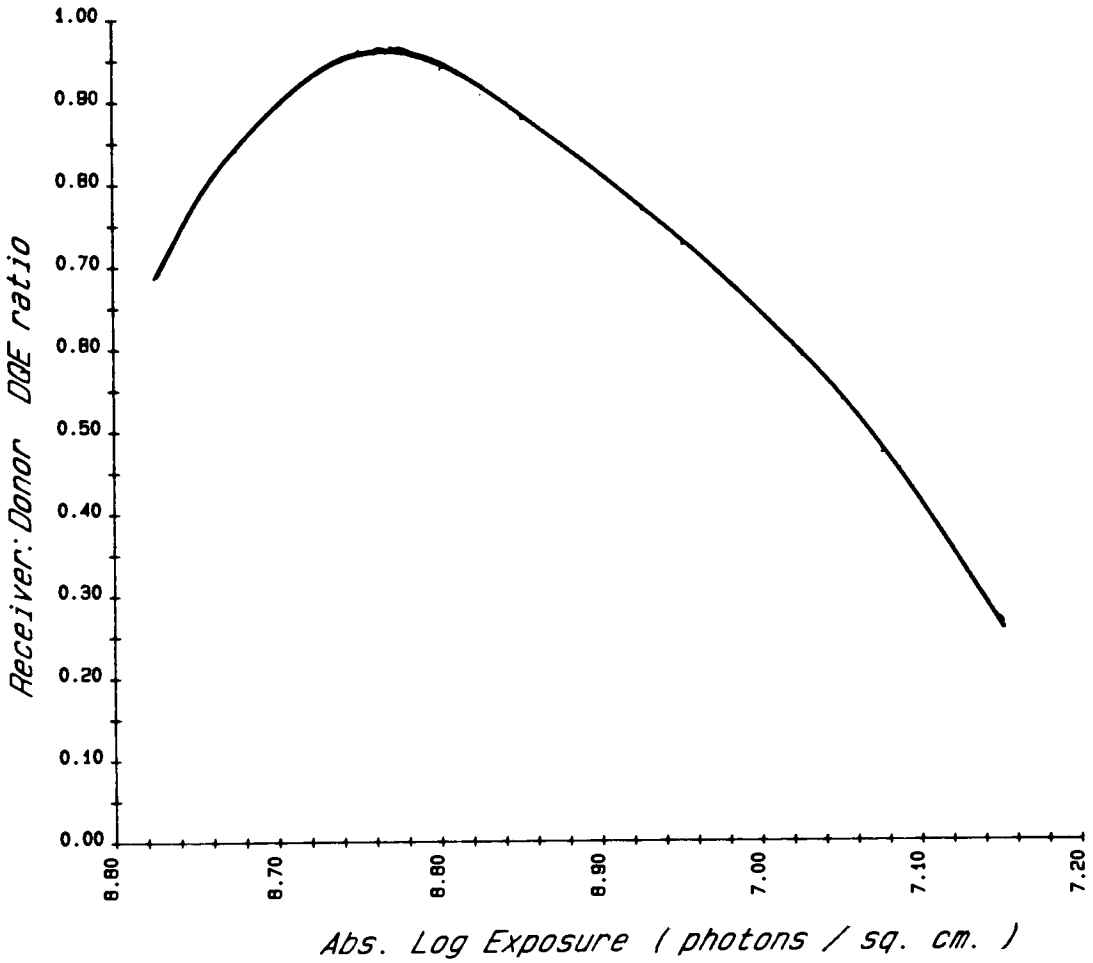

Figure 19 : Ratio of Receiver-Composite:Donor
DQE (& NEQ) ratio vs. log exposure

With further research it should not be difficult to find a different material or processing that would reduce the effect of the Wiener spectrum, while keeping other parameters constant & in turn increase the receiver-composite's DQE. In so doing, the receiver-composite:donor DQE ratio is likely to exceed unity and thus present an opportunity for more efficient quanta detection over that of the donor. Whatever the scheme, it is not difficult to see that a minimal increase of the receiver-composite DQE would accomplish this. As a matter of fact, the same holds for the NEQ of the process also. The reasons why follow.

While NEQ comparisons are typically done on an equi-density basis[51], this form of evaluation makes an implicit assumption that one is interested in, for example, the receiver-composite as a detecting entity by itself. That is, as opposed to an enhancer of an existing process. One would change exposure in the print step to suit some output dynamic range in the former, whereas this is not true for the process at hand. In the context for which visual detection increases were noted by previous workers, the latter is more accurate. With this as a basis, we can answer the second of our questions on both equi-exposure DQE & NEQ through figure 19 alone. The fact that DQE is no more than an exposure normalized NEQ allows us to do this. Therefore, from a SNR viewpoint it appears that the receiver-composite offers no advantage over the donor.

How then can we reconcile the unanimous reports[9-12] of increases in visual detection in the receiver-composite when in fact the NEQ do not reflect these increases? Certainly one way to coordinate the two is to recognize that figure 19 gives no information below an exposure for which the donor's gamma is effectively zero. Since the donor's gamma is zero(see figure 5) then by definition (equation 15) the NEQ & in turn the SNR of the donor for exposures less than this are also zero. This is not the case for the receiver-composite at these same exposure levels, however. One can see from figure 5 that the receiver-composite's gamma remains essentially non-zero for at least one full stop more than for the donor. This is

the key in recognizing that in this exposure region ,the receiver-composite will necessarily have a higher SNR than the donor and in turn, contribute toward increased signal detection. Unfortunetely, in this experiment, sufficient data for confident characterization of the NEQ in this exposure region was not collected and is indeed a shortcoming of this work. Consequently, making any decision concerning the original hypothesis about the NEQ & DQE in this exposure region would not be wise and is best left for verification by future workers.

The above rationale,though certainly plausible, would seem to account for only a fraction of the reported increases in radiographic interpretability; especially when one considers that historically only a small portion of the signal occurs over the area of the characteristic curve just cited. Something more fundamental must be happening. In this author's estimation, & apparently others[48] this "something" is the human visual process.

Unlike unintelligent, memoryless detectors, the human visual process bases its detection & decision making on a complex psychology of pattern recognition tasks. This is the perceptual process of the eye & brain. As pointed out by Goodenough[48], the radiological process can be thought of as a series of five operations. In order, they are exposing, recording, display, detection, & recognition. This paper has quantified the first three & perhaps a portion of the fourth. With an entire host of parameters ranging from the number of signals detected to observer a priori knowledge to consider, it should not be difficult then to understand the mismatch between this studies results & increased visual detection by experienced observers. This is supported by Goodenough in his study of image quality on medical diagnostic decision making. In this he concludes:

> "...there are many unknown factors involved in the pattern recognition step of diagnosis that tend to obviate a general predictive equation of diagnostic accuracy from known physical parameters."

It is speculated that somehow, someway, the human visual process is able to selectively mask the noise from the signal and, in so doing, see "through" the increased noise of the receiver-composite without suppressing the signal. Another thought is that, quite simply, the intensification process increases the SNR for the receiver-composite above a certain visual threshold which did not exist in the donor, namely in the toe of the donor' characteristic curve. This reasoning reflects the insufficient data collection cited previously. Finally, there is even evidence[48] to suggest that some traits which contributed to low NEQ, namely high granularity due to high gamma, may have actually increased human detection performance.

None of the above should be taken as a denunciation of SNR as a detection criteria however. It is simply that SNR does not tell the entire story, especially in cases involving the human visual process. Furthermore, it does not imply that the results of this study cannot be used to optimize what is still the common denominator of all detection criteria, that of SNR. Some ways of doing this are outlined in the following applications section.

4.5 Applications of DQE and NEQ

In the previous section, two of the three questions originally asked in the Introduction were answered. The first two were concerned with comparisons between donor and receiver-composite for 1) maximum DQE and NEQ, and 2) equi-exposure DQE and NEQ. The third question on the optimal "handshake" between donor and receiver-composite was left begging however. This was done because it was more appropriately answered in this section.

Recall that the foundation for the third question lies in SNR optimization considerations for two-stage expose-to-print processes. Rather than treating the donor and receiver-composite as seperable imaging systems, the question becomes, "Is there some way that their interaction can be optimized when considered as a two-stage printing process?". For example, where exposure criteria is critical

(in the recording stage or donor) one would want to base exposure on maximum DQE. On the other hand, if there was no limit to the amount of available energy (the printing stage or receiver-composite) the exposure should be based on maximum NEQ. Therefore, in extending this logic to the autoradiographic process, one would want the exposure at maximum DQE of the donor to coincide with the exposure for maximum NEQ in the receiver-composite. In this way the maximum output of the receiver-composite is statistically matched to the most efficient output of the donor.

By turning to figure 20, we find that the statistical match between donor and receiver-composite is not optimum. The peak DQE of the donor is approximately 1 stop removed from the peak NEQ of the receiver-composite. If however, one was asked to make a best choice for the optimum "handshake" exposure, an exposure of $10^{7.12}$ photons/cm^2 would appear a reasonable compromise since the values for donor DQE and receiver-composite NEQ are both within 90% of their maximum at this exposure.

A parallel scheme to the above that has also been suggested[52] is the composition of several images exposed at DQE_{max} to give a SNR greater than a single image exposed at NEQ_{max}. While this composite of images could be achieved a number of ways[52], the most obvious, but also cumbersome, method would be to physically register the "n" images together. This is, in fact, exactly what occurs in motion picture viewing and is the reason why the image quality appears much better for the "moving" image than it does for a single frame. The basis for this lies in equation 19 which relates the composite SNR of "n" registered images in terms of the NEQ at the exposure for which DQE is a maximum. It is

$$SNR_{(comp)} = (n \cdot NEQ(@ DQE_{max}))^{.5} \qquad (19)$$

The derivation for equation 19 is given in Appendix B. The integer value of "n" for a given application is chosen so that "n" times the exposure at DQE_{max} will be no greater than the exposure at NEQ_{max}. An

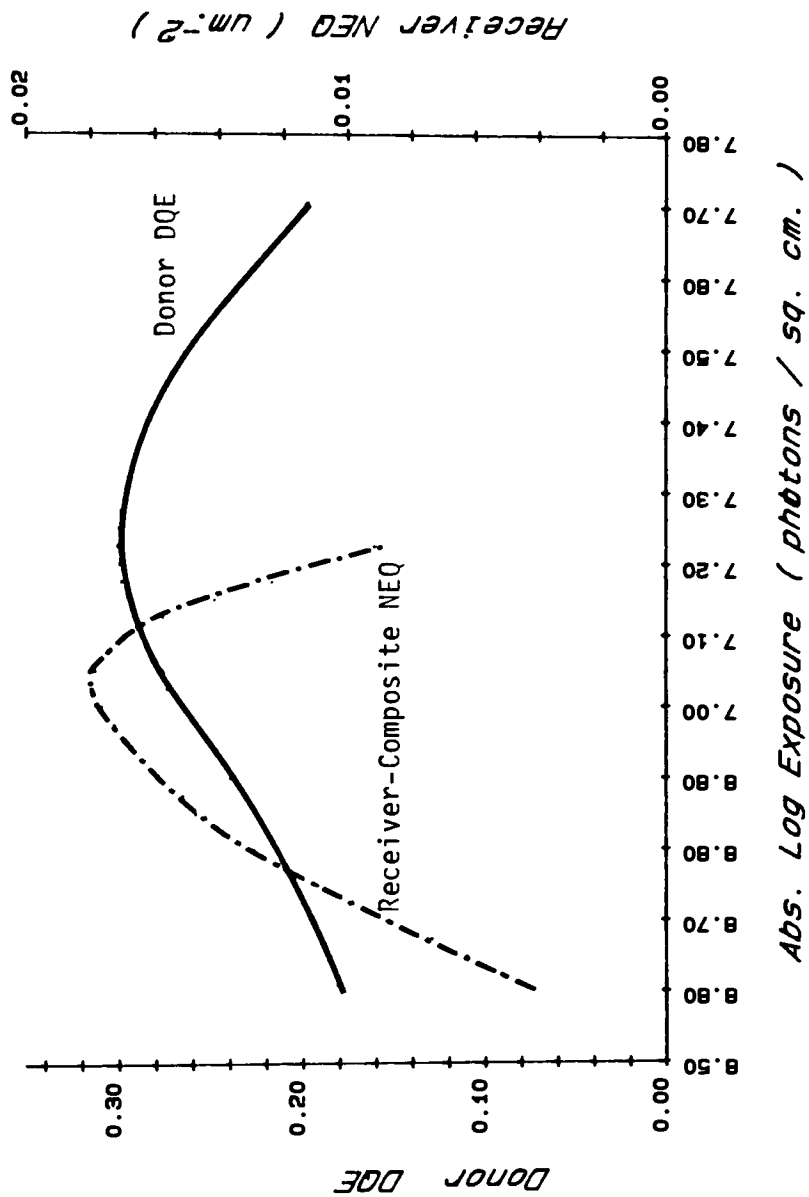

Figure 20: Comparison of Donor DQE(solid) with Receiver-Composite NEQ(dash) for two-stage printing evaluation

analogy for this is, for a given amount of energy can the job be done better through many small hits of the hammer, or with one big hit. In other words, can better SNR be achieved with many lesser exposures or one single one. To answer this question, an example is in order.

Take for instance the donor. In this case "n" turns out to be

$$n = \frac{\text{Exposure @ } NEQ_{max}}{\text{Exposure @ } DQE_{max}} = 10^{(7.55-7.26)} = 2.$$

In order to determine the percent gain in SNR for the composite image, one simply normalizes by the bellwether of SNR, or NEQ_{max}. Therefore, by normalizing equation 19 one obtains

$$SNR_{gain} = \left[\frac{(n \cdot NEQ(\ @\ DQE_{max}))}{NEQ_{max}}\right]^{.5} \qquad (20)$$

Substituting the appropriate donor values into equation 20 then

$$SNR_{gain} = \left[\frac{2 \cdot (.05)}{.081}\right]^{.5} = 1.11$$

In other words, by using a 2 image composite, each image exposed at DQE_{max}, an 11% gain in SNR is achieved as for the same exposure as NEQ_{max}.

Translating equation 20 for the autoradiographic process at hand, the maximum SNR gain can be written as

$$SNR_{gain} = \left[\frac{(2 \cdot n \cdot (NEQ(\ @\ Rec.Com.DQE_{max})_{Rec.Com.})}{(NEQ_{max})_{Donor}}\right]^{.5} \qquad (21)$$

The doubling(2) of the numerator value in equation 21 is due to the fact that because the donor is a double sided emulsion, in actuality two receiver-composites can be had for the price of one donor exposure. Substituting the appropriate values into equation 21, one obtains for n

$$n = 10^{7.55 - 6.88} = 5.62 \rightarrow 5$$

and for SNR_{gain}

$$SNR_{gain} = \left[\frac{2 \cdot 5 \cdot (.013)}{.08}\right]^{.5} = 1.27$$

Therefore by using two receiver film sheets for each of five seperate and lesser exposures at DQE_{max} of the receiver-composite, a 27% increase in SNR is achieved over the NEQ_{max} of the donor.

To be sure, the method of actually registering images as suggested here is probably cumbersome and unfeasible in most working environments. However, the intention here is not so much of a practical nature as much as demonstrating that when working at the limits of detection the type principles advocated here are certainly plausible. It is up to the user to translate these principles into practice for the particular needs at hand.

5. CONCLUSIONS

This research effort has been concerned with the measurement and evaluation of a thiourea S-35 nuclide autoradiographic image enhancement process; especially as it applies to medical diagnostic imagery. Specific attention was paid to that enhancement scheme incorporating a subproportional potassium ferricyanide bleach in the activating solution. This was chosen largely due to the encouraging quantitative and qualitative results with this process by previous workers[9-12].A block diagram of the autoradiographic process studied here is given in figure 22.

One of the important items to come out of this past work was unanimous reports of increased visual detection in the receiver-composite generated images when compared to those of the donor. By quantifying the signal-to-noise ratio (SNR) properties of this autoradiographic process, and comparing their values at the donor and receiver-composite stages, it was hoped that this reasearch could lend some insight into the reasons for the reported visual detection increases. The SNR metrics chosen for this quantification were Detective Quantum Efficiency(DQE) and Noise Equivalent Quanta(NEQ). It was shown how DQE is important for most efficiently detecting quanta, while NEQ is important for detecting a signal with maximum likelihood.

For this work DQE and NEQ were defined as a function of both exposure(q), and rotationally symmetric spatial frequency(w) as:

$$DQE(q,w) = \frac{(\log_{10}e)^2(\gamma(q))^2(MTF(w))^2}{q \cdot W(q,w)}$$

and

$$NEQ(q,w) = DQE(q,w) \cdot q$$

where γ = Differential gamma of the characteristic curve
MTF = Modulation transfer function
W = Wiener spectrum

Quantifying $\gamma(q)$ and q was done through the donor and receiver-composite characteristic curves illustrated in figure 23. From these curves it was shown that, in addition to an approximate 2 stop speed increase, the receiver-composite also exhibited a greater maximum gamma than that of the donor(5.8 vs. 4.2). Because of the receiver-composite's lower D_{max} however, the input exposure latitude for it was limited to about half that of the donor.

In quantifying the MTFs, it was shown that the donor's equivalent bandwidth[40] was 50.% greater than for the receiver-composite. A comparison of these MTFs can be found in figure 24. It was also shown that,in analogy, the changes in MTF in going from the donor to receiver-composite are akin to going from a "medium" to a "fast" radiographic screen/film system. The graphs supporting this are given in figure 25.

In measuring the final contributing parameter, Wiener spectrum, it was found that while both donor and receiver-composite Wiener spectra followed the general shape of Rossman's model, neither of the spectra felloff with MTF^2, as predicted. This indicated sources of noise that were not influenced by the MTF of the processes. It was also shown that for equal densities less than 1.2, the low frequency(i.e.,.40 mm^{-1}) Wiener spectra values were generally an order of magnitude higher in the receiver-composite than in the donor. Figure 26 shows this, along with illustrating that for equal exposures, these same receiver-composite Wiener spectrum values were two orders of magnitude greater than for the donor.

Finally, by mathematically joining the above metrics according to the DQE and NEQ equations, it was shown that the donor $DQE_{max.}$ of .30 exceeded that of the receiver-composite by 50.%. Similarly, the donor $NEQ_{max.}$ of .08 um^{-2} exceeded that of the receiver-composite by 350.%. These results are illustrated in figures 27 and 28. It was further shown that the donor DQE and NEQ continued to exceed that of the receiver-composite even on an equi-exposure basis. It was felt that the reason for this was primarilly due to the largely increased Wiener spectrum values of the receiver-composite

step. From a qualitative viewpoint, it was speculated that the mismatch between lower receiver-composite NEQ and reported visual detection increases was due to contributions of the human visual process that are not strictly predicated on SNR analyses. Quantitatively, it was pointed out that the mismatch may also be due to insufficient data collection over the exposure sample space.

In looking to the future, verification of the results just presented is strongly urged. In so doing however, particular attention should be paid to both an adequate exposure sample space, and error budgets on the individual components leading to the DQE and NEQ metrics. There are, no doubt, many operator error influences confounded in these results that cannot be strictly accounted for. Perhaps in reading this text, future workers may benefit by avoiding any pitfalls they deem present in the experimental methods. It is also suggested that a specific experimental effort be directed towards a study of the noise transfer between donor and receiver-composite. This effort should certainly help in gaining an understanding of the alarming Wiener spectrum increases noted in the receiver-composite as well as acting as a springboard for future studies.

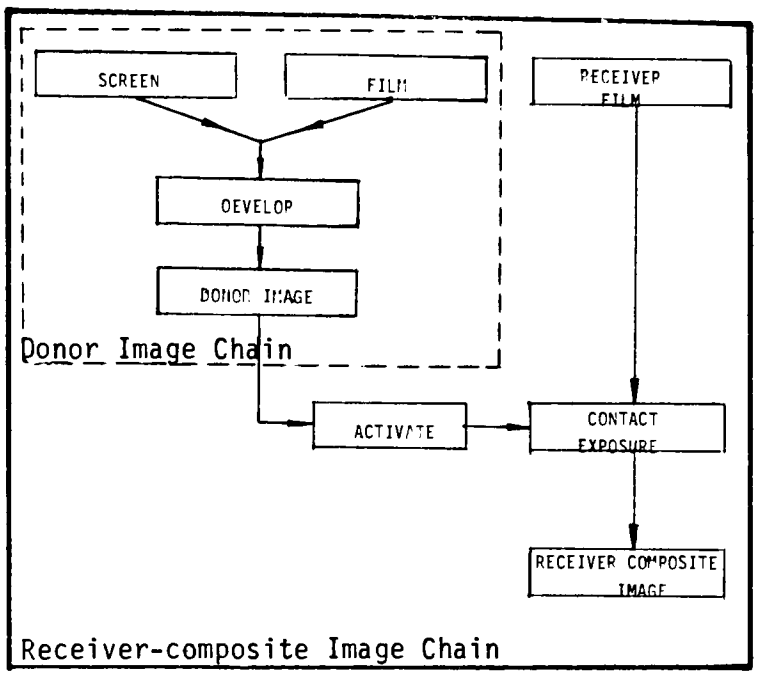

Figure 21: Block Diagram defining Donor (dash) and Receiver-Composite (bold solid) stages.

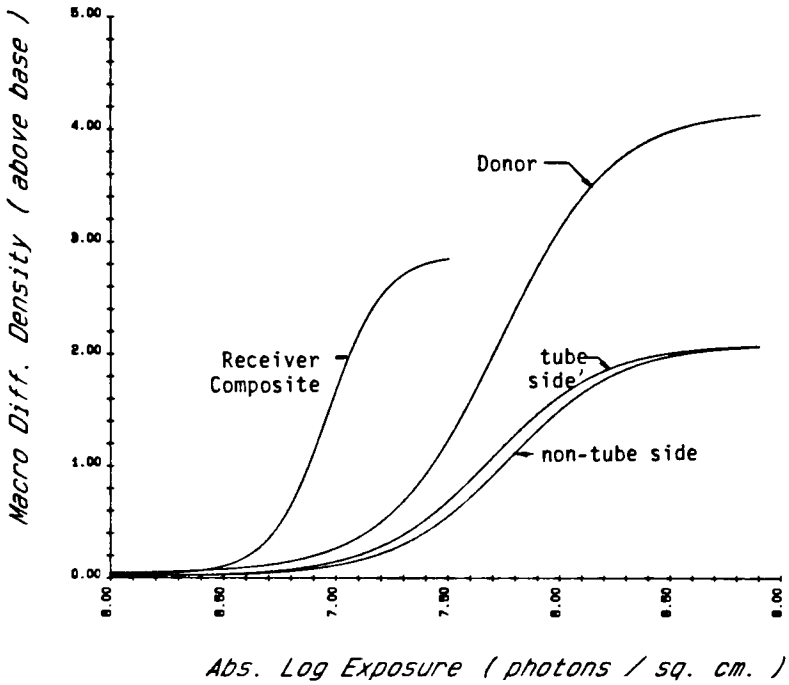

Figure 22: Characteristic Curves for different stages of the Auto-radiographic system tested

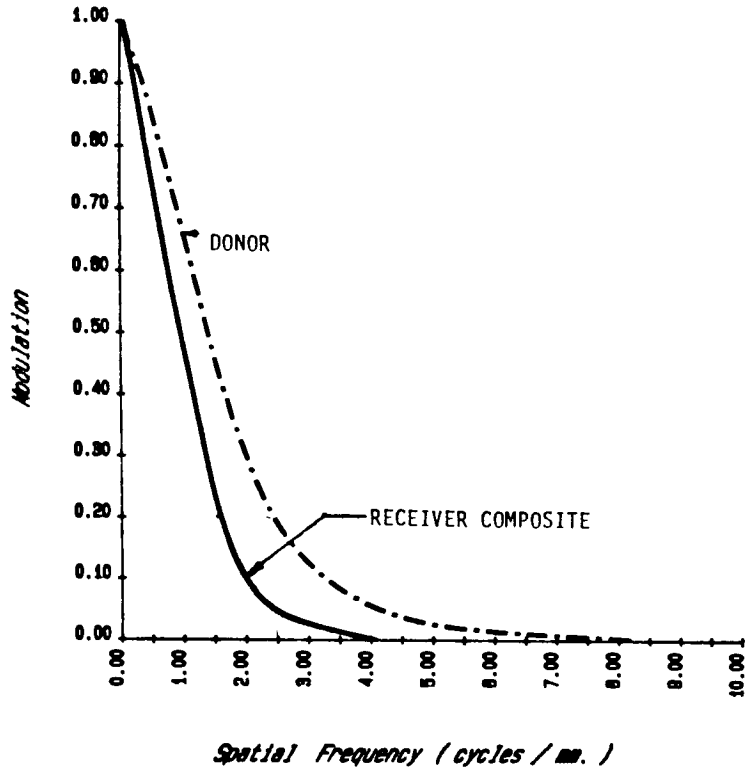

Figure 23: Modulation Transfer Functions for Donor (dash) and Receiver Composite (solid) stages.

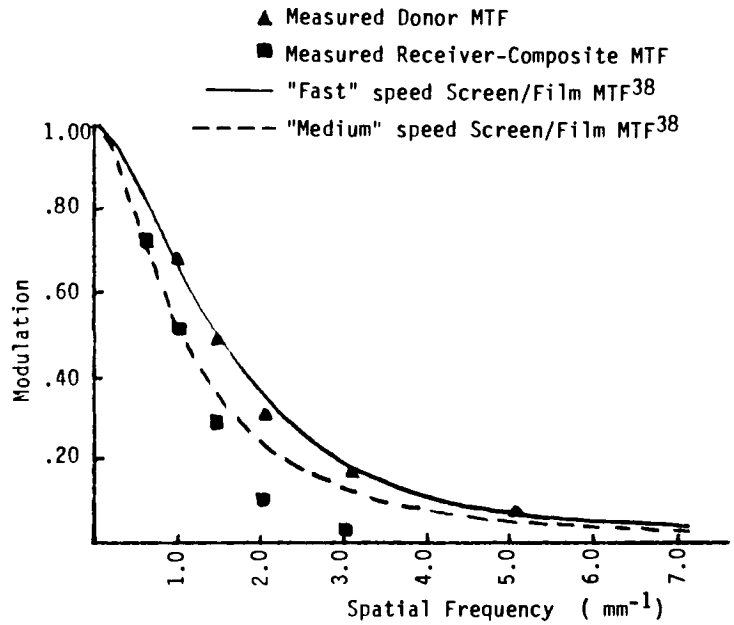

Figure 24: Comparison of Donor and Receiver-Composite MTFs with typical fast and medium speed screen/film systems.

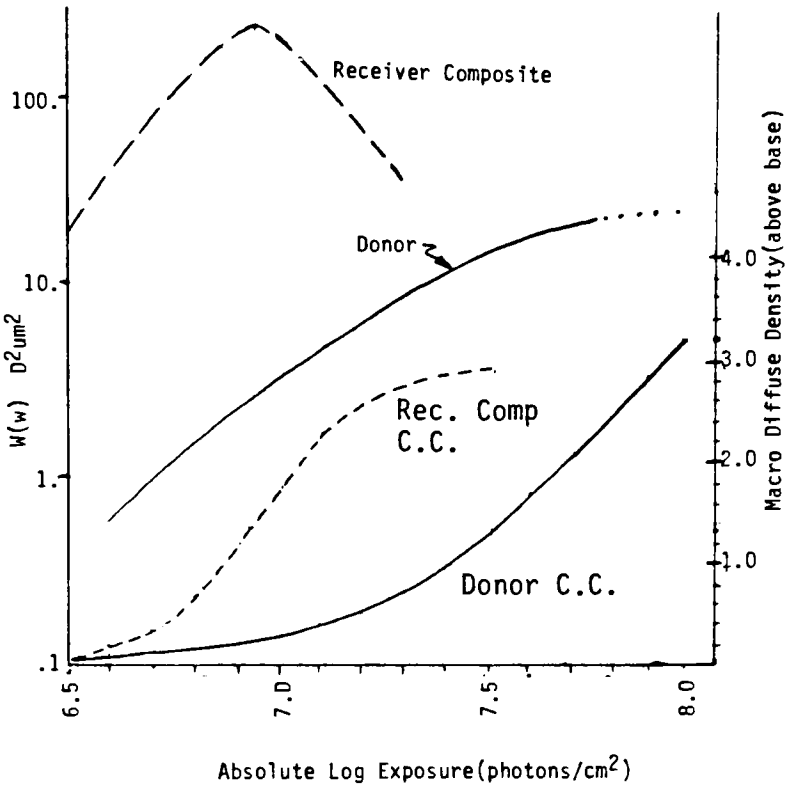

Figure 25: W(.4) for Donor (solid) and Receiver Composite (dash) compared to respective characteristic curves. Noise power on left ordinate & Density on right ordinate.

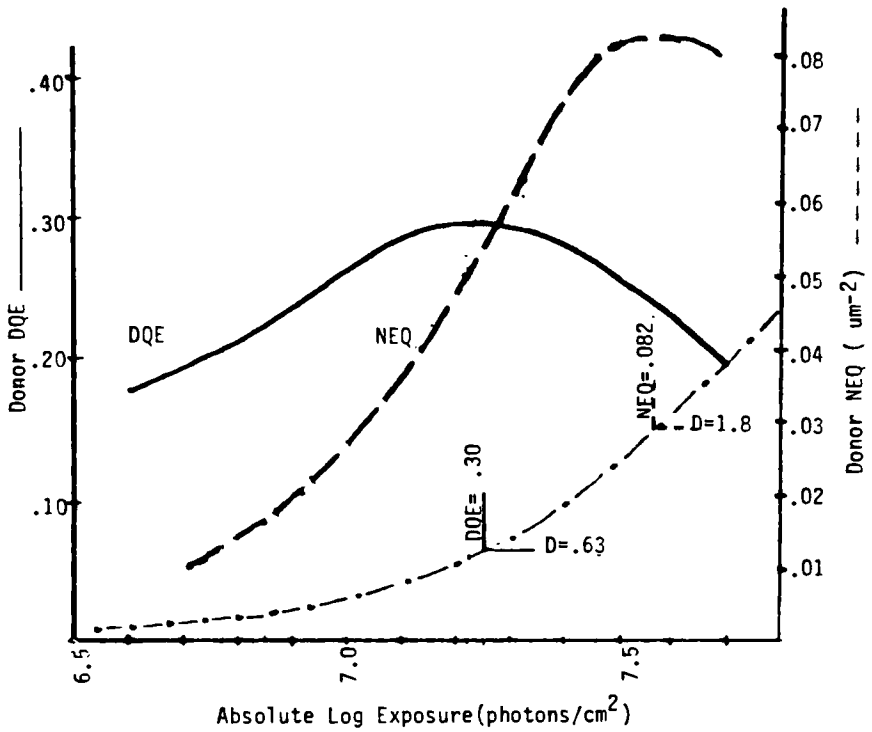

Figure 26: Donor DQE (solid) and NEQ (single dash) curves @ .40 mm^{-1}. Relative Density characteristic curve for comparison.

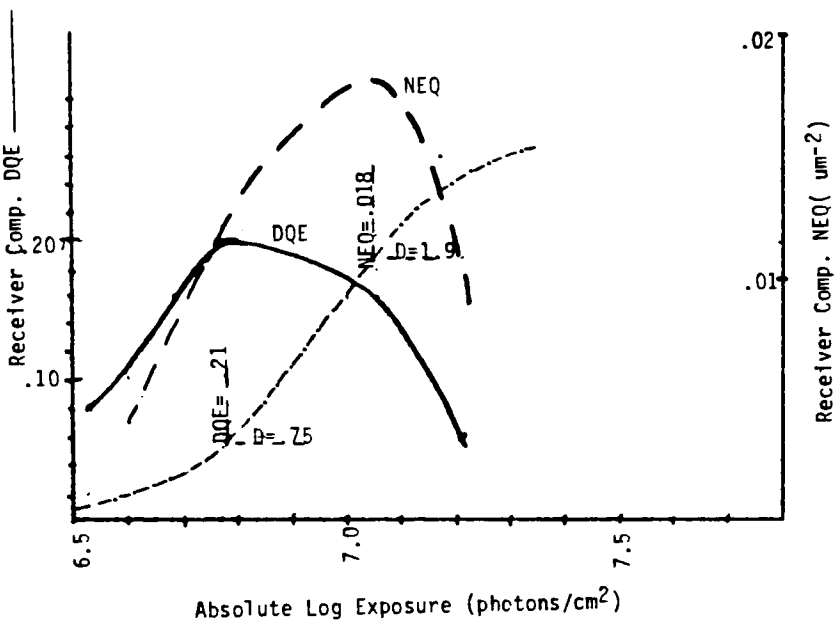

Figure 27: Receiver Composite DQE (solid) & NEQ (single dash) curves @ .40 mm^{-1}. Relative Density characteristic curve for comparison.

6. REFERENCES

1. Anonymous,Stein Der Weisen,35,340(1906).
2. H.E.Wheeler,N.L.Wheeler,and C.W.Durieux,U.S.Patent #2,780,732(1957).
3. M.Thackray,et.al.,Int.J.Appl.Radiat.Isotopes,23,79(1972).
4. E.Ostroff,J.Photoscience,13,213(1965).
5. M.Thackray,Austr.Atomic Ener.Comm.,#AAEC/E317(1974).
6. a)B.Askins,Science,199,684,(197B).b)B.Askins,U.S.Patent #4,101,780(1978).
7. R.Pettijohn,and C.Leung,SRI International,Proj.#PYU8468(1980).
8. T.H.James,and W.Vanselow,J.Phys.Chem.,57,725(1953).
9. D.Dempster,Master Thesis,R.I.T.,SPAS(1978).
10. D.Vachon,Master Thesis,R.I.T.,SPAS(1979).
11. L.Wheaton,R.I.T.,personal communications(1980).
12. L.Wheaton,Master Thesis,R.I.T.,SPAS(1980).
13. A.Rose,J.Soc.Mot.Picture.Eng.,47,273(1946).
14. R.C.Jones,J.Opt.Soc.Amer.,39,327(1949).
15. P.B.Fellgett,J.Opt.Soc.Amer.,39,970,(1949).
16. a)R.Shaw,J.Phot.Sci.,15,78(1967).b)R.Shaw,J.Phot.Sci.,16,170, (1968).
17. H.J.Zweig,Phot.Sci.& Eng.,8,305(1964).
18. G.R.Bird,et.al.,Appl.Opt.,8,2389(1969).
19. J.C.Marchant,J.Opt.Soc.Amer.,54,798(1964).
20. J.C.Dainty,and R.Shaw,Image Science,Academic Press,28(1974).
21. Reference 20,page 156.
22. Reference 20,page 312.
23. R.Shaw,J.Phot.Sci.,17,155(1969).
24. W.A.Baum,Astron.Tech.,Univ.Chicago.Press,213(1962).
25. A.Guttman,Phot.Sci.& Eng.,12,146(1968).
26. R.L.Porteous,and R.Shaw,Royal Astron.Soc.Conf.on Astron.Opt. (1967).

27. H.E.Johns,and J.R.Cunningham,The Physics of Radiology,Charles C. Thomas,735(1977).
28. R.E.Swing,Opt.Eng.,15,559(1976).
29. R.L.Lamberts,J.Opt.Soc.Amer.,51,982(1961).
30. R.Porth,Master Thesis,R.I.T.,SPAS(1984).
31. G.Sanderson,and H.Cleare,Phot.Sci.& Eng.,18,251(1974).
32. P.Burns,and B.Levine,Xerox Internal Report #X2013529(1981).
33. Reference 20,page 276.
34. E.Trabka,J.Opt.Soc.Amer.,59,662(1964).
35. K.Rossman,Amer.J.Roent.,90,863(1963).
36. C.Dainty,Univ.Roch.,personal communications(1982).
37. D.Plewes,Univ.Roch.,personal communications(1981).
38. K.Doi,U.S.Dept.of H.H.S.,Publ.#FDA 82-8187(1982).
39. K.Taylor,et.al.,S.P.I.E. Conf.on Appl.of Opt.Inst.in Medicine VII,173,307(1979).
40. R.Bracewell,The Fourier Transform & Its Applications, McGraw-Hill,151(1978).
41. K.Rossman,J.Opt.Soc.Amer.,52,774(1962).
42. E.W.Selwyn,Photogr.J.,75,571(1935).
43. R.Wagner,and E.Muntz,S.P.I.E.Conf.on Appl.of Opt.Inst.in Medicine VII,173,122(1979).
44. R.Wagner,Phot.Sci.& Eng.,21,252(1977).
45. P.Bevington,Data Reduction and Error Analysis for the Physical Sciences,McGraw-Hill,64(1969).
46. W.Moore,Kodak Res.Lab.,personal communication(1984).
47. R.Shaw,Phot.Sci.& Eng.,17,495(1973).
48. D.Goodenough,Phot.Sci.& Eng.,21,262(1977).
49. R.Halmshaw,J.Phot.Sci.,19,167(1971).
50. Reference 20,page 307.
51. Reference 20,page 162.
52. R.Shaw,J.Phot.Sci.,20,175(1972).
53. W.Smith,Modern Optical Engineering,McGraw-Hill,290(1966).
54. J.Jakubowski,Xerox Corp.,personal communication(1980).

7. APPENDICES

7.1 APPENDIX A

EQUIPMENT, PROCESSING, &
MEASUREMENT PARAMETERS

LIST OF MAJOR EQUIPMENT

- Special Bracke-Seib X-Ray Machine 70 KVP, 105 Volt Primary, Kodak Research Laboratories.
- Kodak XG Radiographic Film
- Kodak NMC Nuclear Medicine Film
- Kodak X-omatic Regular Screens #688250K (front); #699251K (back)
- Macbeth TD-504 Densitometer
- Kodak RP-X-OMAT Film Processor
- Kiethley Model 35020 dosimeter,Model 96020A ion chamber
- Zeiss SMPØ5 microdensitometer
- Inverse Square Exposure Bench,Kodak Research Laboratories

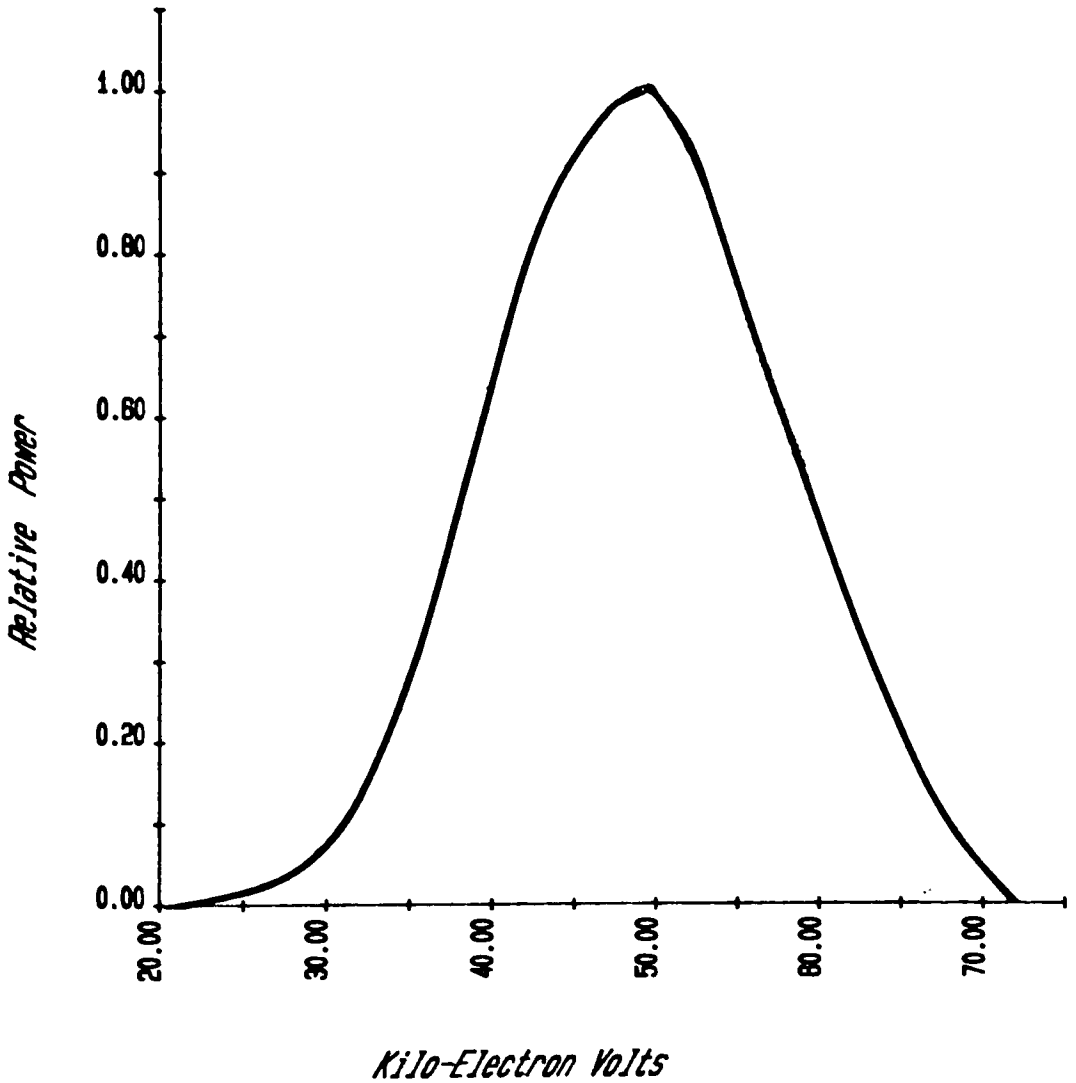

Figure A1: Spectral Power Distribution for nominal 70Kvp X-Ray source with .5 mm copper & 1 mm Aluminum

ACTIVATING SOLUTION PROCESSING

Solution A

25 ml of .4% NaOH Solution

Equivalent of .5 m Ci of S-35

10 ml of .15% S-32 thiourea

Solution B

150 ml of .625% Potassium Ferricyanide solution

Immediately before processing mix equal portions of solutions A & B, and adjust temperature to 70°F and pH to 12.5.

1) Agitate donor strips in A/B mixture for 30 minutes
2) Wash strips for 1 minute
3) Dry strips
4) Contact donor tube side to NMC film emulsion for 1.5 hrs
5) Process NMC film in X-OMAT Processor

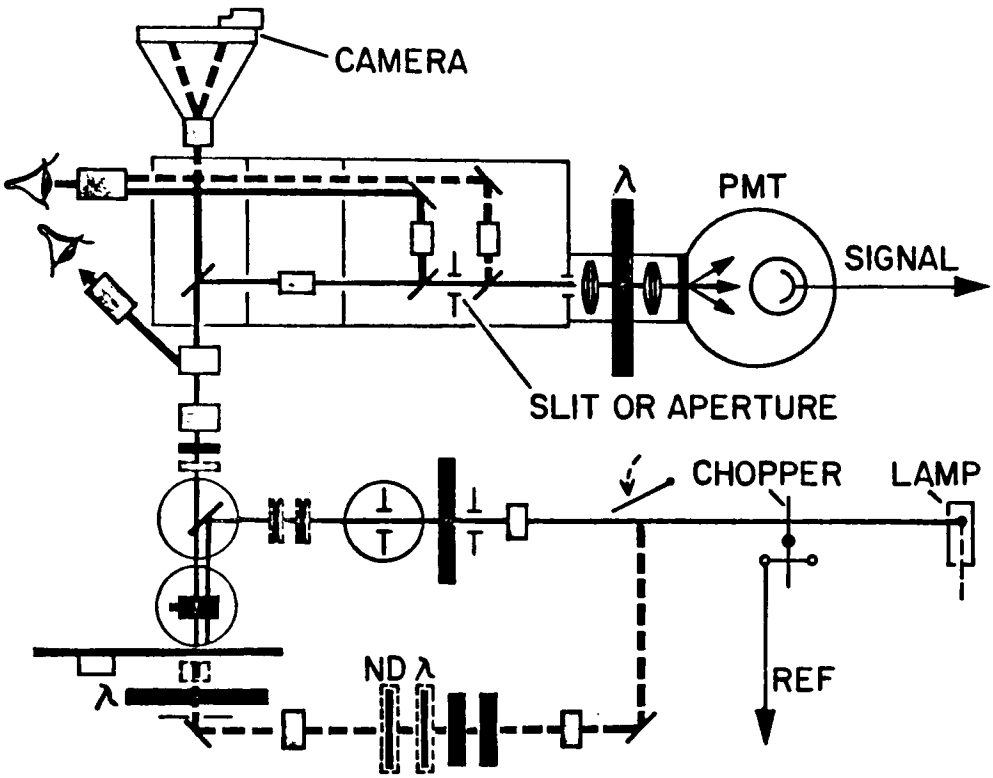

Figure A2: Schematic Diagram of Zeiss SMPØ5 microdensitometer used for densitometer measurements for experiment.[54]

COMMON CONDITIONS FOR MICRODENSITOMETRY

- .08 N.A. efflux objective
- .60 N.A. influx objective
- 14X influx magnification
- $n_o = 40mm^{-1}$
- assumed diffraction limited optics
- effective scanning slit dimensions
  25um x 700um
- sampling interval = 12.5um
- image scan, overfill mode
- 3X overillumination of scanning slit in width (25um) dimension
- 3 reads per sample

7.2 APPENDIX B

CALCULATIONS & CURVE FITS

EXAMPLE CALCULATION FOR PHOTON FLUENCE CALCULATION FROM ROENTGENS.[27]

From reference 27 we have

$$\#\ \frac{\text{photons}}{\text{cm}^2 \cdot \text{roentgen}} = \left[\frac{86.94}{\mu} \cdot \frac{1}{1.59 \cdot 10^{-9}} \cdot \frac{1}{\#\text{Kev}}\right]$$

where μ = Mass attenuation coefficient of air

$\#$ Kev = Number of Kev associated with the spectral source

Since u is a function of Kev and likewise, the weighting of Kev is dependent on the spectral energy distribution of the source, a summation over the broadband source must be done. This source distribution is given in Appendix A. Therefore the working equation to arrive at the LHS of the above equation becomes

$$\sum_{i=20}^{72\ \text{Kev}} \Phi(i) \left[\frac{86.94}{u(i)} \cdot \frac{1}{1.59 \cdot 10^{-9}} \cdot \frac{1}{i}\right]$$

where $\Phi(i)$ = Relative power associated with the i^{th} Kev

$u(i)$ = Mass attenuation coefficient at the i^{th} Kev

i = Kev

The result of this summation was then multiplied by the calibrated measure of 1.204 milliroentgens to arrive at a photon fluence of $10^{7.49}$ photons/cm^2 at a density of 1.2 above base for the donor.

CALCULATIONS FOR MICRODENSITOMETER DEPTH-OF-FOCUS, LINEARITY, AND EFFECTIVE INCOHERENCE CONDITIONS

DEPTH-OF-FOCUS

From Smith[51] the depth-of-focus, Δ, for diffraction limited systems is

$$\Delta = \pm \frac{\lambda}{2\,N\,(N.A.)^2} = \frac{\lambda}{N\,(N.A.)^2}$$

for λ = 550 nm
N = 1.5 (emulsion index of refraction)
Δ = 230 um total for donor film

The required numerical aperture would have to be $\leqslant$ .040. This low a numerical aperture being unavailable the single emulsion depth was only considered. It was only 40 μm deep. Therefore, a relaxation of the numerical aperture to $\leqslant$ .096 was calculated. An available .08 N.A. efflux objective was used. This being the lowest numerical aperture objective available, an over fill mode was predicated.

LINEARITY

Using Swing's[28] nomenclature,

Maximum frequency of interest = n_o = 40. mm^{-1}
Cutoff frequency of efflux optics = σ_o = 290. mm^{-1}

The linearity conditions are

$$\epsilon \geqslant 1 + \frac{n_o}{\sigma_o} = 1.14$$

where $$\epsilon = \frac{N.A._{influx}}{N.A._{efflux}}$$

Therefore using $N.A._{influx}$ = .60

$$\epsilon = \frac{.6}{.08} = 7.5 > 1.14$$

Therefore the linearity requirements were satisfied.

EFFECTIVE INCOHERENCE

Effective scanning slit width calculation

In order to prefilter for 40. mm^{-1} with a rectangular slit, a

$$\frac{mm}{40.} = .025 = 25 \text{ micrometer slit width was used}$$

Effective Incoherence

$$p > 4 + Q(n_o + \sigma_o)$$

where $p = \dfrac{\text{width of microdensitometer source slit}}{\text{coherence interval of source}}$

For this experiment

$$p = \frac{1050 \text{ um}}{25 \text{ um}} = 42.$$

and $$42 > 4 + Q(.330)$$

Solving for Q

$$Q < 115.15 \text{ micrometers}$$

where Q = reduced image of the source aperture on the sample
Therefore the influx magnification, M_{influx} must satisfy

$$M_{influx} = \frac{\text{width of microdensitometer source slit}}{Q}$$

or

$$M_{influx} > \frac{1050 \text{ micrometers}}{115.15 \text{ micrometers}} = 9.12$$

Since

$$14 > 9.12$$

the effective incoherence conditions were then met with the .60 N.A. influx objective using an auxiliary ocular to give the total 14x magnification.

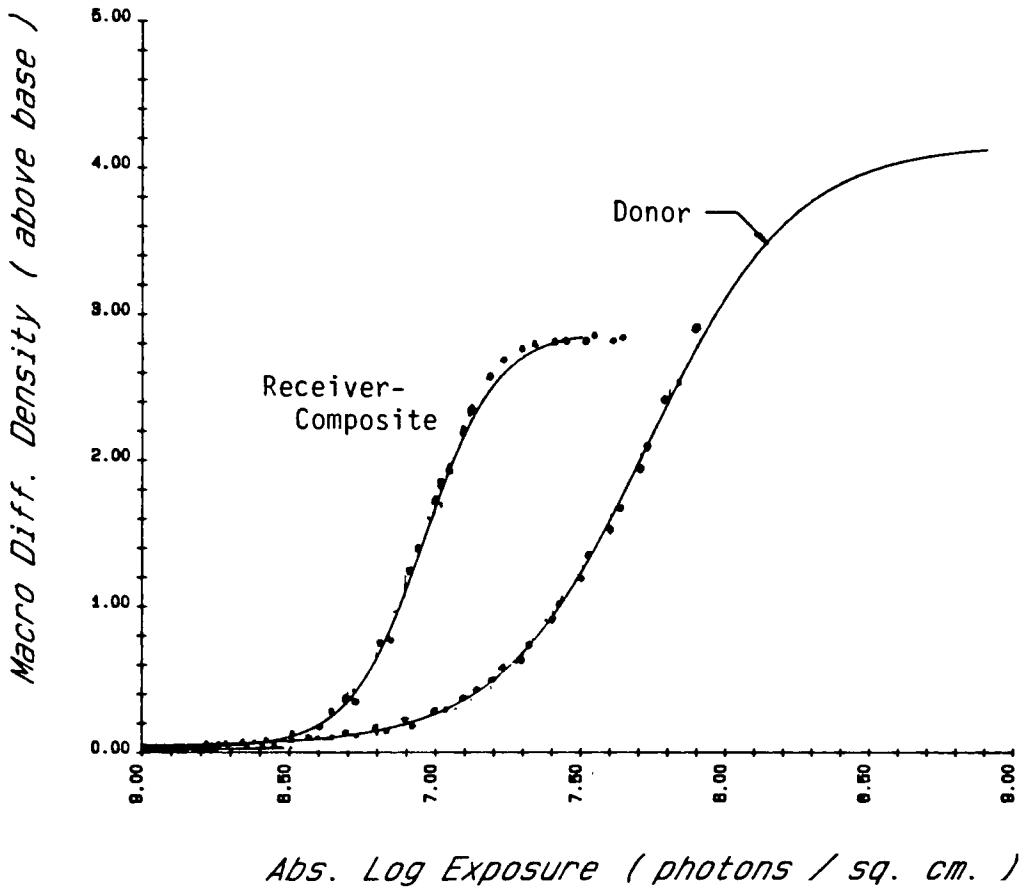

Figure B1: Comparison of raw data with characteristic curve fits

Donor RMSE	= .0178
Receiver-composite RMSE	= .0287
Tube & non-tube RMSE	= .0185

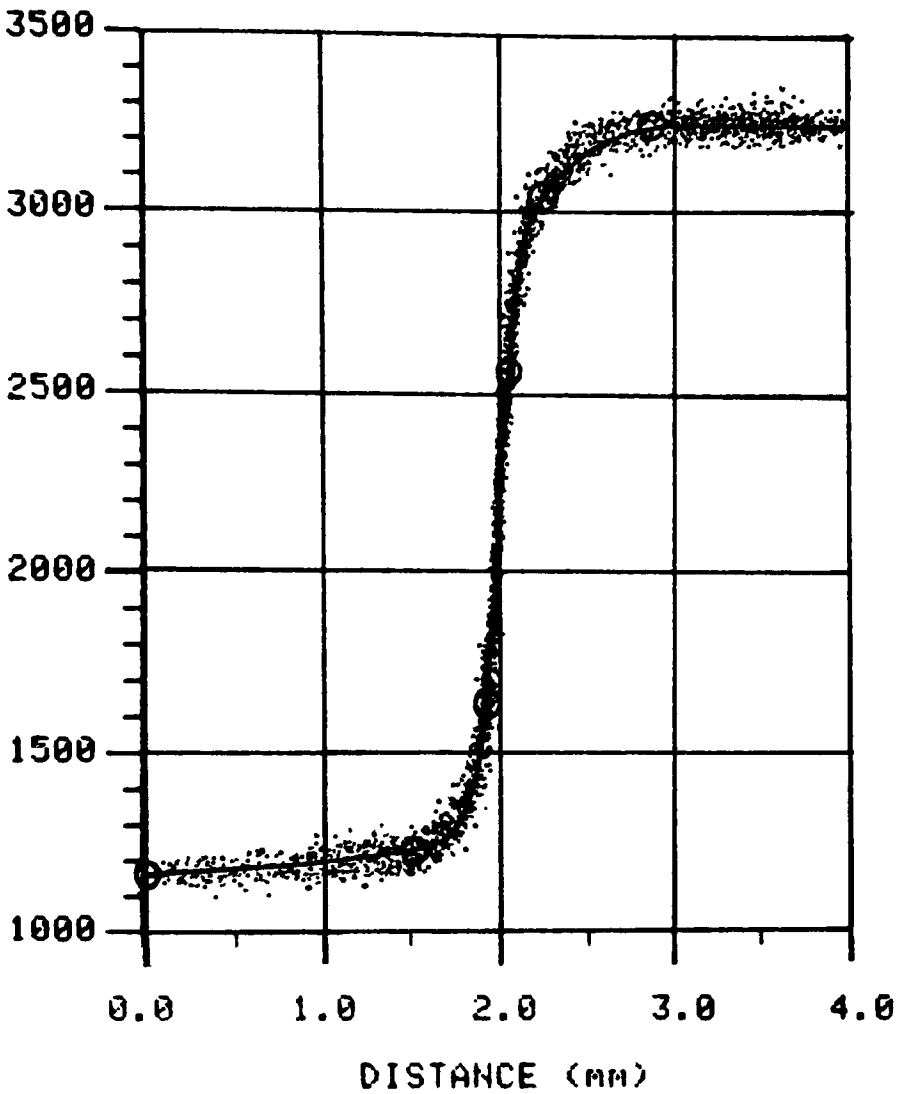

Figure B2: Comparison of raw data with cubic spline fit of edge profile. Knots indicated by circles.

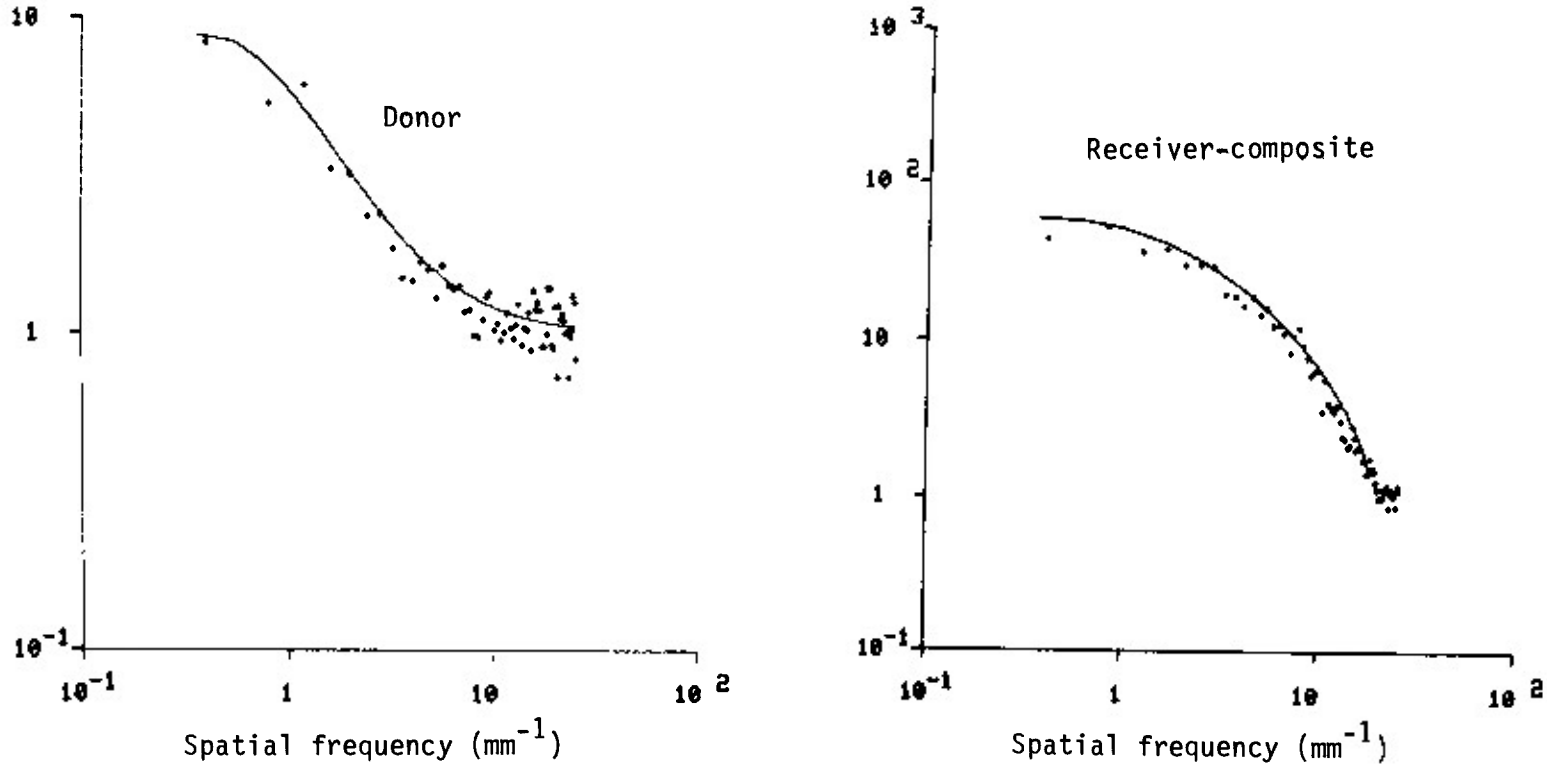

Figure B3: Example Wiener spectrum fits for single sided donor density of .63 above base(left) and receiver-composite density of .30 above base

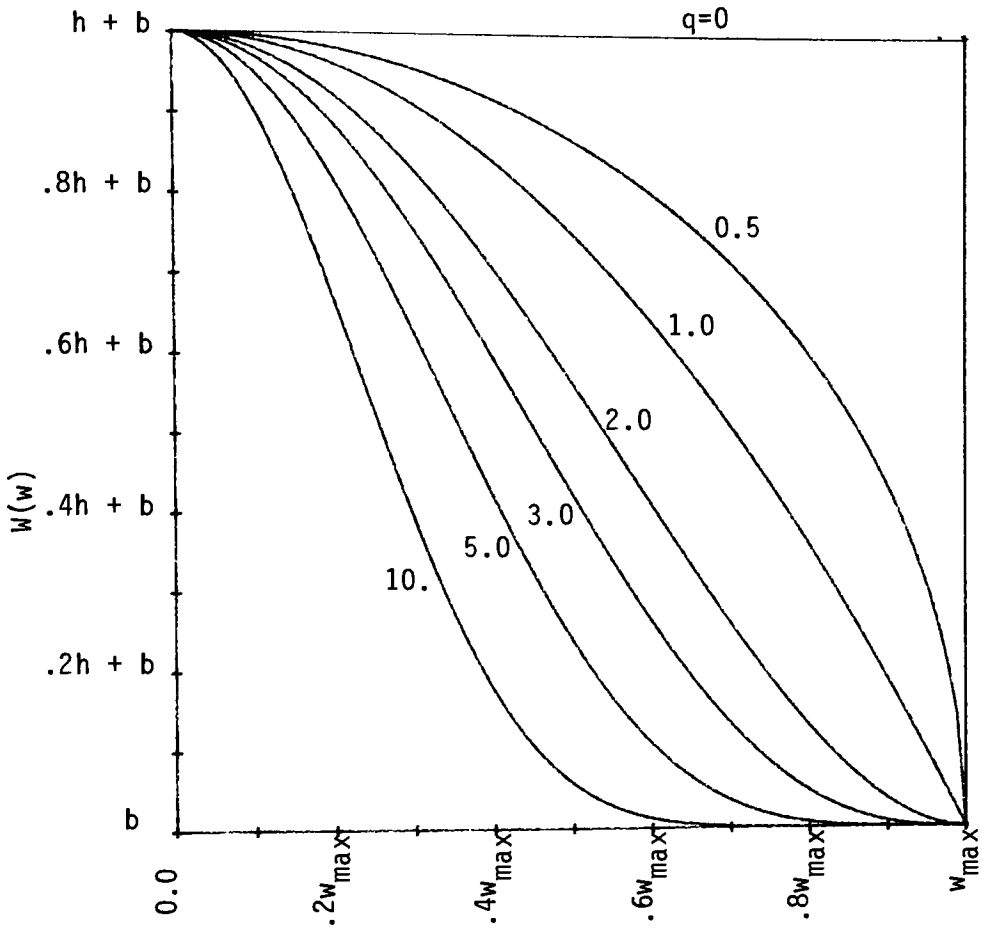

$$W(w) = h\left(1 - \left(\frac{w}{w_{max}}\right)^2\right)^q + b$$

Figure B4: Family of Curves used for donor & receiver-composite Wiener spectrum fits.

DERIVATION OF COMPOSITE SNR FOR REGISTERED IMAGES

let S_i = Signal of the $i^{\underline{th}}$ component

σ_i = Noise of the $i^{\underline{th}}$ component

$$\left(\frac{S}{N}\right)_{comp} = \frac{S_1 + S_2 + \ldots + S_n}{((\sigma_1)^2 + (\sigma_2)^2 + \ldots (\sigma_n)^2)^{1/2}}$$

for equal signals and noise

$$\left(\frac{S}{N}\right)_{comp} = \frac{nS}{(n\sigma^2)^{1/2}} = \sqrt{n}\,\frac{S}{\sigma}$$

$$\left(\frac{S}{N}\right)_{comp} = \sqrt{n}\,\left(\frac{S}{N}\right)$$

$$\left(\frac{S}{N}\right)^2_{comp} = n\,\left(\frac{S}{N}\right)^2$$

$$\left(\frac{S}{N}\right)^2_{comp} = n\,(NEQ(q))$$

$$\left(\frac{S}{N}\right)_{comp} = (n \cdot NEQ\,(DQE_{max}))^{1/2}$$

The assumptions involved are that the individual noise components are independent of each other and truly additive in nature.

7.3 APPENDIX C

SUPPLEMENTAL GRAPHS

LIST OF FIGURES
FOR APPENDIX C

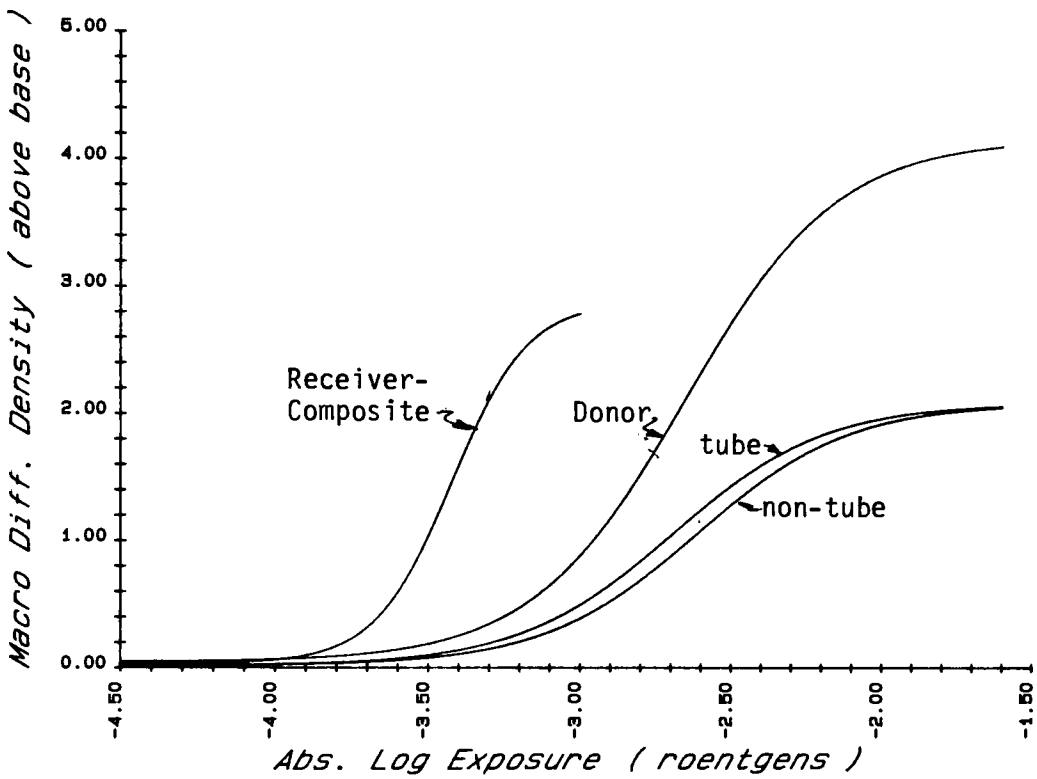

Figure C1: Characteristic Curves of
different stages in roentgens

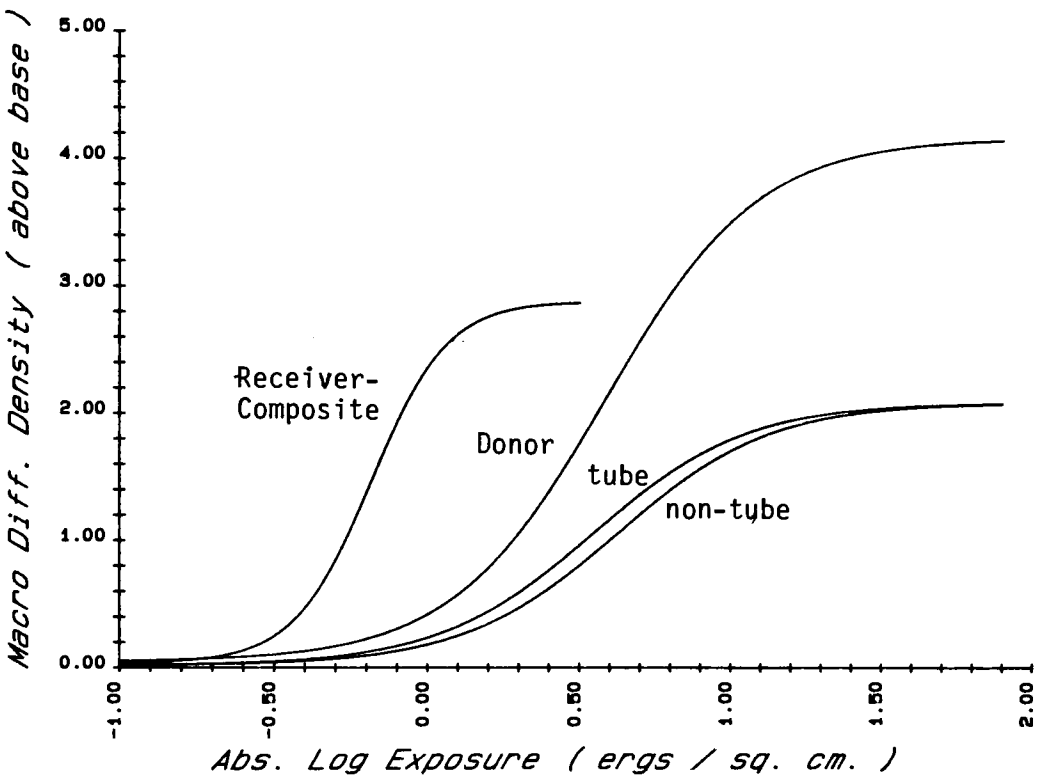

Figure C2: Characteristic curves at different stages in ergs/cm^2

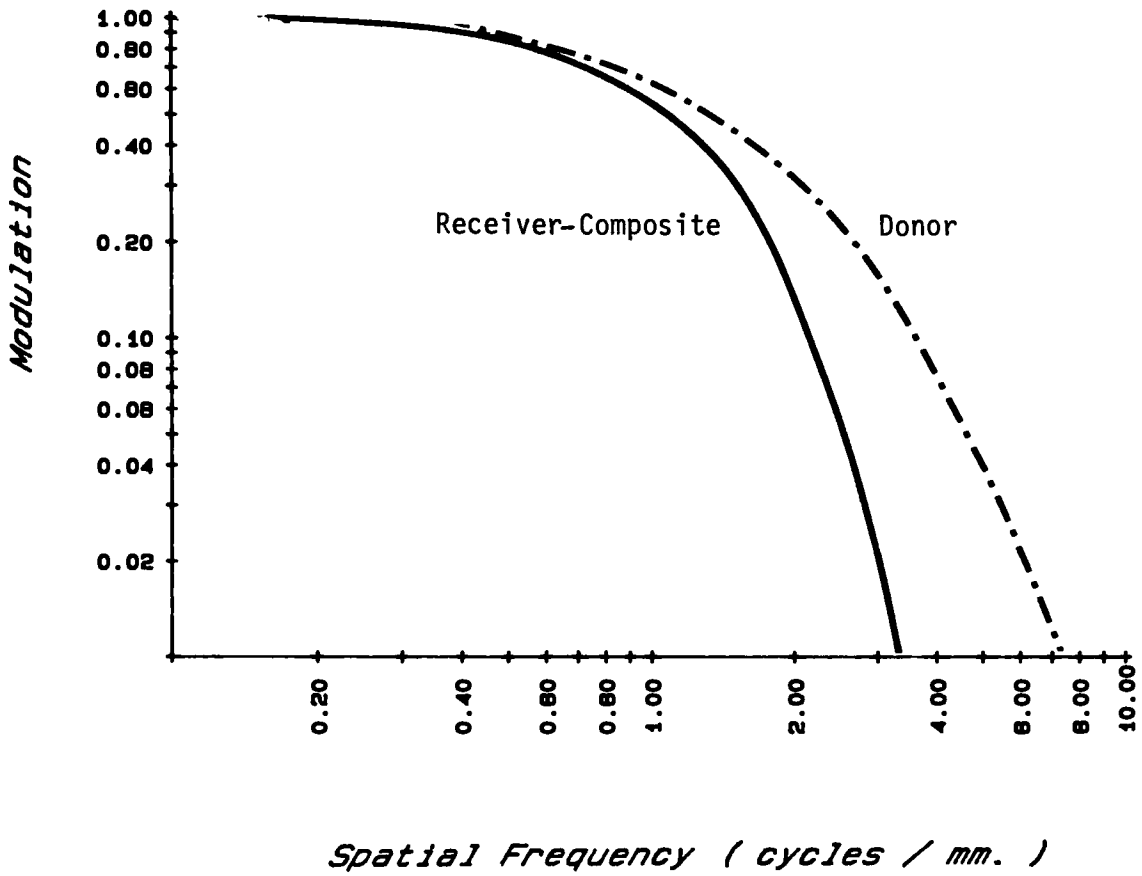

Figure C3: MTFs on log-log coordinates for
Donor and Receiver-Composite

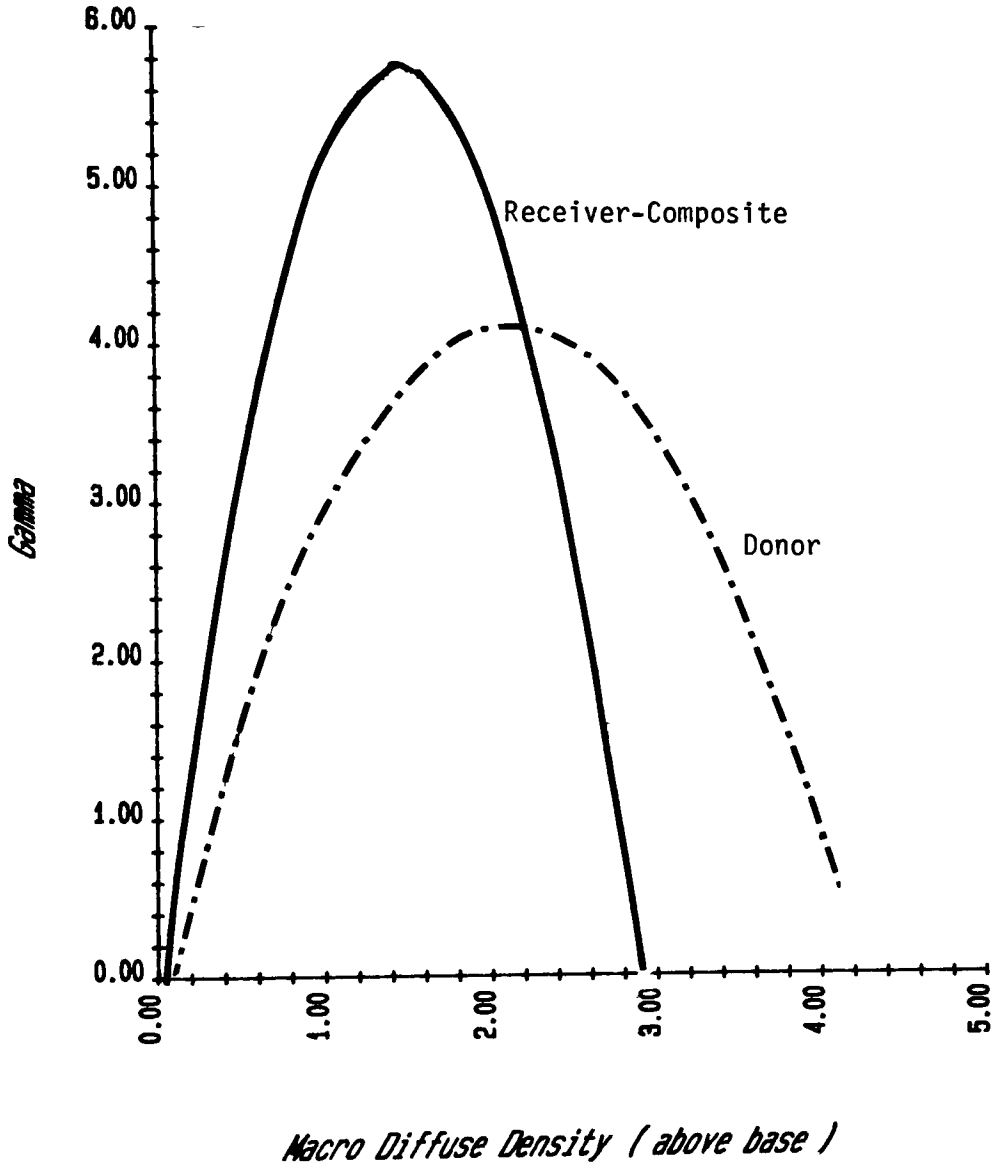

Figure C4: Gamma vs. Macro-Diffuse Density
for Receiver-Composite & Donor

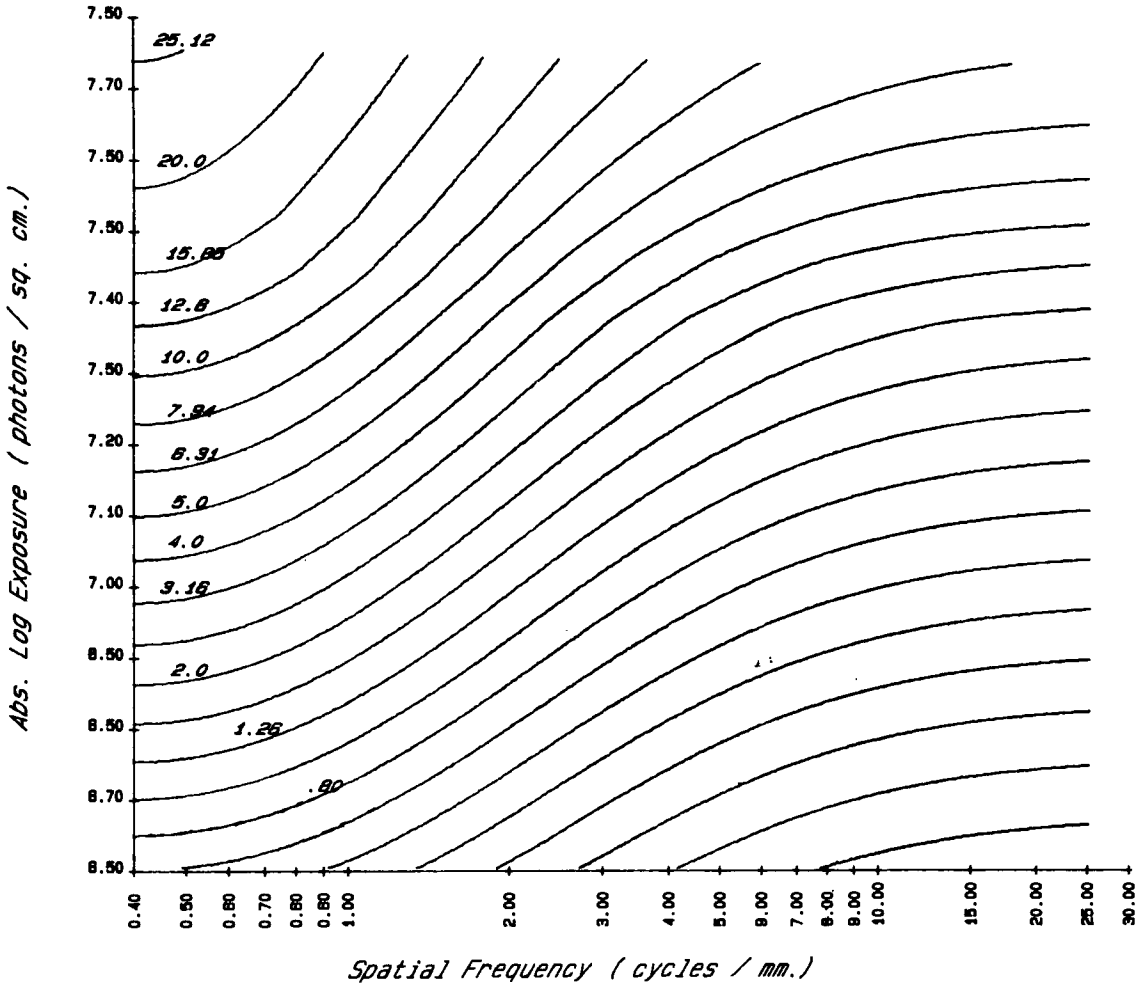

Figure C5: Donor Wiener spectrum contour plots vs. log exposure & spatial frequency

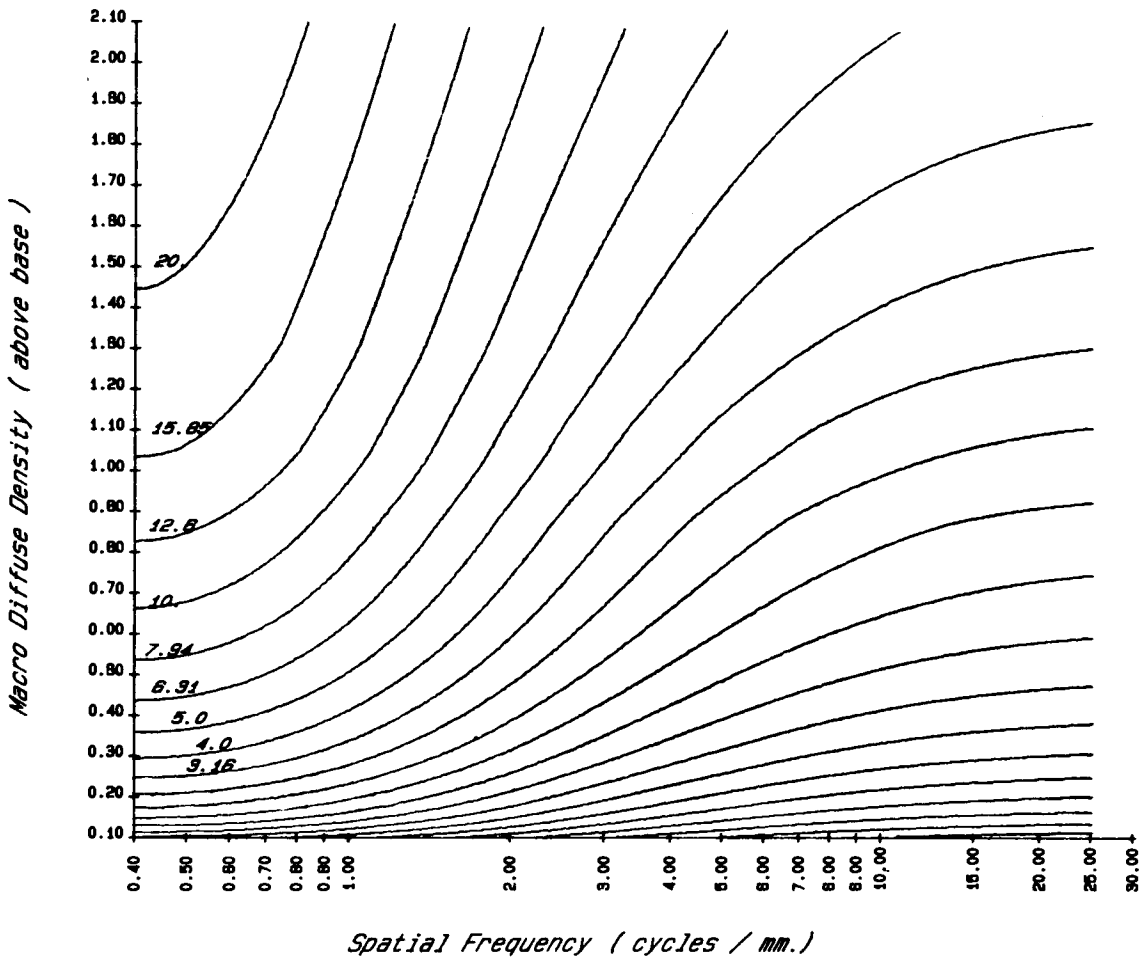

Figure C6: Donor Wiener spectrum contour plots vs. Macro-diffuse density and spatial frequency

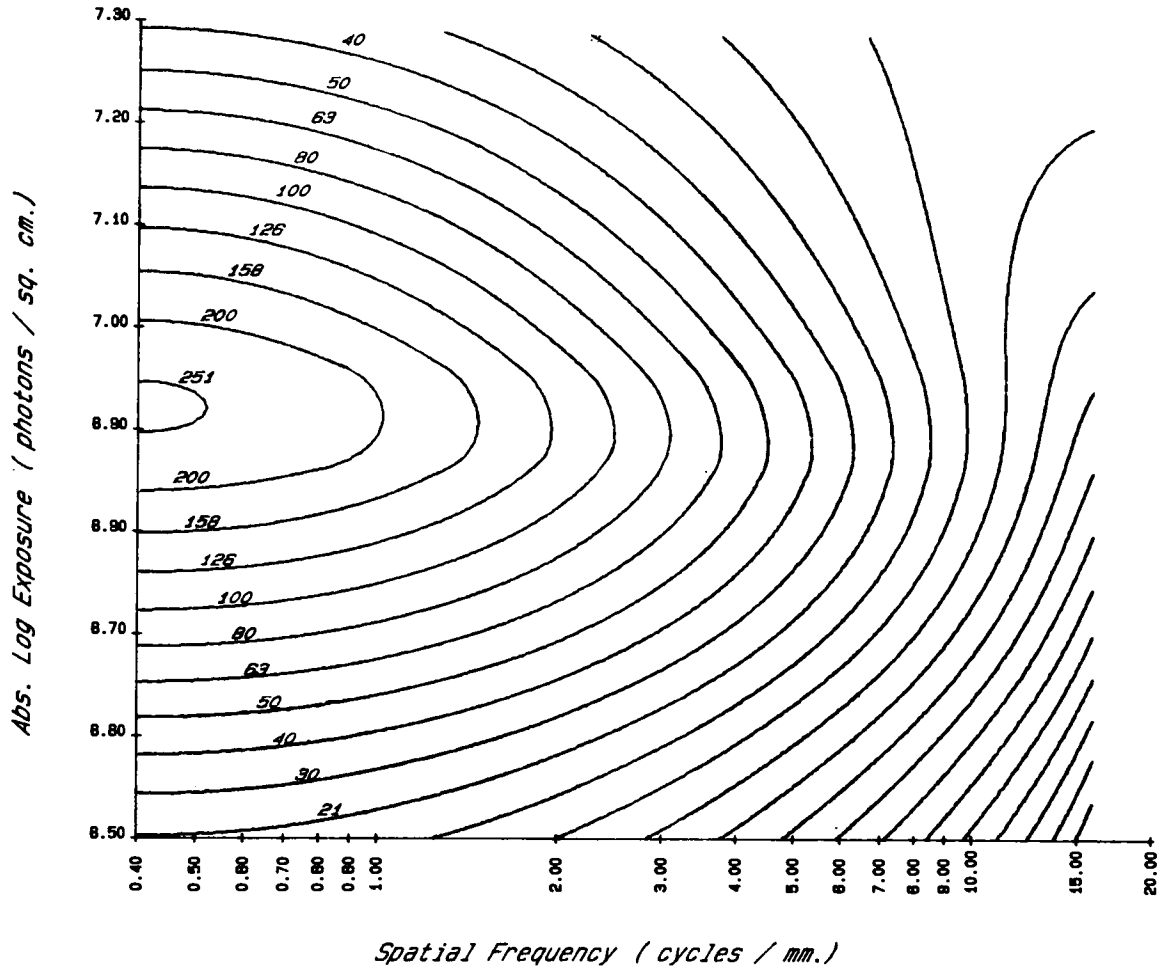

Figure C7: Receiver-Composite Wiener spectrum contour plots vs. log exposure & spatial frequency

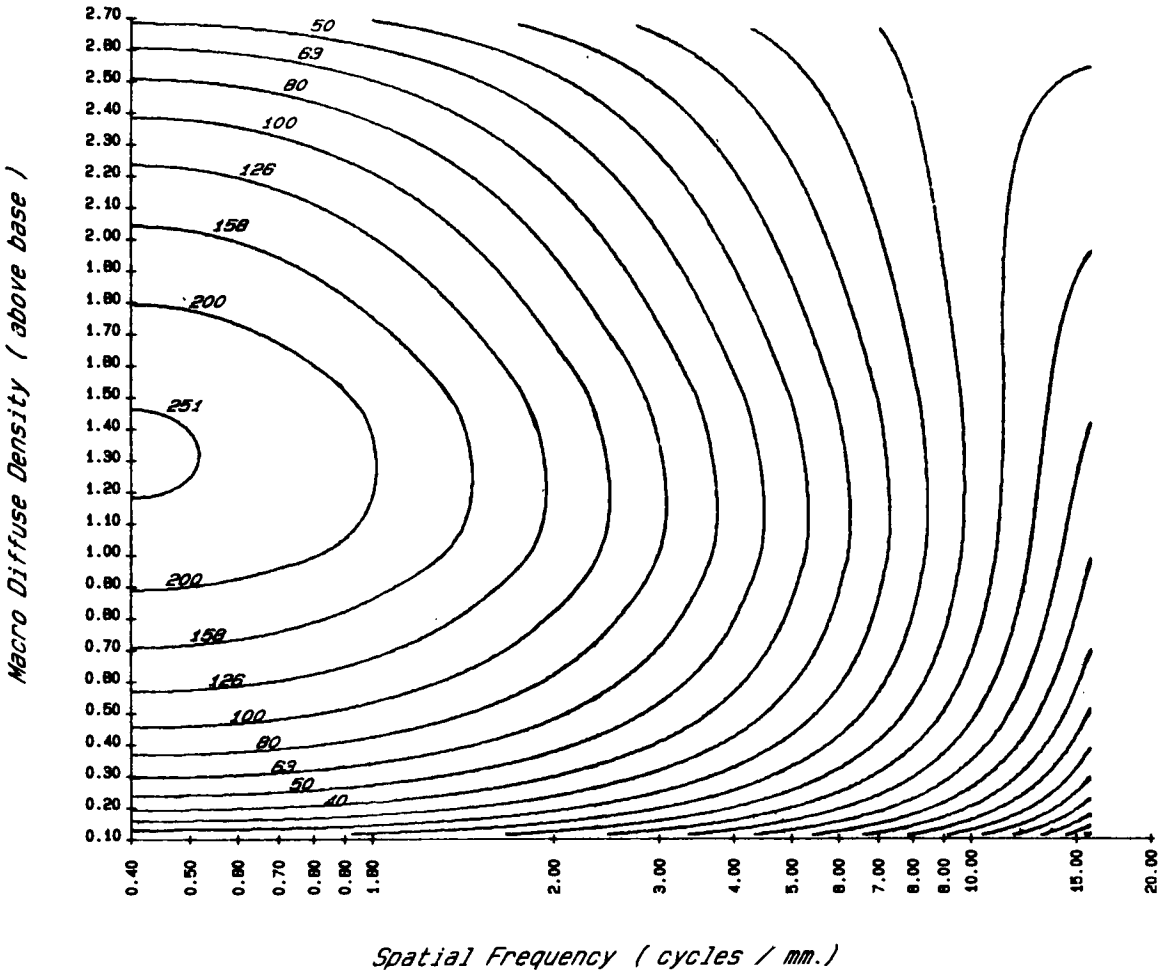

Figure C8: Receiver-Composite Wiener spectrum contour plots vs. Macro-diffuse density & spatial frequency

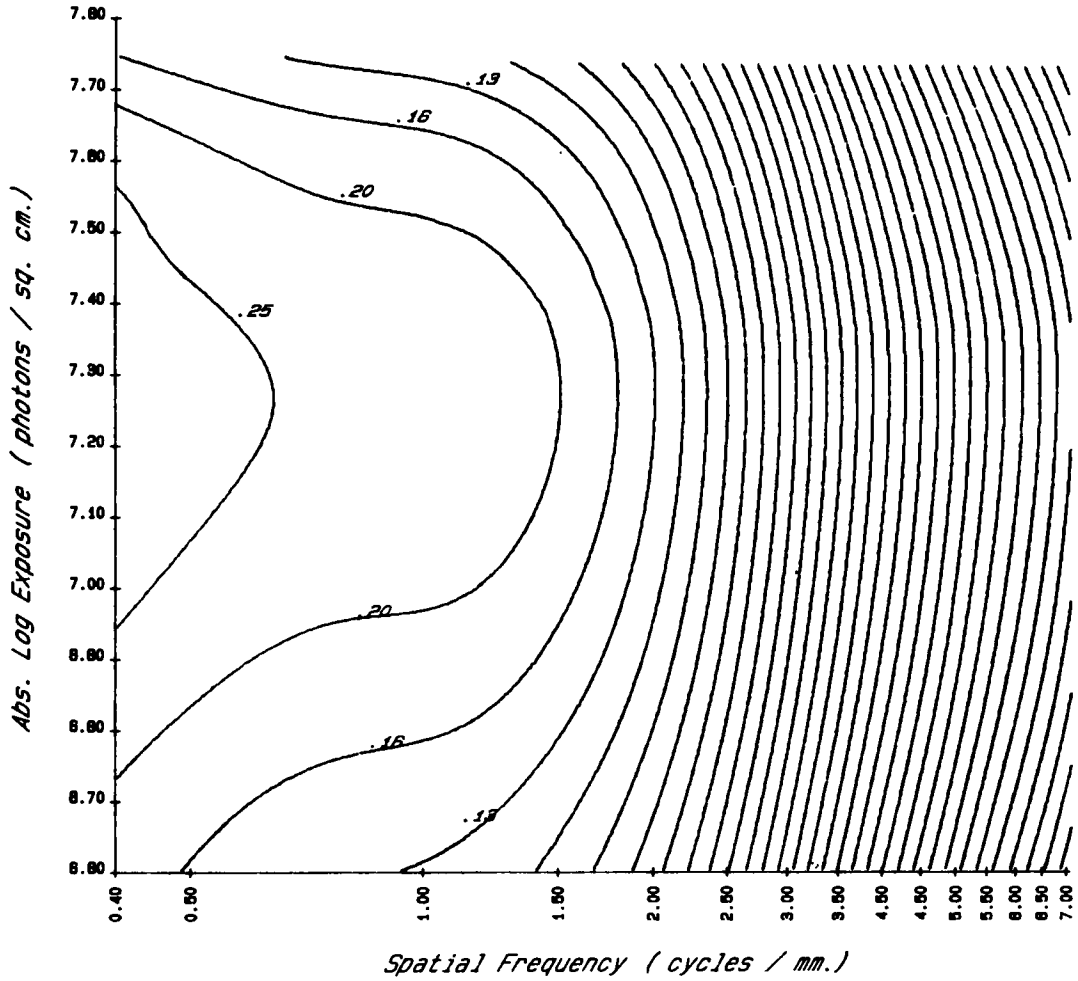

Figure C9: Donor DQE contour plots vs. log exposure & spatial frequency

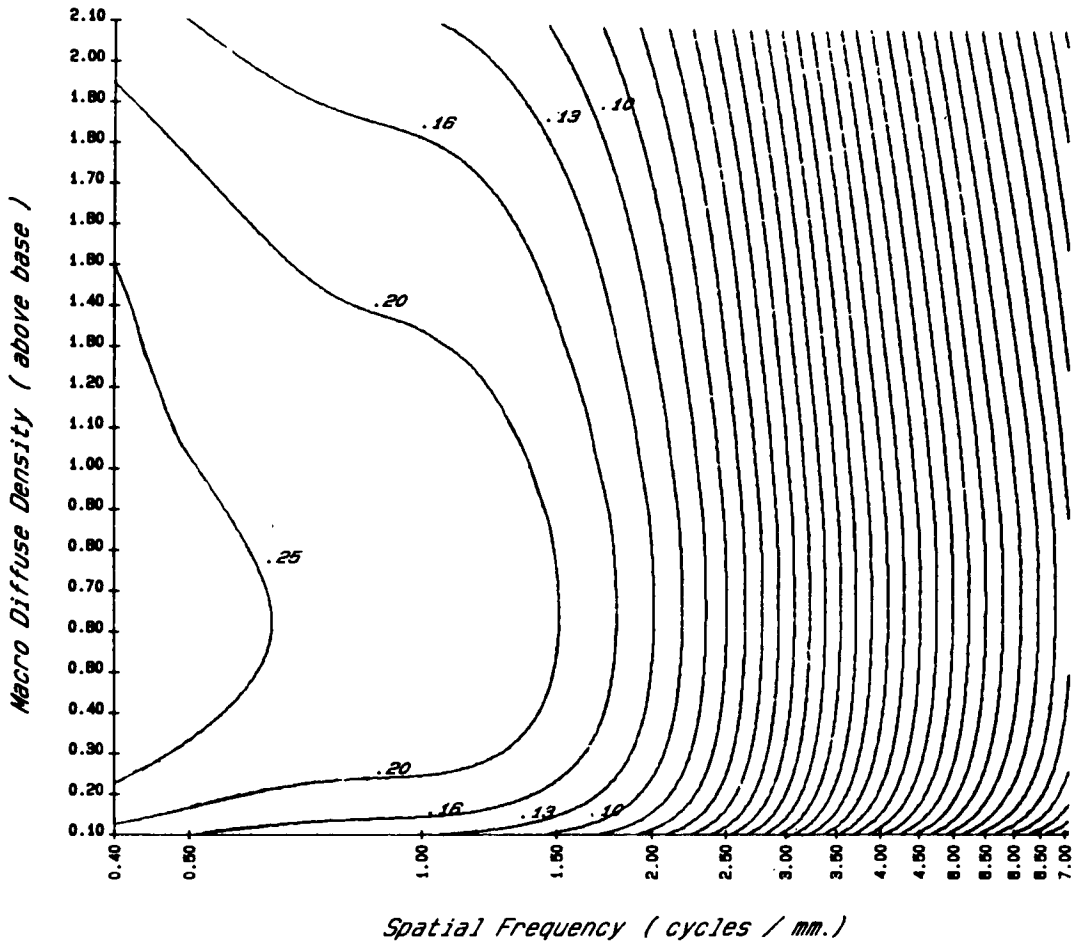

Figure C10: Donor DQE contour plots vs.

Macro-diffuse density & spatial frequency

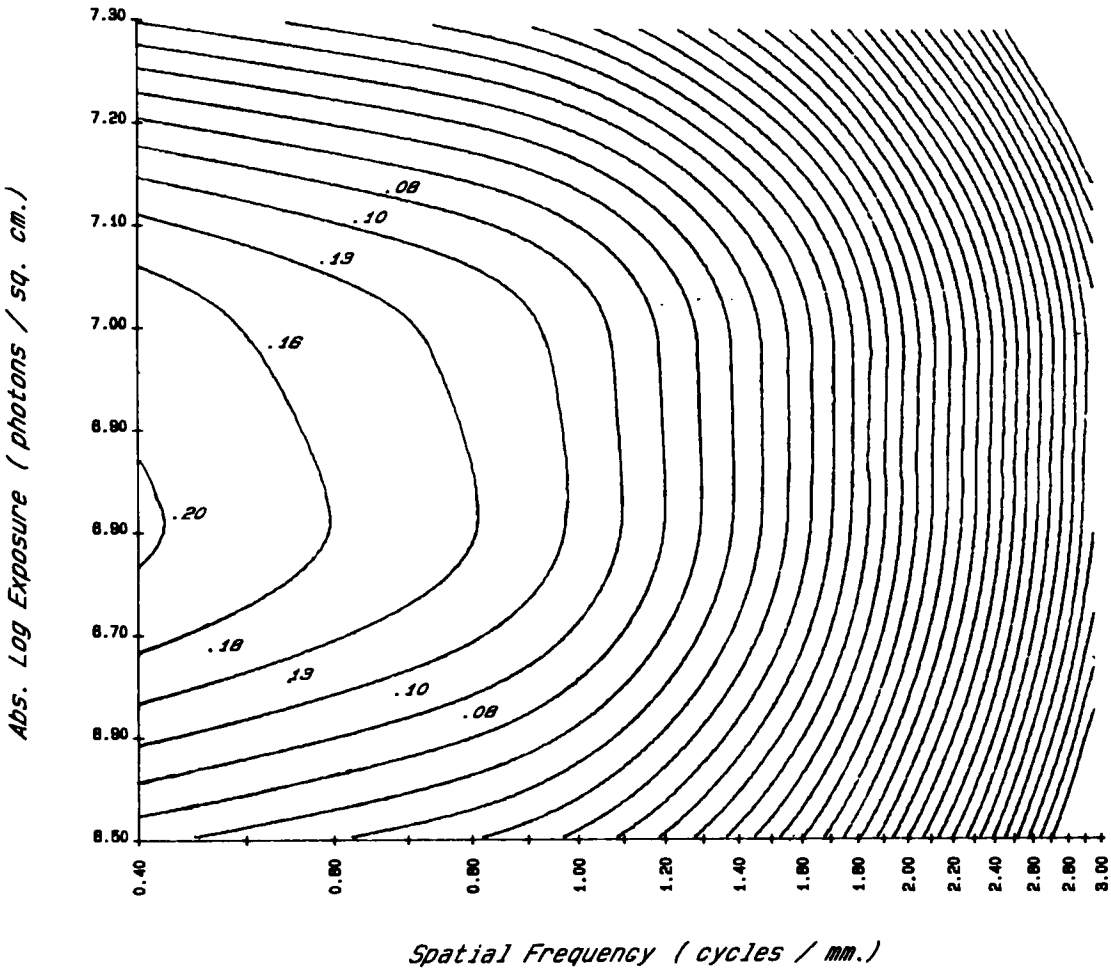

Figure C11: Receiver-Composite DQE contour plots
vs. log exposure & spatial frequency

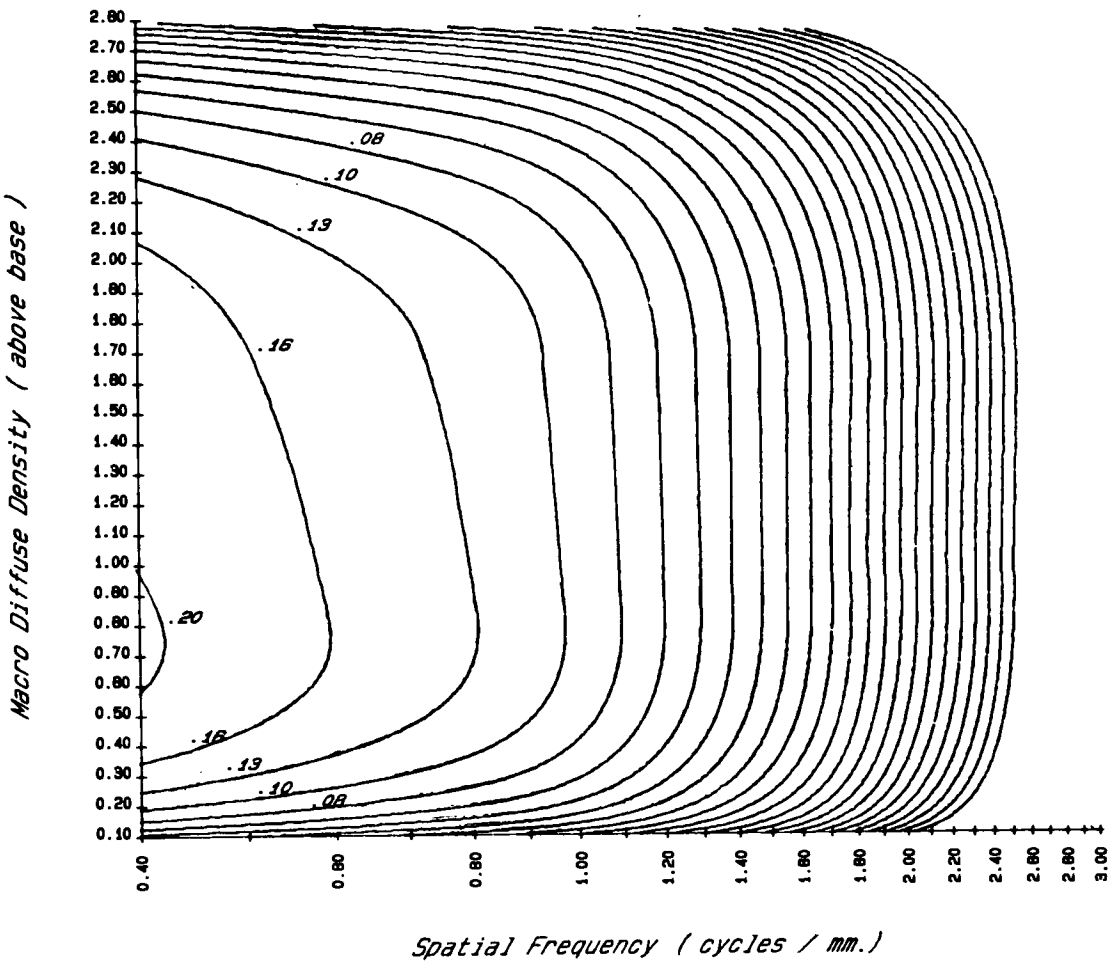

Figure C12: Receiver-Composite DQE contour plots vs. Macro-diffuse density & spatial frequency

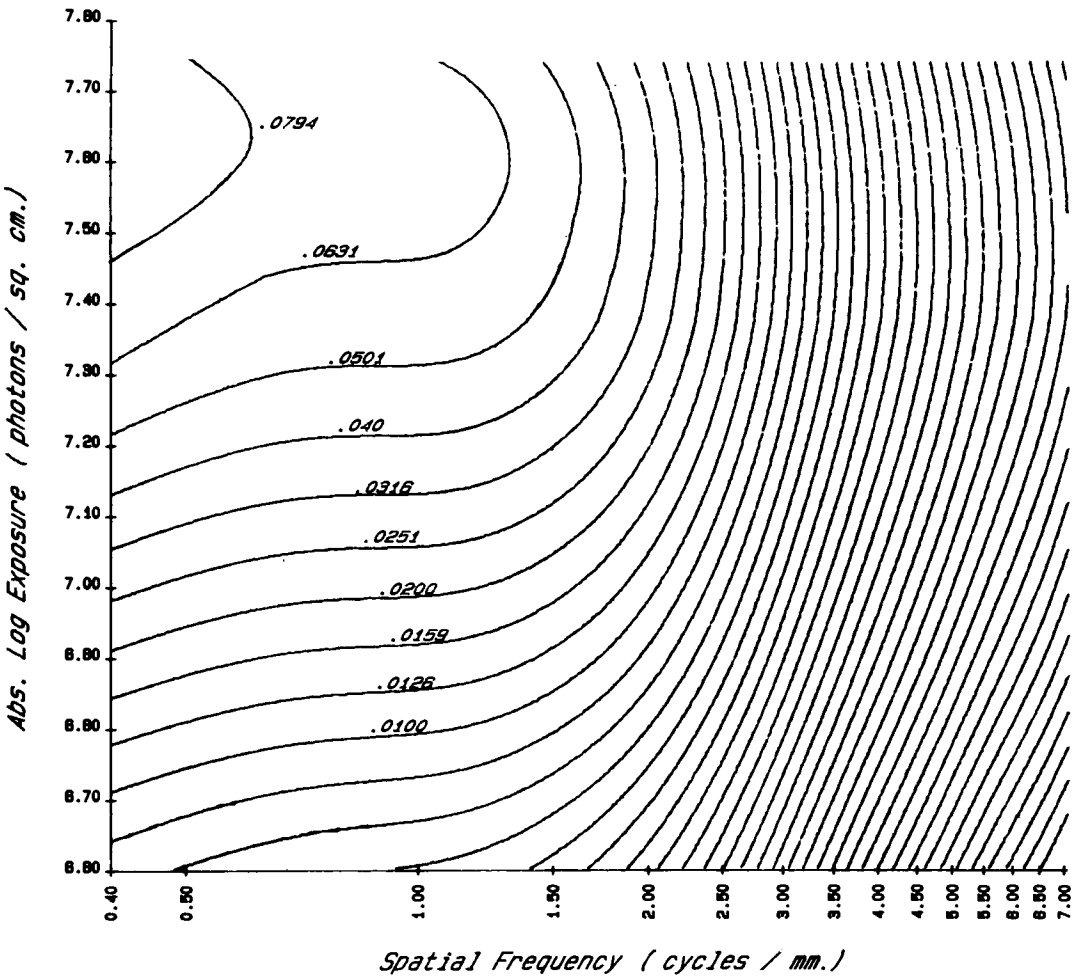

Figure C13: Donor NEQ(um^{-2}) contour plots vs.
log exposure & spatial frequency

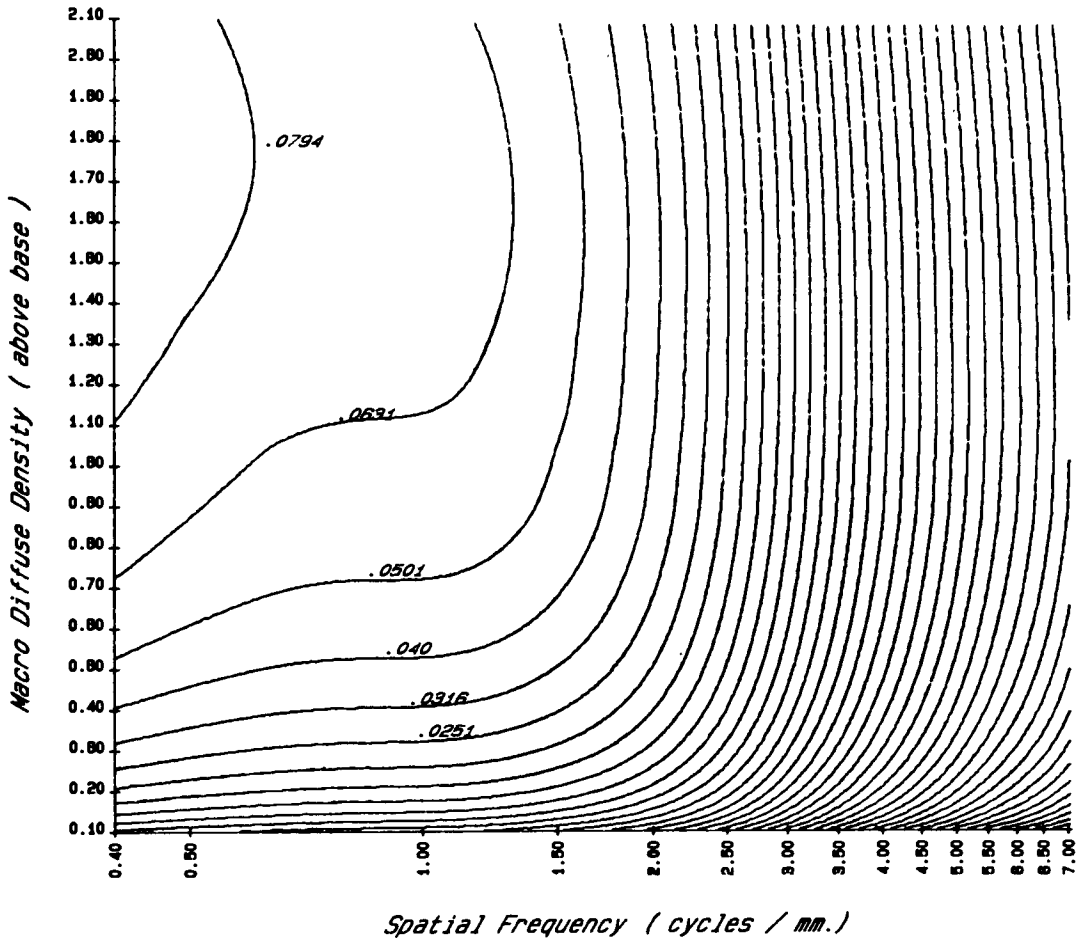

Figure C14: Donor NEQ(um^{-2}) contour plots vs. Macro-diffuse density & spatial frequency

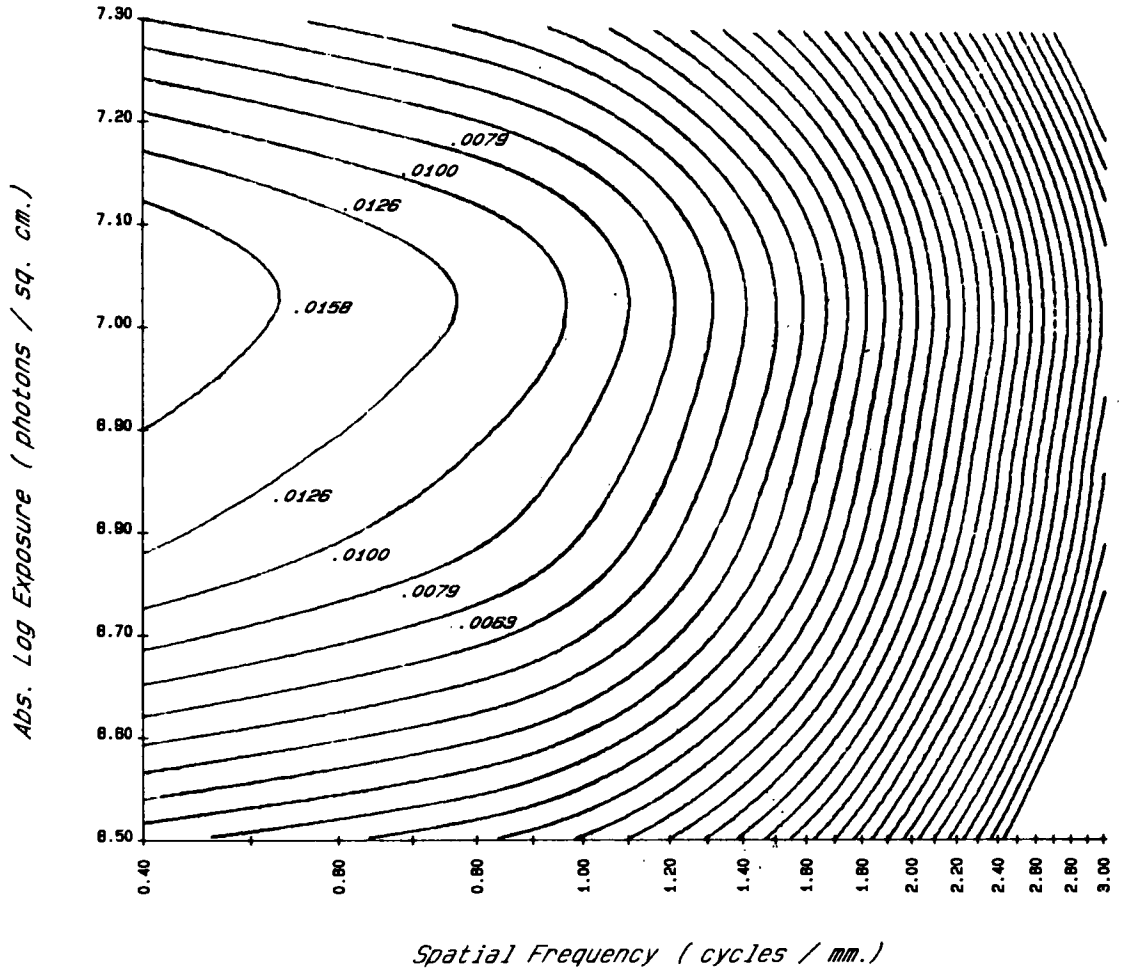

Figure C15: Receiver-Composite NEQ(um^{-2}) contour plots vs. log exposure and spatial frequency

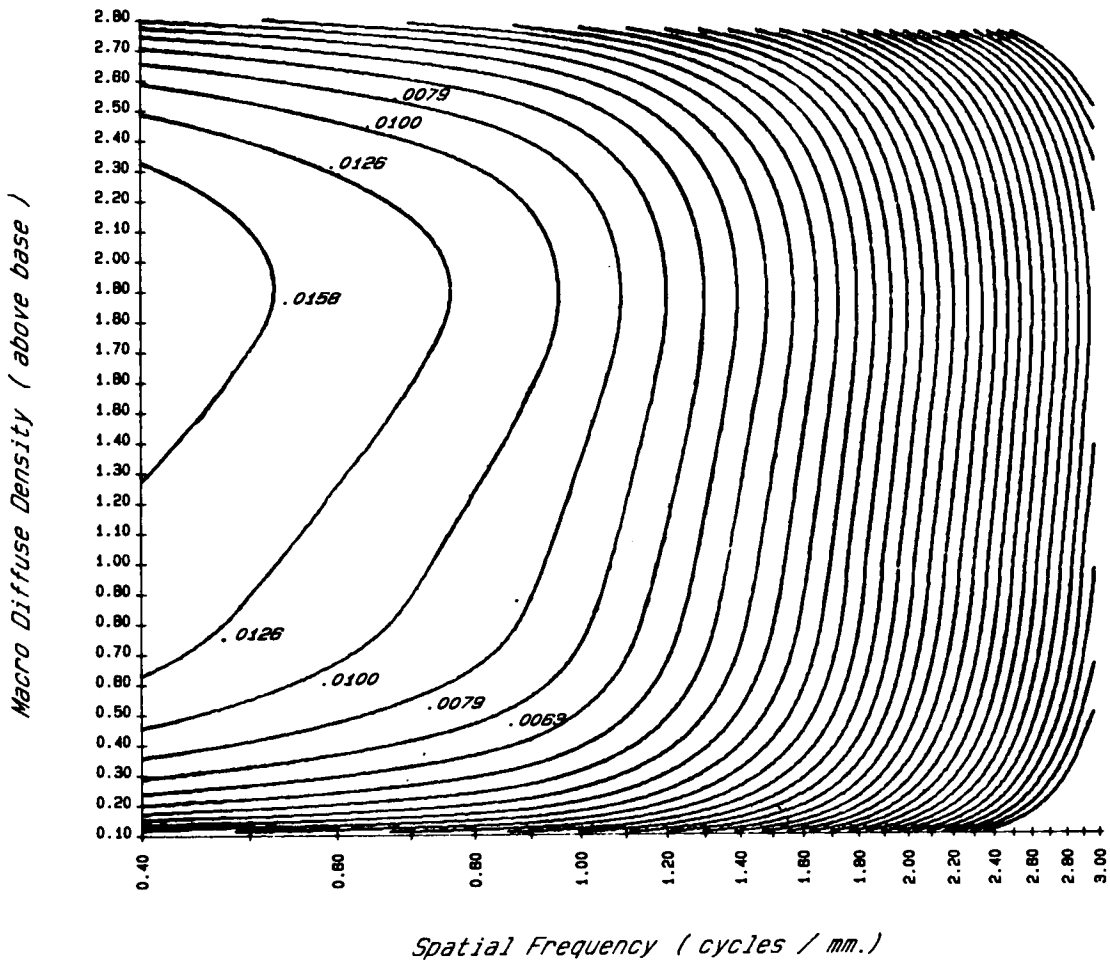

Figure C16: Receiver-Composite NEQ(um^{-2}) contour plots vs. Macro-diffuse density and spatial frequency

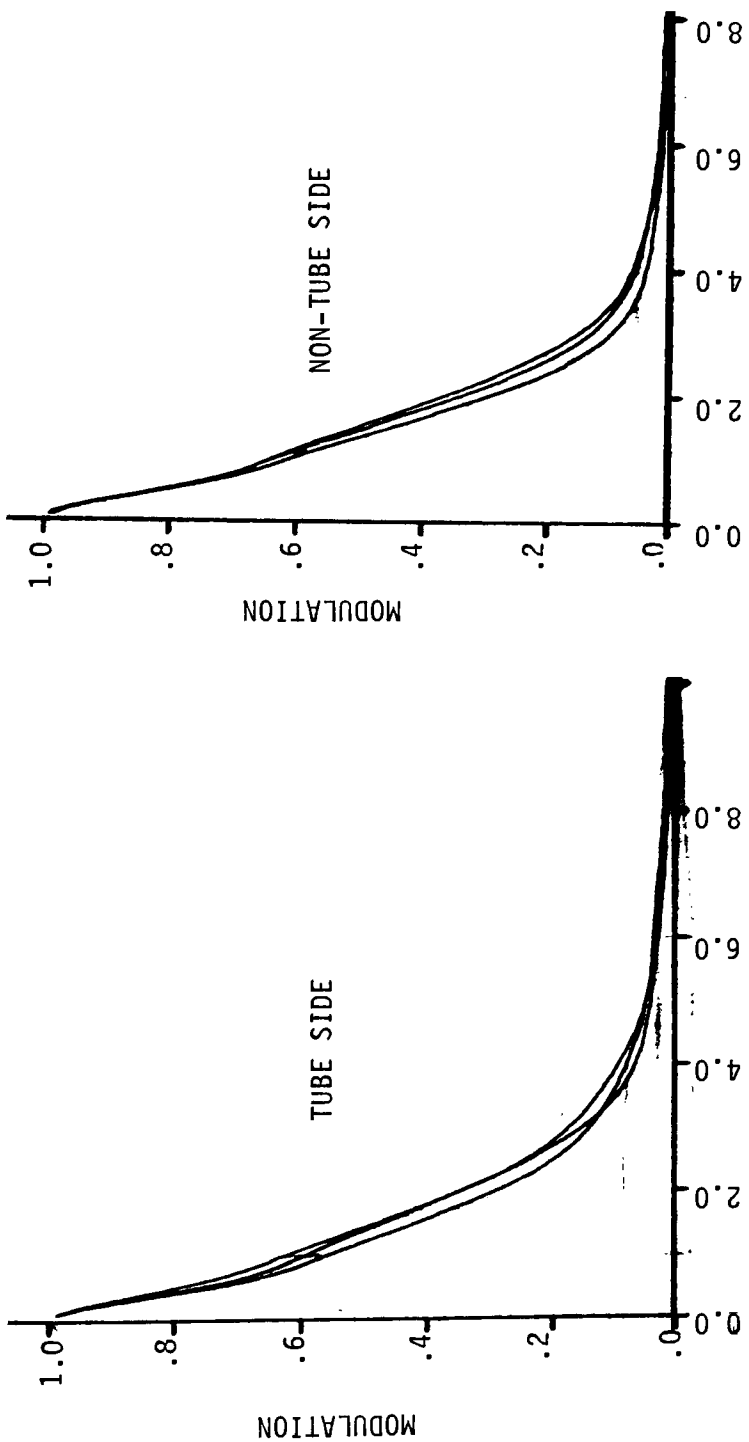

Figure C17: Comparison between Tube & Non-Tube side MTFs for Donor.

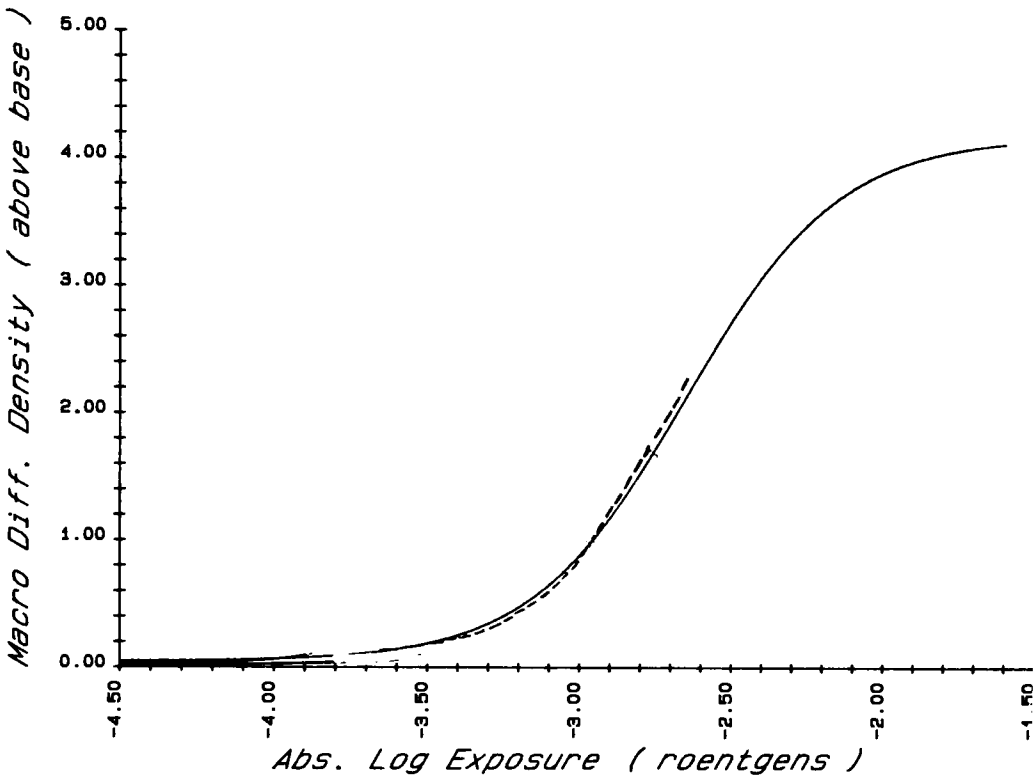

Figure C18: Comparison of relative characteristic curve shapes between this experiment (solid) and results of reference 38 (dash) for Donor.

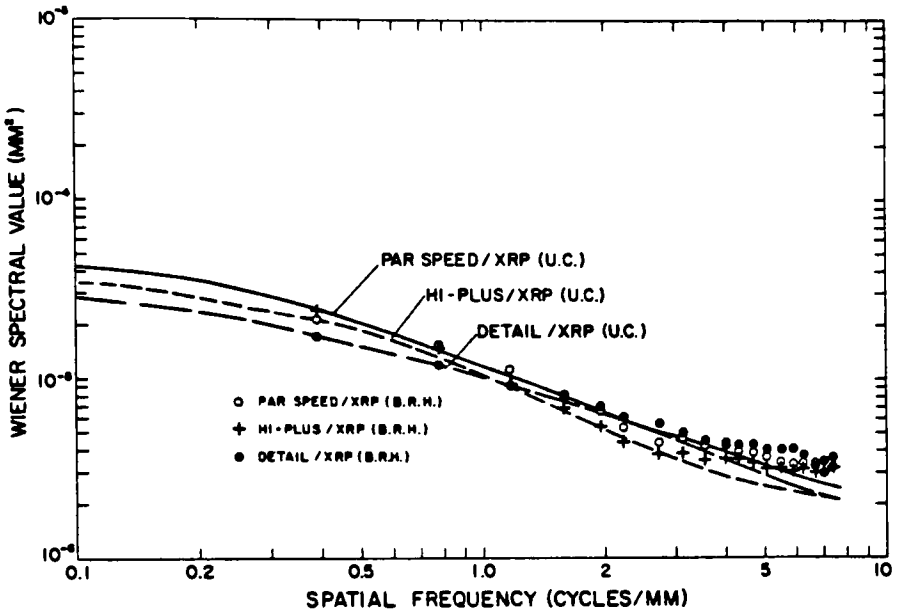

Figure C19: Typical absolute Wiener spectrum values in Macro D^2mm^2 for screen/film radiographic systems.(from reference 38)

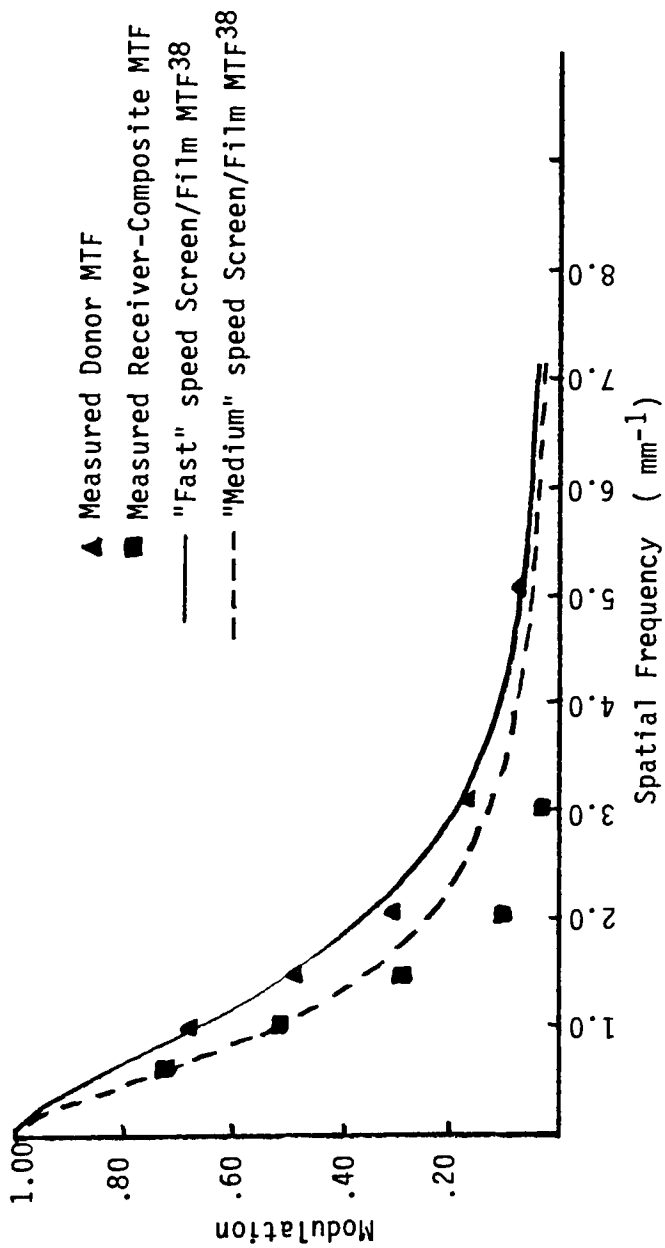

Figure C20: Comparison of Donor & Receiver composite MTFs to typical medium & fast film/screen systems.

7.4 APPENDIX D

COMPUTER PROGRAMS

```
      SUBROUTINE SPL2Z(DATAX,DATAY,ND,XNOT,NK,Y,M,RMSE,AVABE)
C
C     SPL2Z IS A FORTRAN CALLABLE SUBROUTINE WHICH CALCULATES THE
C     LEAST SQUARE CUBIC SPLINE SUBJECT TO THE CONSTRAINT THAT THE
C     SLOPE MUST BE ZERO AT THE ENDPOINTS.
C     XNOT IS THE VECTOR OF KNOT LOCATIONS
C     DATAX AND DATAY ARE THE VECTORS OF THE ABSCISSA AND ORDINATE
C     VALUES OF THE DATA.
C     MAXIMUM NUMBER OF DATA POINTS-400
C     MAXIMUM NUMBER OF KNOTS-7
      DIMENSION DATAX(1),DATAY(1),XNOT(1),M(1),Y(1)
      DIMENSION H(6),A(7,7),B(7,7),C(7,7)
      DIMENSION AINV(49)
      DIMENSION ZZ(2800)
      DOUBLE PRECISION AINV,D
      REAL M,H
C
C CHECK ORDER OF KNOTS AND REORDER IF NECESSARY
C
 5    DO 10 I=1,NK-1
      IF (XNOT(I+1).GE.XNOT(I)) GO TO 10
      E=XNOT(I+1)
      XNOT(I+1)=XNOT(I)
      XNOT(I)=E
      GO TO 5
 10   CONTINUE
C
C SET ELEMENTS OF MATRICIES A,B,& C EQUAL TO ZERO
C
      DO 20 I=1,NK
      DO 20 J=1,NK
 20   A(I,J)=B(I,J)=C(I,J)=0.0
C
C CREATE VECTOR H
C
      DO 30 I=1,NK-1
 30   H(I)=XNOT(I+1)-XNOT(I)
C
C CREATE MATRIX A
C
      DO 40 I=1,NK-1
      A(I,I+1)=A(I+1,I+1)=A(I+1,I)=H(I)
 40   A(I,I)=(A(I,I)+H(I))*2.
      A(NK,NK)=A(NK,NK)*2.
C
C CONVERT MATRIX A INTO A VECTOR AINV
C
      K=0
      DO 50 I=1,NK
      DO 50 J=1,NK
      K=K+1
 50      AINV(K)=A(I,J)
```

```
C
C INVERT MATRIX A
C
      CALL DMINV(AINV,NK,D,M,Y)
      IF(D.EQ.0.DO)TYPE "*** MATRIX A IS SINGULAR ***"
C
C CREATE MATRIX B
C
      DO 60 I=1,NK-1
      B(I,I+1)=B(I+1,I+1)=B(I+1,I)=6./H(I)
 60   B(I,I)=(B(I,I)+6./H(I))*(-1.)
      B(NK,NK)=B(NK,NK)*(-1.)
C
C CREATE MATRIX C BY POST MULTIPLYING AINV BY B
C
      DO 70 I=1,NK
      DO 70 J=1,NK
      D=0.DO
      DO 65 K=1,NK
 65   D=D+AINV(I+(K-1)*NK)*B(K,J)
 70   C(I,J)=D
C
C ABCSISSA VALUES ARE ASSUMED TO BE IN ASCENDING ORDER AT THIS POINT
C
C SET ELEMENTS OF MATRIX Z EQUAL TO ZERO
C
      DO 90 I=1,NK*ND
 90   ZZ(I)=0.0
C
C CREATE MATRIX Z FROM DATAX,H, & C
C
      K=1
      DO 100 I=1,ND
      NQ=(NK-1)*ND
      IF(DATAX(I).LT.XNOT(1)) GO TO 101
      IF(DATAX(I).GE.XNOT(NK)) GO TO 102
 92   IF(XNOT(K).LE.DATAX(I).AND.DATAX(I).LT.XNOT(K+1)) GO TO 93
      K=K+1
      GO TO 92
 93   DU=XNOT(K+1)-DATAX(I)
      DL=DATAX(I)-XNOT(K)
      W1=DU**3/(6.*H(K))-DU*H(K)/6.
      W2=DL**3/(6.*H(K))-DL*H(K)/6.
      W3=DL/H(K)
      W4=DU/H(K)
      DO 95 J=1,NK
      NX=(J-1)*ND
 95   ZZ(NX+I)=W1*C(K,J)+W2*C(K+1,J)
      NZ=(K-1)*ND
      ZZ(NZ+I)=ZZ(NZ+I)+W4
      NW=K*ND
      ZZ(NW+I)=ZZ(NW+I)+W3
```

```
      GO TO 100
  101 ZZ(I)=1.0
      GO TO 100
  102 ZZ(NQ+I)=1.0
  100 CONTINUE
C
C CALCULATE THE LEAST SQUARES ESTIMATE OF VECTOR Y
C
      CALL LINREG(ZZ,DATAY,Y,NK,ND)
C
C CALCULATE RECONSTRUCTED DATA VALUES RESIDUALS,RMSE
C AND AVERAGE ABSOLUTE ERROR.
      RMSE=AVABE=ERRSUM=0.0
      DO 110 I=1,ND
      SUM=0.0
      DO 105 J=1,NK
      NU=(J-1)*ND
  105 SUM=SUM+ZZ(NU+I)*Y(J)
      RES=SUM-DATAY(I)
      ERRSUM=ERRSUM+RES
      RMSE=RMSE+RES**2
  110 AVABE=AVABE+ABS(RES)
      RMSE=SQRT(RMSE/ND)
      AVABE=AVABE/ND
C
C CALCULATE VECTOR M FROM M=CY
C
      DO 120 I=1,NK
      SUM=0.0
      DO 115 J=1,NK
  115 SUM=SUM+C(I,J)*Y(J)
  120 M(I)=SUM
      RETURN
      END
```

```
      SUBROUTINE SPLVAL(X,S,XNOT,Y,M,NK,K)
    DIMENSION XNOT(NK),Y(NK),M(NK)
    REAL M
    IF(X.LT.XNOT(1)) GO TO 101
    IF(X.GE.XNOT(NK)) GO TO 102
10  IF(XNOT(K).LE.X.AND.X.LT.XNOT(K+1)) GO TO 20
    K=K+1
    GO TO 10
20  DU=XNOT(K+1)-X
    DL=X-XNOT(K)
    XH=XNOT(K+1)-XNOT(K)
    DIV=6.*XH
    S=(DU**3*M(K)+DL**3*M(K+1)+DL*(6.*Y(K+1)-M(K+1)*XH*XH)
    1   +DU*(6.*Y(K)-M(K)*XH*XH))/DIV
    GO TO 100
101 S=Y(1)
    GO TO 100
102 S=Y(NK)
    GO TO 100
100 CONTINUE
    RETURN
    END
```

```
      SUBROUTINE SPLFTZ(F,TM,TP,TR,TI,Y,Q,XNOT,NK)
      DIMENSION Y(NK),XNOT(NK),Q(NK)
      IF(F.EQ.0.0) GO TO 31
      PI=3.14159265358979323846264338327 95
   10 W=2*PI*F
      W2=W*W
      W3=W*W*W
      ARGA=W*XNOT(1)
      ARGB=W*XNOT(NK)
      CA=COS(ARGA)
      CB=COS(ARGB)
      SA=SIN(ARGA)
      SB=SIN(ARGB)
      SUMR=(Q(NK)*CB-Q(1)*CA)/W2
      SUMI=(Q(NK)*SB-Q(1)*SA)/(-W2)
      L=NK-1
      DO 20 I=1,L
      SUMR=SUMR-(Q(I+1)-Q(I))*(SIN(W*XNOT(I+1))-SIN(W*XNOT(I)))/
     1   (W3*(XNOT(I+1)-XNOT(I)))
      SUMI=SUMI-(Q(I+1)-Q(I))*(COS(W*XNOT(I+1))-COS(W*XNOT(I)))/
     1   (W3*(XNOT(I+1)-XNOT(I)))
   20 CONTINUE
      TR=SUMR/(Y(NK)-Y(1))
      TI=SUMI/(Y(NK)-Y(1))
      TM=SQRT(TR*TR+TI*TI)
      TP=ATAN2(TI,TR)
      GO TO 30
   31 TM=TR=1.0
      TI=TP=0.0
   30 RETURN
      END
```

```
      SUBROUTINE LINREG(X,Y,B,NC,NR)
      DOUBLE PRECISION SUM,XPX
      DIMENSION B(NC),Y(NR),X(NR,NC)
      DIMENSION XPX(49),XPY(7),LL(7),MM(7)
C
C     X IS A MATRIX OF PREDICTORS,DIMENSIONED (NR,NC)
C     Y IS A VECTOR OF RESPONSES
C     B IS A VECTOR OF LEAST SQUARES COEFFICIENTS
C
C     FORM X.X MATRIX
C
      M=0
      DO 10 J=1,NC
      DO 10 K=1,NC
      SUM=0.DO
      DO 9 I=1,NR
    9 SUM=SUM+X(I,J)*X(I,K)
      M=M+1
   10 XPX(M)=SUM
C
C     INVERT X.X MATRIX USING IBM SSP DOUBLE PRECISION MINV
C
      CALL DMINV(XPX,NC,SUM,LL,MM)
C
C     REPORT SINGULAR X.X MATRIX
C
      IF(SUM.EQ.0.DO) TYPE.  ***XPX MATRIX IS SINGULAR***
C
C     FORM X.Y MATRIX
      DO 14 J=1,NC
      SUM=0.DO
      DO 15 I=1,NR
   15 SUM=SUM+X(I,J)*Y(I)
   14 XPY(J)=SUM
C
C     CALCULATE B VECTOR
C
      M=0
      DO 5 I=1,NC
      SUM=0.DO
      DO 6 J=1,NC
      M=M+1
    6 SUM=SUM+XPX(M)*XPY(J)
    5 B(I)=SUM
      RETURN
      END
```

```
      SUBROUTINE DMINV(A,N,D,L,M)
      DIMENSION A(1),L(1),M(1)
      DOUBLE PRECISION A,D,BIGA,HOLD
      D=1.
      NK=-N
      DO 80 K=1,N
      NK=NK+N
      L(K)=K
      M(K)=K
      KK=NK+K
      BIGA=A(KK)
      DO 20 J=K,N
      IZ=N*(J-1)
      DO 20 I=K,N
      IJ=IZ+I
   10 IF(DABS(BIGA)-DABS(A(IJ))) 15,20,20
   15 BIGA=A(IJ)
      L(K)=I
      M(K)=J
   20 CONTINUE
      J=L(K)
      IF(J-K) 35,35,25
   25 KI=K-N
      DO 30 I=1,N
      KI=KI+N
      HOLD=-A(KI)
      JI=KI-K+J
      A(KI)=A(JI)
   30 A(JI)=HOLD
   35 I=M(K)
      IF(I-K) 45,45,38
   38 JP=N*(I-1)
      DO 40 J=1,N
      JK=NK+J
      JI=JP+J
      HOLD=-A(JK)
      A(JK)=A(JI)
   40 A(JI)=HOLD
   45 IF(BIGA) 48,46,48
   46 D=0.D0
      RETURN
   48 DO 55 I=1,N
      IF(I-K) 50,55,50
   50 IK=NK+I
      A(IK)=A(IK)/(-BIGA)
   55 CONTINUE
      DO 65 I=1,N
      IK=NK+I
      HOLD=A(IK)
      IJ=I-N
      DO 65 J=1,N
      IJ=IJ+N
```

```
      IF(I-K) 60,65,60
60    IF(J-K) 62,65,62
62    KJ=IJ-I+K
      A(IJ)=HOLD*A(KJ)+A(IJ)
65    CONTINUE
      KJ=K-N
      DO 75 J=1,N
      KJ=KJ+N
      IF(J-K) 70,75,70
70    A(KJ)=A(KJ)/BIGA
75    CONTINUE
      D=D*BIGA
      A(KK)=1./BIGA
80    CONTINUE
      K=N
100   K=K-1
      IF(K) 150,150,105
105   I=L(K)
      IF(I-K) 120,120,108
108   JQ=N*(K-1)
      JR=N*(I-1)
      DO 110 J=1,N
      JK=JQ+J
      HOLD=A(JK)
      JI=JR+J
      A(JK)=-A(JI)
110   A(JI)=HOLD
120   J=M(K)
      IF(J-K) 100,100,125
125   KI=K-N
      DO 130 I=1,N
      KI=KI+N
      HOLD=A(KI)
      JI=KI-K+J
      A(KI)=-A(JI)
130   A(JI)=HOLD
      GO TO 100
150   RETURN
```

```
C CLAUDE
      REAL DATA(52,200),ADATA(100,2),TRAN(200),WORK(202)
C
CCCC
```

```
      DO 16 L=1,NPTS,2
      C=(TRAN(L)**2)+(TRAN(L+1)**2)
16    ADATA((L+1)/2,2)=ADATA((L+1)/2,2)+(C/FLOAT(NENS))
14    CONTINUE
      DO 17 I=1,NPTS/2
17    ADATA(I,2)=ADATA(I,2)*EL*SMDS/NPTS*DC
C     MAKE CORRECTIONS FOR SLIT MTF AND OPTICS MTF
      DO 18 J=2,NPTS/2
      U=(J-1)*DFR
      ARG=U*SLWI*PI
      SLCOR=(ARG**2)/(SIN(ARG)**2)
      ANCOR=(1.-(U*(1./.8*DFLIM)))**2
      CF=ANCOR/SLCOR
      ADATA(J,2)=ADATA(J,2)/CF
      IF(CF.LT..2) KTP=J
      GO TO 181
18    CONTINUE
C     DETERMINE CONFIDENCE LIMITS ON SPECTRUM FOR DGFR ¢ 100
181   DGFR=NENS*2
      CSUL=.5*((-1.96+SORT(2.*DGFR-1.))**2)
      CSLL=.5*((1.96+SQRT(2.*DGFR-1.))**2)
      UV=DGFR/CSUL
      BV=DGFR/CSLL
C     OUTPUT DATA
      WRITE(116,19) (ADATA(K,1),ADATA(K,2)), K=1,KTP
      WRITE(116,19)
      WRITE(116,19) (ADATA(K,1),ADATA(K,2)*UV), K=1,KTP
      WRITE(116,19)
      WRITE(116,19) (ADATA(K,1),ADATA(K,2)*BV), K=1,KTP
19    FORMAT(2G4.4)
      END
```

8. VITA

Born, raised, and educated in Lorain, Ohio, the author pursued his college education in Photographic Science and Instrumentation at Rochester Institute of Technology. While a student at R.I.T. he was awarded the Fuji Photo Scholarship, along with serving as president of the joint student chapters of the Society for Photographic Scientists and Engineers, & Society of Motion Picture and Television Engineers. Gaining practical work experience through employment at the National Photographic Interpretation Center, and graduate assistantships at R.I.T., a working knowledge of photographic system physics was developed. This was further augmented through full-time work experience in image quality metrics, image structure modelling, microdensitometry, and digital image processing while employed at Xerox Corp. and Eastman Kodak Co.